District-Scale Geothermal System Performance Evaluation using Thermodynamic and Environmental Analysis

By

Lauren Katherine Thomas

A thesis submitted in partial fulfillment of the requirements for the degree of

Master of Science

Geological Engineering

At the

University of Wisconsin-Madison

2019

District-Scale Geothermal System Performance Evaluation using Thermodynamic and Environmental Analysis

By

Lauren Katherine Thomas

Approved by

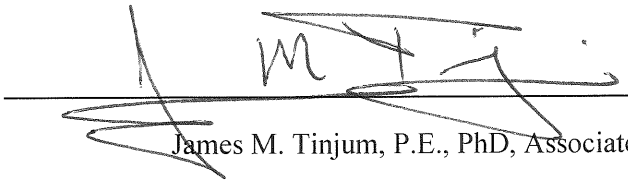

James M. Tinjum, P.E., PhD, Associate Professor

Executive Summary

The focus of the work presented in this thesis aims to improve geothermal heat system efficiency by investigating subsurface thermal properties that influence system performance over the lifetime of the system, as well as quantify the environmental impacts associated with geothermal systems. This work is done through the development of a heat budget and life cycle assessment tool that can assist with more efficient geothermal system design and operation that best benefit the end-user.

The heat budget combines long-term temperature measurements of a district-scale geothermal heat exchange system in Verona, Wisconsin and the thermal properties of the borefield subsurface to calculate the change in borefield heat storage over time. This allows for a heat budget, or understanding of the heat being transported into and out of the borefield, to be developed. Given the cooling-dominated heat load that the borefield is carrying, quantifying the amount of heat independently exiting the borefield allows for a more in-depth understanding of how "leaky" the heat reservoir is. The heat budget investigation in this thesis determined that the borefield behaves as a leaky reservoir of heat. Because of the cooling-dominated heat load combined with the cool climate in Wisconsin, having a natural means of heat escape supports borefield longevity and prevents a reduction in system efficiency due to borefield overheating. This understanding of borefield behavior is useful in making better-informed operational decisions, especially on a district-scale, as there is less speculation regarding where heat travels once placed in the borefield. These improvements in district-scale geothermal systems allow for data-based, sustainable growth in the geothermal sector by providing information that allows for optimizing borefield design for more efficient geothermal systems.

This thesis also investigates the feasibility of implementing a deep direct-use geothermal heat recovery system by investigating the environmental impacts of the system through a Life Cycle Assessment (LCA). The LCA was performed using a spreadsheet tool that was simultaneously developed to provide further insight into the cradle-to-grave environmental impacts. This analysis offers insight into the environmental and economic costs associated with the system, and allows a user to determine if a deep-direct use geothermal system is a feasible option for their site. While geothermal systems are often considered sustainable energy sources, further investigation into the environmental performance of these systems reveal significant impacts associated with various components of DDU systems throughout the lifecycle of the system. The results of the assessment of the proposed system show significant environmental impacts associated with the acquisition of raw materials and electricity required to operate the system. Even with these sizable environmental costs, the proposed geothermal system has potential to offset the emissions associated with the traditional fuel source alternatives that are currently being utilized on the existing campus in approximately 10 years.

Acknowledgements

I would like to thank the members of my advising committee — Professors James Tinjum, Dante Fratta, and Dave Hart – for their many years of guidance, advice, and knowledge. Without their direction and individual skillsets, the work presented here would never have been pursued. It was Professor Tinjum that offered an undergraduate research position to me as a junior, and saw the potential to continue my research career as a graduate student. That first opportunity opened countless doors that would not have been encountered without his effort and care. Professor Dante Fratta created an environment that was the perfect ratio of challenging and supportive, and I am extremely appreciative of the way he advocates for his students and their long-term success. Professor Dave Hart approached every problem with optimism, and his experience in this field took our work to a new level of discovery. Being part of this research group has undoubtedly benefited my personal and professional growth, and I am incredibly grateful to have been advised by this committee.

I owe the greatest debt of gratitude to my parents, Paul and Melanie Thomas. They have ceaselessly supported me through the highs and lows of life, and never doubted that I would succeed. The values that they instilled in me at a young age have made my achievements possible; namely, the importance of hard work and curiosity. Their countless sacrifices for my benefit have ignited my determination for self-improvement and persistent growth. Rachael, my big sister, has served as an incredible example of perseverance and stoicism, while also being a provider of endless laughter and love. Morgan Sanger, my peer, roommate, and dear friend, merits special mention as my daily motivator and source of unending assurance as we worked through this graduate program together. In addition, Kia Race, Cameron Evans, Madeline Sova, and Jane Scott have been exceptional friends and sources of support.

Within the Geological Engineering family, there are far too many names to thank individually, but Xiaodong “Buff” Wang deserves recognition as an outstanding lab manager who has always made himself available to assist with anything ranging from a simple curiosity to a detailed lab test setup. Among research cohorts, Adam McDaniel must be especially thanked for his years of teaching, both relating to geothermal and the general challenges of life. His support and guidance has shaped who I am as an engineer and person. Mitch Laken has my sincerest thanks for his consistent assistance with data calibration, excellent attitude whilst tackling challenging research problems, and being a reliable partner during visits to Vault 14. Thank you to all my graduate student peers who were always willing to offer their help, as well as create a fun and welcoming environment at work. The GLE family has been an enormous part of my life for six years and it will always hold a special spot in my heart.

I would also like to thank Epic Systems and the Wisconsin Department of Transportation for allowing me to work on and contribute to projects that supported my pursuit of this degree. In addition, my research was supported by the University of Illinois, for which I am grateful. Lastly, thank you to the UW-Madison Department of Civil and Environmental Engineering for offering Teaching Assistantships that supported my time here. Any opinions, findings, conclusions, or recommendations expressed in this material are those of the authors and do not necessarily reflect the views of collaborators and funding organizations.

Table of Contents

Chapter 1.0: Introduction

Ground-source heat pumps (GSHP) are part of a heating and cooling system that utilizes relatively constant subsurface temperature to serve as a heat source or heat sink. GSHP systems can be implemented on a variety of scales, ranging from small residential systems to large district-scale systems that serve multiple buildings. GSHP systems have numerous advantages over conventional heating and cooling technologies, mostly related to higher energy efficiency and lower environmental costs (Green Building Alliance, 2019). Transferring energy within a GSHP system is operationally more efficient than other heating and cooling alternatives when designed and operated properly. There is difficulty in predicting performance over the lifetime of a GSHP system, as subsurface heat transfer varies widely depending on the geologic units that the system is interacting with. Furthermore, a significant amount of the environmental costs throughout the lifecycle, such as raw material extraction and construction impacts, of various geothermal systems are widely unknown. The focus of the work presented in the following chapters aims to further understand subsurface thermal behavior that influence GSHP performance over the lifetime of the system, offer insight into improving GSHP performance, and provide a tool that can help quantify the environmental impacts associated with geothermal systems.

This work begins in Chapter 2 with a review of previous work done by the Geothermal and Energy Geotechnics Research Group at UW-Madison. In 2014, this group became partners with Epic Systems (Epic), a world-renowned healthcare software provider with a 10,000+ employee campus located just west of Verona, Wisconsin. At the time, Epic was in the preliminary phases of construction of their fourth district-scale geothermal borefield to supply expanding heating and cooling needs. Due to severely imbalanced (excess heating) annual building loads, Epic had previously experienced overheating and subsequent capacity and efficiency decreases in their first

three fields. The UW team was tasked with monitoring and advising the usage of the fourth and largest borefield to mitigate these past problems. The unique contribution that the UW could provide for this project was provision of a fiber optic distributed temperature sensing (FO DTS) system to monitor a three dimensional grid of field temperatures through the installation of a complex network of buried fiber optics. Chapter 2 presents a continuation of a dynamic, double-ended, centralized, and remotely accessible FO DTS calibration regime, including additional temperature measurements and analysis of Borefield 4 performance. This chapter also works in tandem with Appendix A, where updates and changes to the calibration methodology were made to reduce noise and address disturbances to the system. While the permanent FO DTS system installed at Borefield 4 provides previously unknown information regarding subsurface temperature response, it does not offer insight into how the system is retaining and/or releasing heat. When analyzing borefield efficiency and heat storage potential, temperature data alone does not allow for an understanding of how the system retains or releases heat.

Chapter 3 then aims to build upon the knowledge obtained using the FO DTS data in order to further understand borefield heat storage. This chapter introduces the novel concept of a heat budget to analyze long-term borefield temperature response, heat storage, and heat exchange performance in Borefield 4. The FO DTS data collected at Borefield 4, paired with input and output exchange water temperatures in all four borefields, inform operational decisions of how to split the heating and cooling demand between the four borefields. Beyond this information, using the collected data to calculate the amount of heat injected into, being stored, and naturally dissipating from Borefield 4 allows us to determine if the borefield is acting as a thermal reservoir or radiator, or some combination thereof. The aim of this chapter is to use the knowledge gained from the heat budget to make better-informed operational decisions regarding the optimization of using

Borefield 4 as a heat sink for the campus load imbalance so as to extend future thermal capacity and, most importantly, performance.

Chapter 4 investigates the environmental impacts of a novel geothermal system through a Life Cycle Assessment (LCA) of a potential deep direct-use geothermal system in the Illinois Basin. The LCA was performed using a spreadsheet tool that allows for a general assessment of the cradle-to-grave environmental impacts of a geothermal system. This spreadsheet can be altered to assess deep-direct use geothermal systems with various design parameters, including number of injection and production wells, injection and production well(s) depth, and distance to building(s) served. This analysis offers insight into the environmental impacts associated with geothermal systems, and allows a user to determine if a deep-direct use geothermal system is a feasible option for their site in terms of environmental costs.

The final chapter is a brief discussion regarding the future work that can be done, including suggestions for ways to build upon the work performed at Epic Systems, ideas for new areas of investigation, and recommendations for continuation of the work done in this paper. Appendices include supplements to the chapters outlined above. Appendix A includes an in-depth review of the changes and alterations made to the FO DTS calibration methodology utilized at Borefield 4 and provides insight into how to improve and maintain a permanent FO DTS system. Appendix B is a catalog of the relevant data and scripts used for the heat budget calculation and fiber optic data calibration. Appendix C serves as an instruction manual and guide for the deep direct-use LCA spreadsheet tool, including a review of the inputs and assumptions that are necessary for a complete estimate of environmental impacts. Finally, Appendix D is the supplemental information regarding the LCA project, including a catalog of the assumptions made to perform the LCA.

Chapter 2.0: Background

2.1: Ground Source Heat Pumps

Ground source heat pumps (GSHP) are a source of geothermal space heating and cooling with a growing market. GSHPs take advantage of the fact that the earth maintains relatively constant temperatures below the surface in a range of one to 450 meters deep. The earth is cooler than the ambient air in the summer and warmer than the ambient air in the winter. This thermal resistivity helps shift the cooling load to the season where it is needed. In a GSHP system, networks of closed pipes allow water to transport heat energy from the ground to the surface, where a compressor concentrates the heat and allows a standard heating, ventilation, and air conditioning (HVAC) system to distribute the heat. If cool air is desired, the process is reversed; unwanted heat from the building is drawn from the interior and dispersed into the ground.

The three main components of a GSHP system are heat pumps and ground heat exchangers (GHX), and surface distribution. The heat pump transfers heat from the heating/cooling distribution system to the earth connection. For residential applications and small commercial systems, a single heat pump unit often will suffice. Larger commercial or industrial systems will typically require multiple units that are all connected to a common fluid loop. The GHX makes use of deep vertical holes (boreholes) or a horizontal arrangement of sealed loops of high-density polyethylene (HDPE) piping buried below the surface. Vertical arrangements generally provide higher heat transfer capacity than horizontal installations; however vertical arrangements typically have higher capital costs.

The most significant differential cost of GSHP systems are the initial capital costs of the GHX system, specifically the installation of well and surface components. Because of this, it is important to construct the GSHP system to provide sufficient current and future heating and

cooling capacity without oversizing the system. Lifetime performance of GSHP systems has proven difficult to predict, and this lack of confidence when sizing systems has led to poor economic and environmental outcomes. While a number of predictive models have been developed to size GSHP systems, these models often focus on the performance of mechanical components of the system (Puttagunta, 2010). Subsurface heat transfer is typically estimated under the assumption of one homogenous unit, rather than with a system interacting with a variety of thermophysical parameters. In reality, thermophysical parameters of the subsurface vary with depth and location within the borefield, which is why predictive models that ignore the heterogeneity of the subsurface often oversize GSHP systems. The continuation of these assumptions does not allow for improving future GSHP designs that interact with a heterogeneous subsurface. The ability to understand, monitor, and predict GSHP performance throughout the lifetime of the system can be improved by investigating the variability of the subsurface and how it affects long-term performance of GSHP systems.

2.2 Fiber Optic Distributed Temperature Sensing

Distributed temperature sensing technology uses the scattering of light to create temperature profiles along the fiber optic cables through which the light passes. As a light pulse propagates through a fiber, it interacts with the surrounding matter to form a scattering event. Raman scattering is an inelastic scattering event with two possible outcomes. The first is that the surrounding matter absorbs the energy and the emitted photon has a lower energy than the absorbed photon (Suarez, 2011). This is called Stokes Raman scattering. The second outcome is that the material loses energy and the emitted photon has a higher energy than the absorbed photon, called anti-Stokes scattering. The ratio of Stokes to anti-Stokes photons is a function of the temperature where the scattering event took place (Boiarski, 1993).

Interrogators generate pulses of light that propagate down the cable. When scattering events occur, a portion of the incident light propagates back to the interrogator. The interrogator contains a photo-diode that measures the amplitudes of the Stokes and anti-Stokes Raman backscatter. This light data can be used to calculate temperature data along the cable (Hausner, 2011). The fiber and interrogator can be set up for a single or double ended measurement. For single ended, the light is sent down one end of the fiber for the set duration, which creates one profile, and then moves on to the next fiber. In a double ended setting, the fiber optic cable is looped back and reattached to the interrogator, allowing light to propagate down both ends of the fiber. This method reduces the effects of differential attenuation, as two profiles are created (Selker, 2006).

While most DTS instruments available include pre-installed calibration routines, these routines are not accurate, as they may return temperatures with an accuracy of +/- 1-2 °C. Error of this magnitude is not appropriate for many environmental applications, so a more robust calibration is required (Hausner, 2011).

2.3 Double-ended Calibration

Double-ended calibration refers to measurements where laser pulses are injected and monitored from both sides, alternating after each measurement interval. This method allows for direct calculation of differential attenuation along the fiber optic cable (Giesen, 2012). When cables are homogenous without splices, this calibration method may not be required, but when splices do occur, direct observation of the attenuation is important when obtaining accurate temperature measurements. Another advantage of double-ended calibration is that it only requires calibration baths near the DTS instrument, which is beneficial in cases where it could be difficult to place calibration baths along the cable (Giesen, 2012).

The temperature of a fiber optic cable can be calculated using Equation 1, shown below. At position z (m), the Raman Stokes, $P_s(z)$, and anti-Stokes, $P_{aS}(z)$, signals are used to calculate temperatures.

$$T(z,t) = \frac{\gamma}{ln\frac{P_S(z,t)}{P_{aS}(z,t)} + C - \int_0^z \Delta\alpha(z')dz'} \qquad [1]$$

where γ (K) represents the change in energy between the photon at the laser and the scattered Raman photon, C is a parameter that encompasses laser and DTS properties, and $\Delta\alpha$ (m^{-1}) is the differential attenuation between the Stokes and anti-Stokes signals (Hausner, 2011). The integral represents the product of length and differential attenuation of the Stokes and anti-Stokes radiation caused by differences in absorption. This integral can be referred to as the "cumulative differential attenuation."

During a double-ended measurement, pulses are sent into the fiber from one end of the cable during the first measurement period, and then from the other end during the second measurement period (Selker, 2006). These two directions are called "forward", starting at z = 0, and "reverse", starting at z = L, where L is the length of the cable. If a small reference section of the cable remains a constant temperature, Equation 2 can be used to solve for differential attenuation, $\Delta\alpha$.

$$\int_z^{z+\Delta z} \Delta\alpha(z')dz' = \frac{ln\left(\frac{P_S(z+\Delta z)}{P_{aS}(z+\Delta z)}\right)_{\Rightarrow} - ln\left(\frac{P_S(z)}{P_{aS}(z)}\right)_{\Rightarrow} + ln\left(\frac{P_S(z)}{P_{aS}(z)}\right)_{\Leftarrow} - ln\left(\frac{P_S(z+\Delta z)}{P_{aS}(z+\Delta z)}\right)_{\Leftarrow}}{2} \qquad [2]$$

Where the arrows indicate whether the measurement is forward (⇒) or reverse (⇐). If the value for attenuation for every Δz is summed, starting at z = 0, an average differential attenuation along the cable for each section can be determined (Giesen, 2012).

Once $\Delta\alpha$ is determined for each section of the fiber, a piecewise function can be made to combine the results determined for each section of fiber. After the piecewise function is created, the log power ratios and $\Delta\alpha$ are determined at each bath, as they will be used to determine constants γ and C. Once the values of constants γ and C are found, they can be substituted into Equation 1 to determine temperature down the length of the cable.

In addition to the calibration process described above, it is possible to further calibrate this temperature data to provide a smoother plot with less fluctuation in temperature between time steps. This is done by finding an average γ value across the length of fiber. This fixed gamma value is then used to let the constant C be variable through the cable. A schematic of the overall calibration set up can be seen in Figure 1 (McDaniel, Dynamic Calibration for Permanent Distributed Temperature Sensing Networks, 2018).

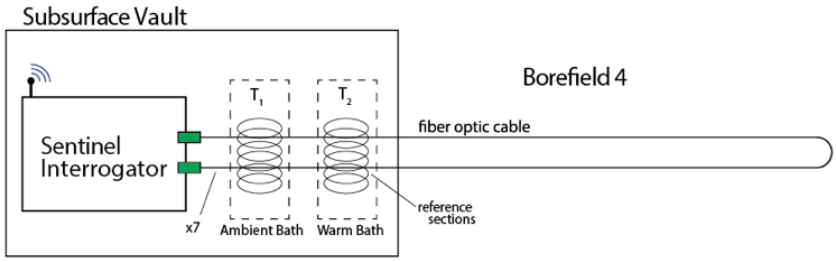

Figure 1. Schematic of double-ended calibration set up used at Epic (McDaniel, Dynamic Calibration for Permanent Distributed Temperature Sensing Networks, 2018)

2.4 Previous work at Epic

The FO DTS system currently being used at Epic Systems is a double-ended dynamically calibrated system installed in Borefield 4, which is the newest geothermal exchange field on Epic's campus. Borefield 4 provides the largest portion of the heating and cooling capacity of the four borefields on site. Sentry wells in the borefield are equipped with fiber loops, and piezometer wells are equipped with a fiber loop to the base of the 150 m deep borefield. A schematic of the temperature monitoring well (TMW) set up can be seen in Figure 2.

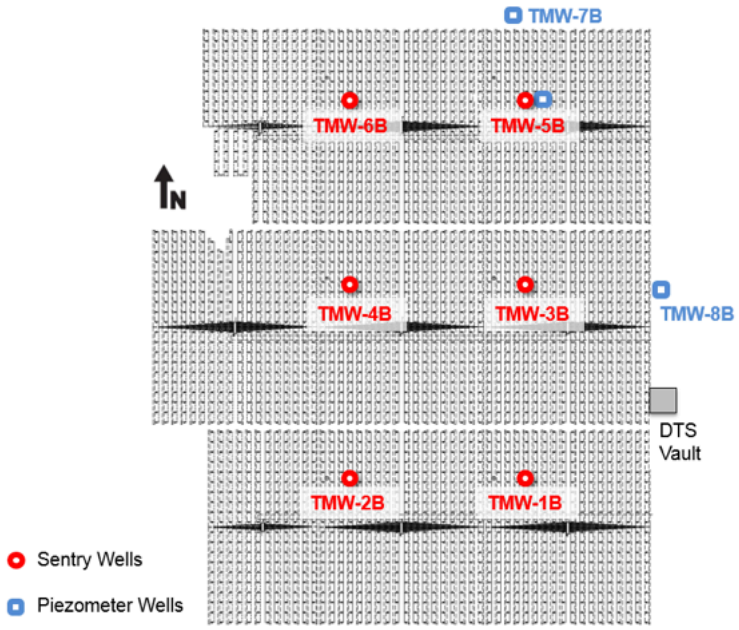

Figure 2. Location of temperature monitoring wells within Borefield 4.

Activation of Borefield 4 was initiated in phases. Phase 1, consisting of the southern third of the borefield, started in October of 2014. Phase 2, comprising the remaining northern two thirds of the borefield, was activated in September of 2015. The operational heating and cooling loads of all four borefields and pond have been monitored since January of 2015. The fiber optic instrumentation of the borefield was initiated with the southern third becoming operational in May of 2015, approximately seven months after heat injection began. The remaining two thirds of the borefield have been monitored since December of 2015.

A dynamic calibration method was developed to interpret the DTS data collected at Borefield 4 (McDaniel, 2018). This calibration method and the resulting color floods provide more knowledge about the subsurface temperature response to Epic's heat loads. Furthermore, when paired with the geology of the area, significant conclusions were made regarding the management of heating and cooling loads at Epic. The temperature data collected for Borefield 4 suggested that saturated rock transferred heat more effectively than dry rock, dry rock heated up slower than the same rock below the water table, there is accelerated cooling associated with highly voided rock, and the shale formations at the base of the borefield had poor heat transfer potential (McDaniel, 2018).

TMW-1B (Figure 3) supports the hypothesis that subsurface heat transfer is heterogeneous. Furthermore, the effect of the water table on the rate of heat transfer is notable, as there a decrease in temperature within the Prairie du Chien group. This formation is known to have significant voids, which would increase water flow. In Figure 4, TMW-2B provides similar observations to TMW-1B. One notable difference is that there is a topography change to the west side of the field, meaning that TMW-2B extends into the Eau Claire shale at the base of the borefield. Figure 4 shows that the Eau Claire shale serves as a thermal barrier at the bottom of the system, as seen by the vertical thermal gradient. The Tunnel City formation shows low rates of heat transfer compared to the surrounding lithology, as the clay and feldspathic materials create a lower thermal diffusivity (McDaniel, 2018).

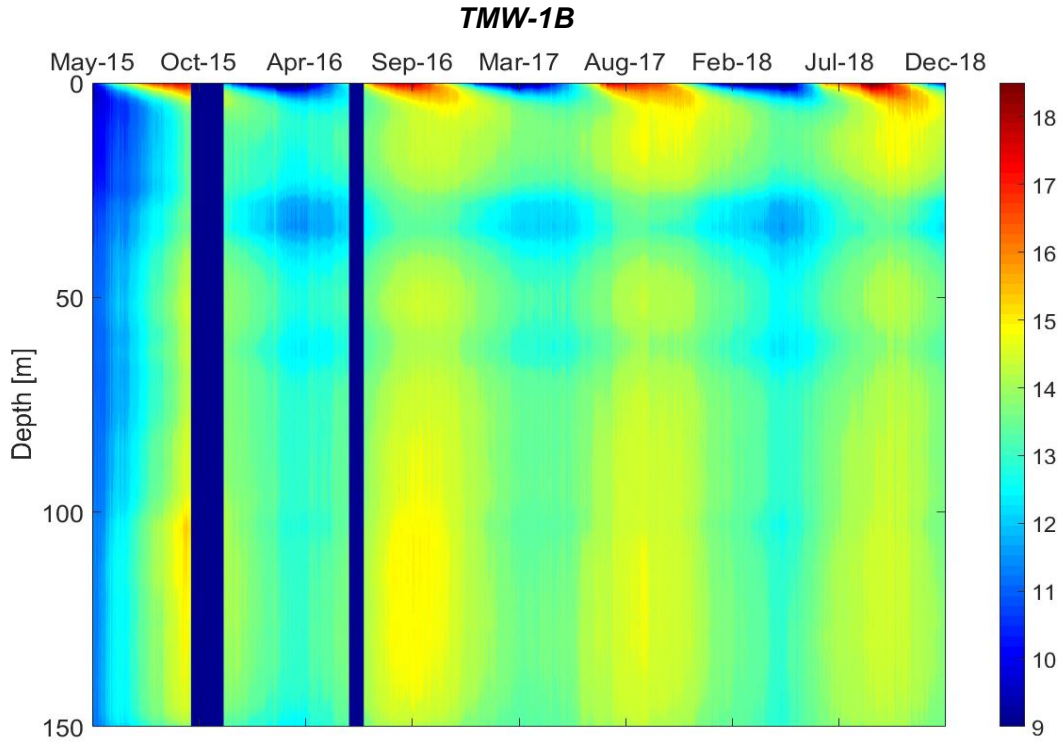

Figure 3. Results from Temperature Monitoring Well 1.

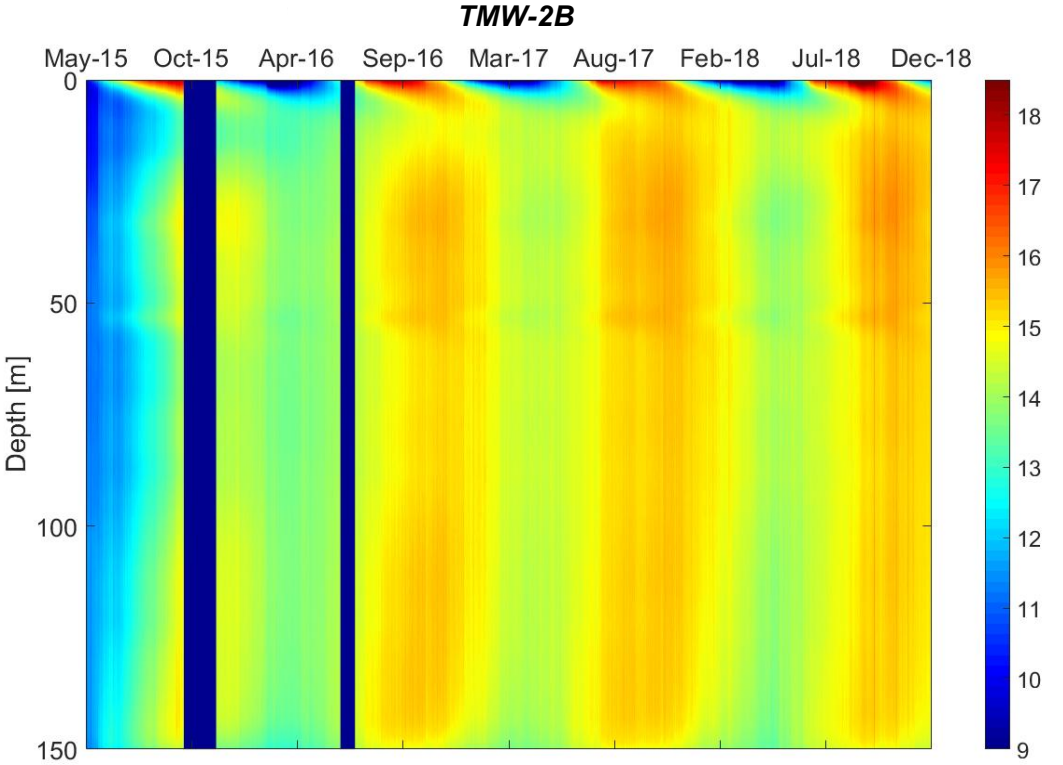

Figure 4. Results from Temperature Monitoring Well 2.

Temperatures in TMW-3B and TMW-4B (Figures 5 and 6) are already elevated at the beginning of the plot, this is because data collection began 2.5 months after phase 2 and phase 3 activation. There is a lag in heating of the part of the Prairie du Chien group that is above the water table, which indicates that dry rock has a lower thermal diffusivity. A notable difference between TMW-3B and TMW-4B is that TMW-4B displays the low heat movement through the Tunnel City formation, while TMW-3B shows relatively homogenous heat flow in the differing units.

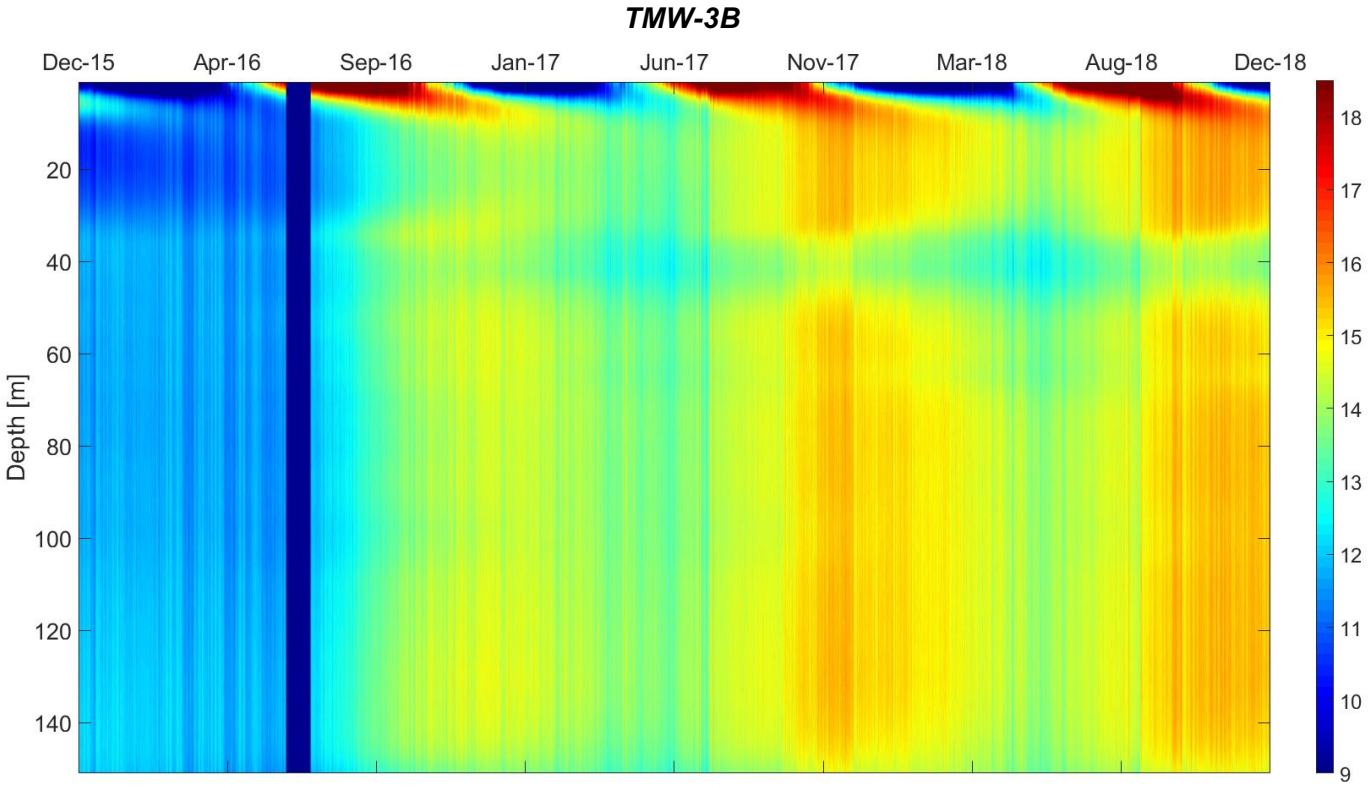

Figure 5. Results from Temperature Monitoring Well 3.

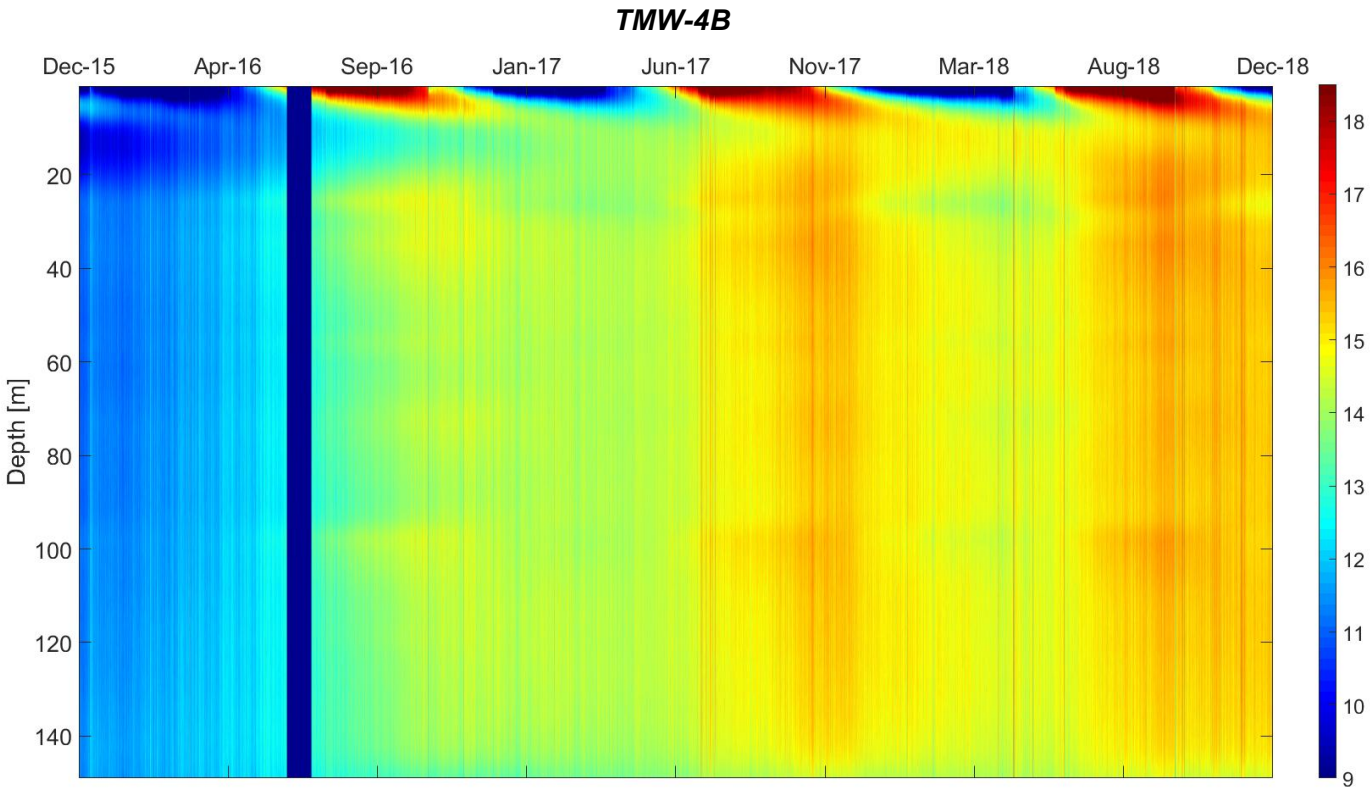

Figure 6. Results from Temperature Monitoring Well 4.

Phase 3 of Borefield 4 is represented in TMW-5B and TMW-6B. TMW-5B (Figure 7) shows the effects of voids in the geology with cooler pockets near the bottom of the Prairie du Chien formation. TMW-6B (Figure 8) shows the most local variation in heat flow of any well in the borefield. There are four windows of preferential heat flow within the plot, which provide insight into how heat flow in the borefield might not be laterally continuous (McDaniel, 2018).

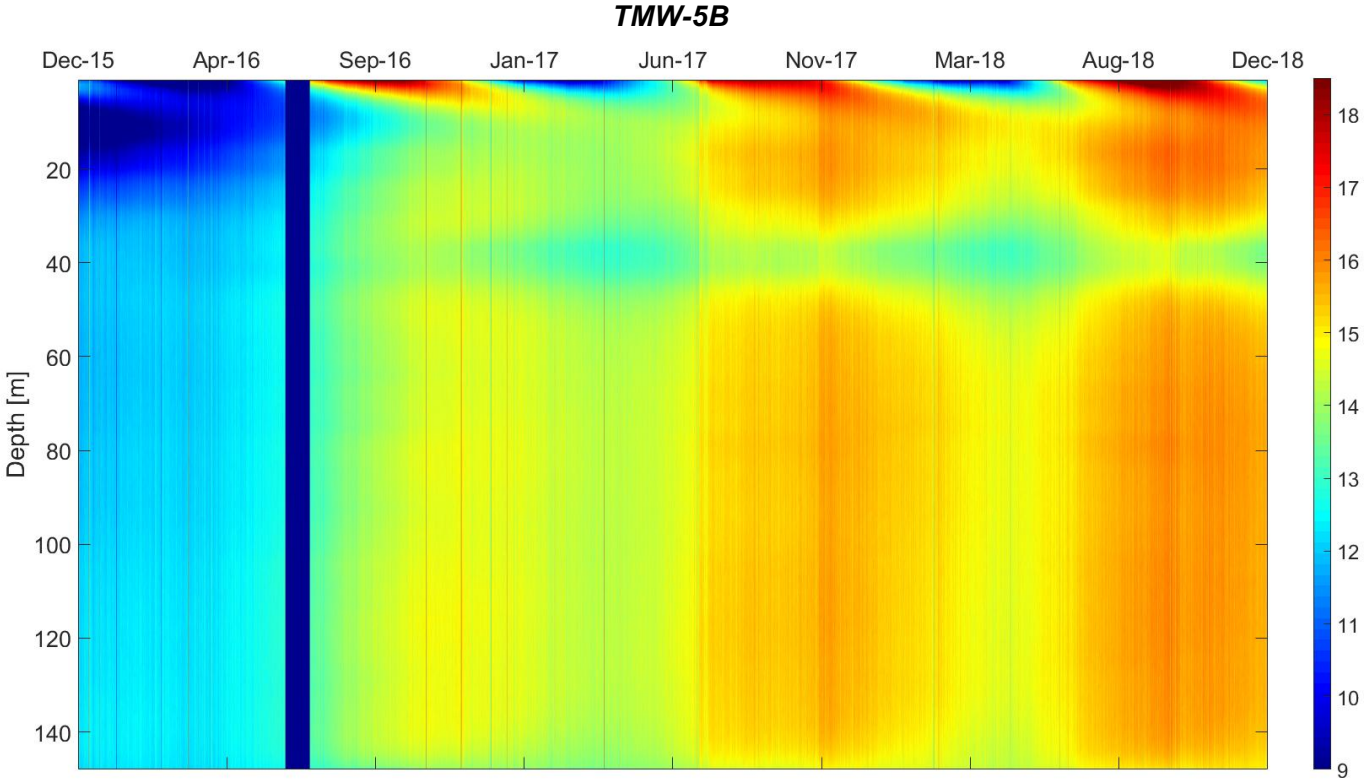

Figure 7. Results from Temperature Monitoring Well 5.

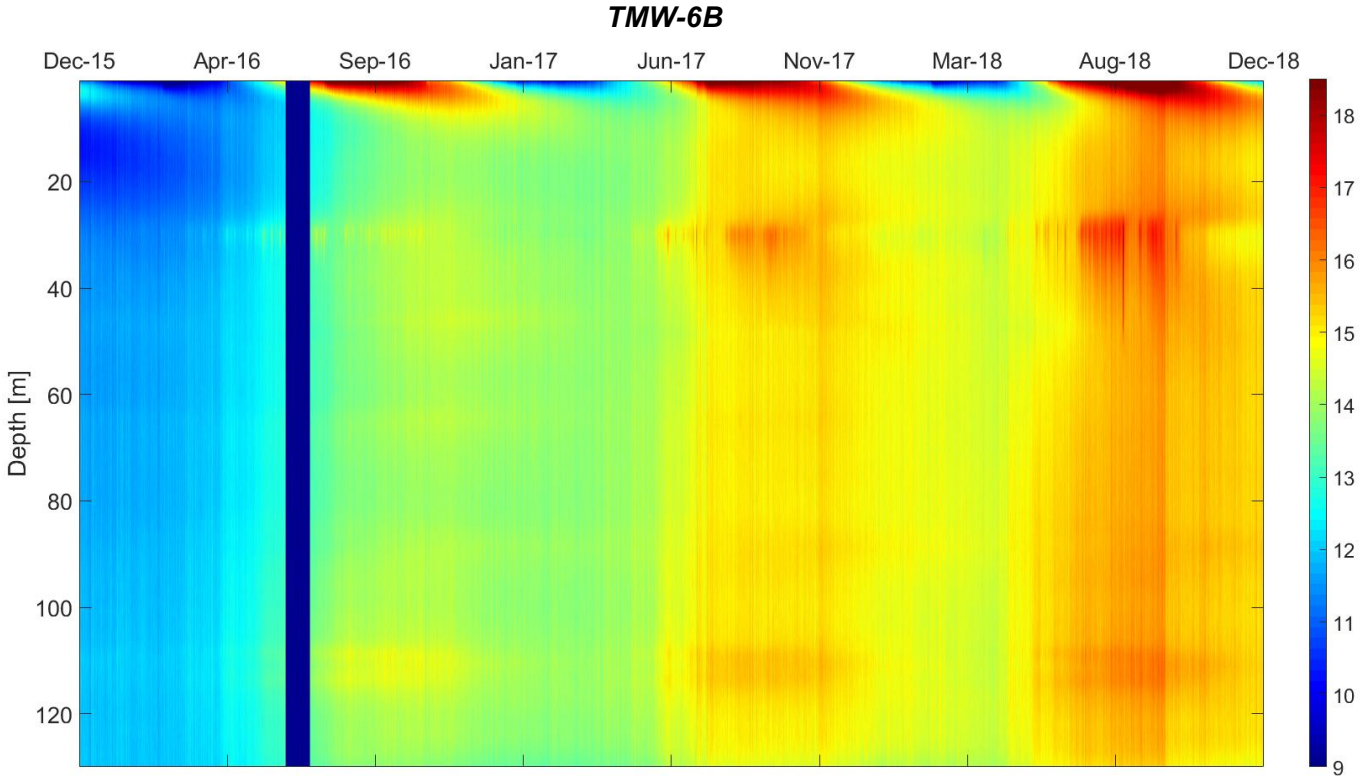

Figure 8. Results from Temperature Monitoring Well 6.

TMW-7B and TMW-8B (Figures 9 and 10) are two temperature monitoring wells that are outside of Borefield 4. The purpose of these wells are to observe how groundwater flow interacts with heat exchange in the borefield. The shallow and deep aquifers, as mentioned earlier, are seen in the temperatures of TMW-7B and TMW-8B. In the shallow aquifer, data suggests that the groundwater flow has moved heat south, and the differing groundwater movement in the deep aquifer is shown by higher temperatures.

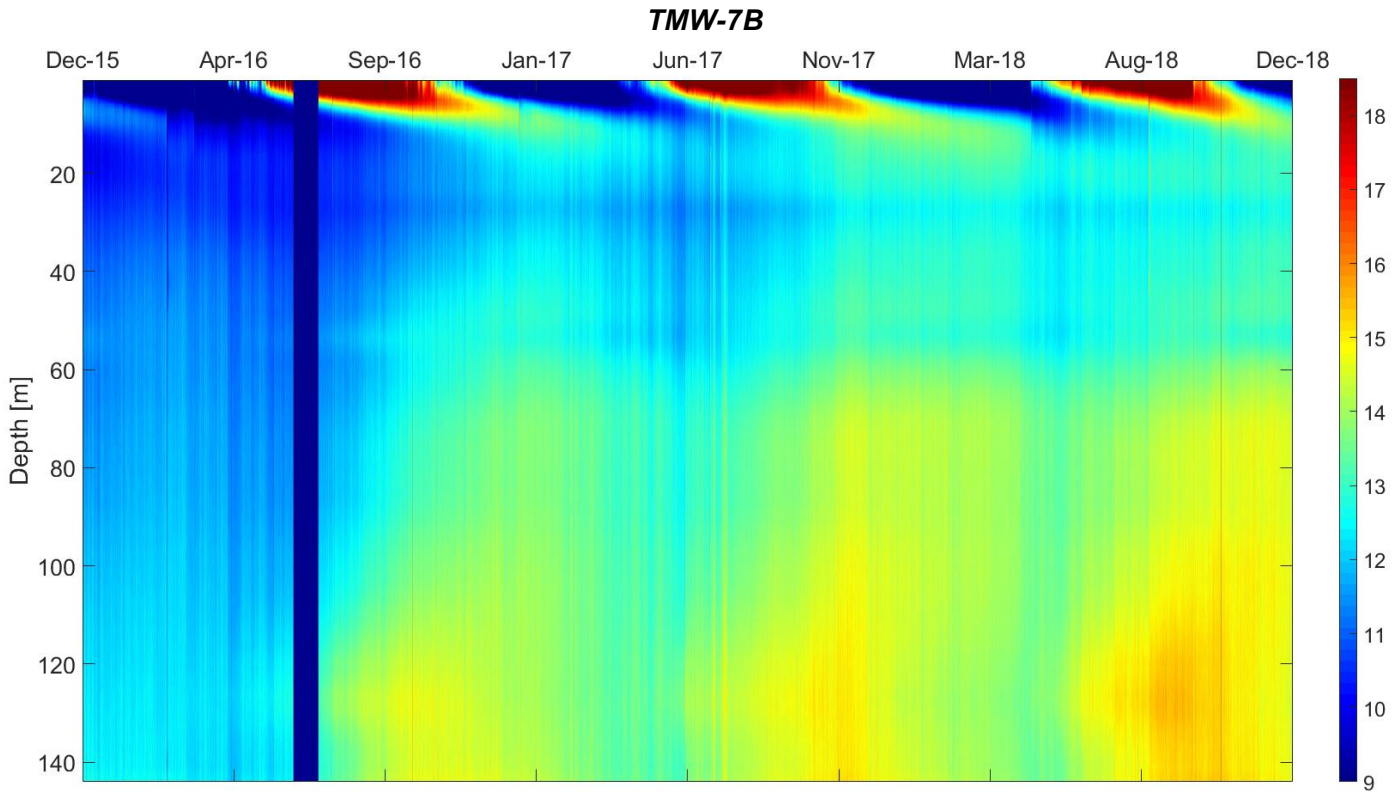

Figure 9. Results from Temperature Monitoring Well 7.

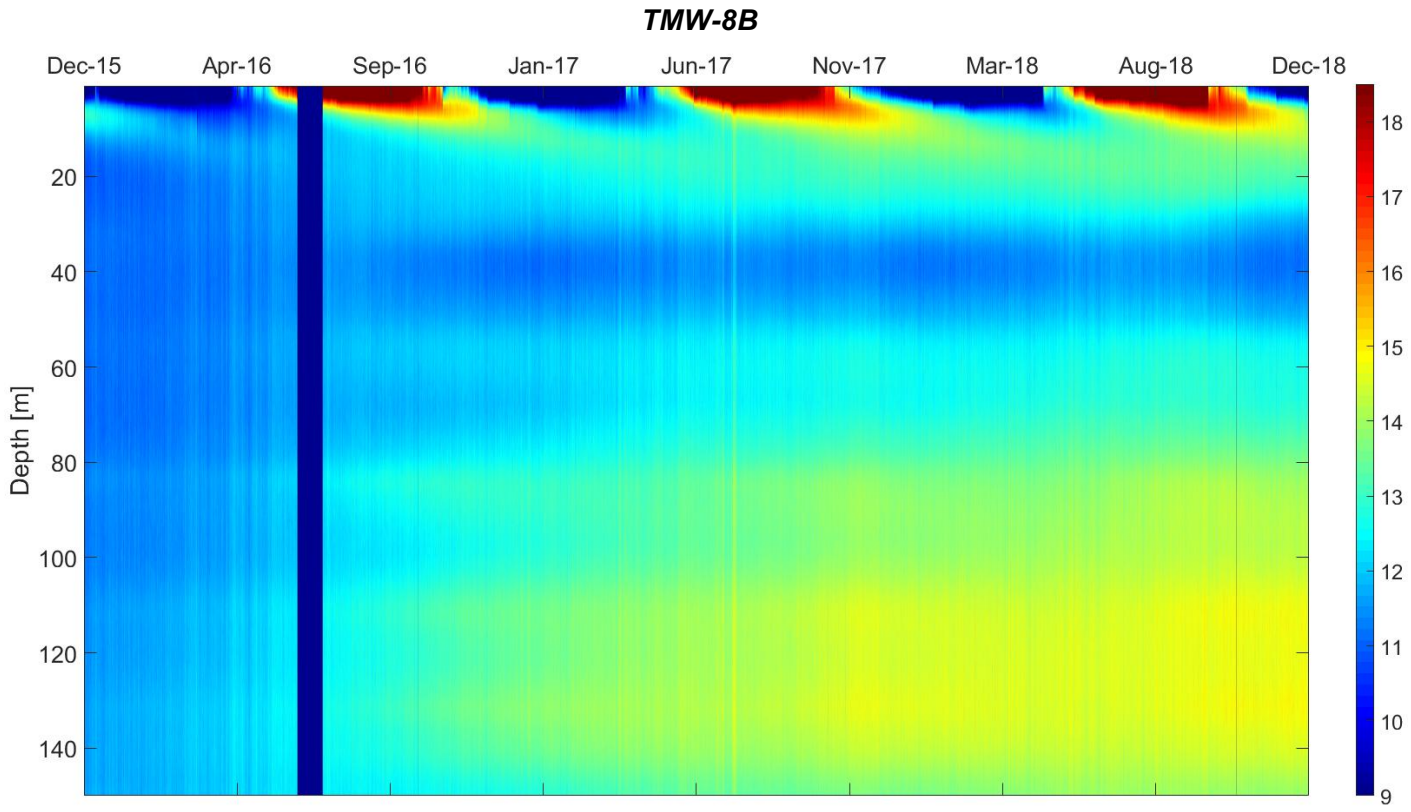

Figure 10. Results from Temperature Monitoring Well 8.

While these temperature results proved to be useful for making inferences regarding borefield behavior, there is still a considerable amount of noise (false temperature fluctuations) in the data. Furthermore, the current calibration setup is sensitive to seasonal temperature fluctuations and is not robust enough for permanent data collection at Borefield 4. An investigation of the noise seen in the DTS results and a discussion of suggested calibration improvements can be found in Appendix A.

Chapter 3.0: Energy Budget and Heat Flow calculation at Borefield 4

3.1 Abstract

Epic Systems is a healthcare software company in Verona, Wisconsin with a campus that houses approximately 10,000 employees in 20 buildings. Epic heats and cools its campus with four district-scale geothermal heat exchange borefields with 48.5 MW of capacity, and a cooling pond that provides an additional 4.2 MW of cooling capacity for limited time intervals. Epic has an imbalanced heat load as a result of a cooling-dominated campus in a cold climate. Borefield 4, the fourth and largest borefield on campus, bears the largest portion of the heat load with approximately 2,500 ground heat exchangers. At 360 meters (north-south) by 280 meters (east-west) by 152 meters deep, Borefield 4 has approximately 15.4 million cubic meters of rock to serve as a thermal reservoir.

Borefield 4 has been instrumented with eight fiber optic temperature monitoring wells down to the base of the borefield. This fiber optic data in Borefield 4 paired with input and output exchange water temperatures in all four borefields inform operational decisions of how to split the heating and cooling demand between the four borefields. Beyond this information, using the collected data to calculate the amount of heat injected into, being stored, and naturally dissipating from Borefield 4 allows us to determine whether or not the borefield is acting as a reservoir or radiator of heat. The aim of this study is to use the knowledge gained from this heat budget to make better-informed operational decisions regarding the optimization of using Borefield 4 as the primary heat sink for the campus load imbalance so as to extend future thermal capacity.

3.2 Introduction

The planet's average surface temperature has risen 0.9 degrees Celsius since the late 19th century (NOAA, 2019). Global temperature rise, an event driven largely by increased carbon

dioxide and other human-made emissions into the atmosphere, can be mitigated by utilizing low-emission energy sources. Ground-source heat pumps (GSHP) are low enthalpy systems used for space heating and cooling with low primary energy consumption compared to conventional fossil fuel temperature control. A large benefit of GSHP systems is the low emissions associated with them, with 33-50% CO_2 emissions savings globally (Fridleifsson, 2008). Geothermal heat exchange systems can be implemented on a variety of scales, ranging from small residential systems to large-scale systems supporting multiple buildings. District-scale systems can be highly competitive with other space heating fuel sources, and geothermal often shows itself to be the lowest cost alternative in today's energy market (Thorsteinsson & Tester, 2009). Because of the increasing demand for low-emission energy alternatives increase, implementation of district-scale geothermal systems should be more heavily considered.

One notable district-scale borefield is the Epic Systems GSHP system in Verona, Wisconsin. University of Wisconsin-Madison researchers have monitored this system for over three years using fiber optic distributed temperature sensing (DTS), which is a technique that can be used to obtain temperature measurements along quasi-continuous profiles in space and time. While DTS technology is often only used for short-term monitoring, long-term or permanent monitoring can offer further insight into borefield operation and efficiency.

The work in this paper combines long-term temperature measurements of a district-scale geothermal heat exchange system in Verona, Wisconsin and the thermal properties of the borefield subsurface to calculate the change in borefield heat storage over time. This allows for a heat budget, or understanding of the heat being transported into and out of the borefield, to be developed. This understanding of borefield behavior and borefield heat storage potential is beneficial for long-term operation. The heat budget can be used to determine if Borefield 4 is

acting as a thermal reservoir or radiator. Given Epic's cooling-dominated heat load, quantifying the amount of heat independently exiting the borefield allows for a more in-depth understanding of how "leaky" the heat reservoir is. Furthermore, the heat budget assists with the analysis of borefield operation in order to make better-informed long-term operational decisions based on the borefield heat storage potential.

3.3 Background

Epic Systems Corporation, or Epic, is a healthcare software company headquartered in Verona, Wisconsin, 11 miles south of Madison. The climate in Verona is cool, with temperatures dropping below freezing five months out of the year. Epic has a growing campus that houses approximately 10,000 employees in 20 office buildings. Overall, Epic's campus approaches energy neutrality through the use of a 10-MW-capacity wind farm, 1.5 MW-capacity in solar panels, and district-scale geothermal heating and cooling. Epic's geothermal system consists of four district-scale borefields with 6,172 u-pipe ground heat exchangers (GHX) that provide 48.5 MW of cooling capacity and a cooling pond with 1,300 coiled loops that provide 4.2 MW of cooling for limited intervals. While Verona's climate is relatively cool, Epic's campus is cooling-dominated and often distributes excess heat to the four borefields and cooling pond. Borefield 4 bears the largest portion of the campus heat load, with 2,596 GHXs that provide nearly 26 MW of cooling capacity (McDaniel, 2018).

3.4 Materials & Methods

3.4.1 Field Site

Borefield 4 is located in the northeast corner of the Epic campus. The borefield is 360 meters (north-south) by 280 meters (east-west) by 152 meters deep with 2,596 GHXs that provide 25.6 MW of cooling capacity.

The bedrock geology at Borefield 4 is predominantly dolomite, shale, and sandstone. Beneath 10 meters of gravel and sand fill, the first bedrock encountered is a dolomite formation within the Prairie du Chien group. The next 10 meters is the clean quartz arenite layer of the Jordan sandstone. Beneath the sandstone layer is interbedded siltstone and dolostone from the St. Lawrence formation, Next is 35 meters of the Tunnel City formation that contains clay and feldspar cements that reduce the overall thermal conductivity of the unit. The Wonewoc sandstone is below and is a quartz arenite similar to that of the Jordan sandstone. The bottom of Borefield 4 consists of the shaley layer of the Eau Claire formation, which has the lowest thermal conductivity of the profile. A representative geologic profile of Borefield 4 can be seen in Figure 11.

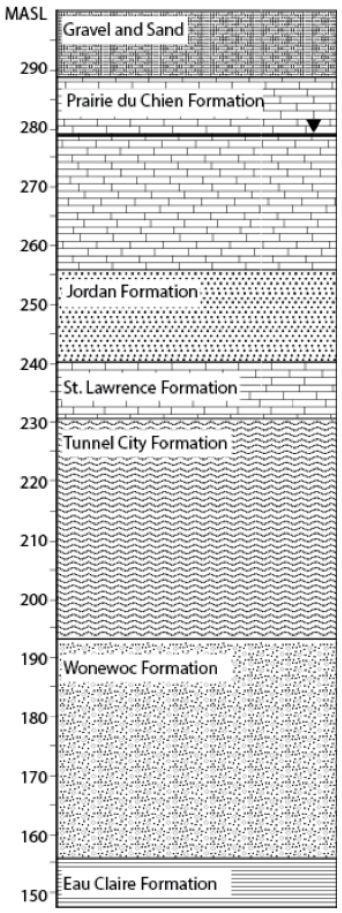

Figure 11. Representative geologic profile of Borefield 4.

In addition to geology, groundwater flow is also important to monitor when analyzing heat transfer of the borefield. The Tunnel City formation separates a shallow and deep aquifer in Borefield 4. Within the shallow aquifer, water flows south west towards the Sugar River. In the deep aquifer, water flow direction changes between flowing

towards the Sugar River and flowing south east towards a municipal pumping well. The average flow direction in the deep aquifer is south.

3.4.2 Instrumentation

Borefield 4 has been instrumented with temperature monitoring wells (TMW) with fiber optic loops down to the base of the borefield. There are five sentry wells within the bulk volume of the borefield, and three piezometer wells, one within the bulk volume and two along the outside perimeter of the borefield. The piezometer wells are screened in the shallow aquifer, the deep aquifer, and have a fiber optic loop installed to the base of the borefield. A map of the borefield can be seen in Figure 12.

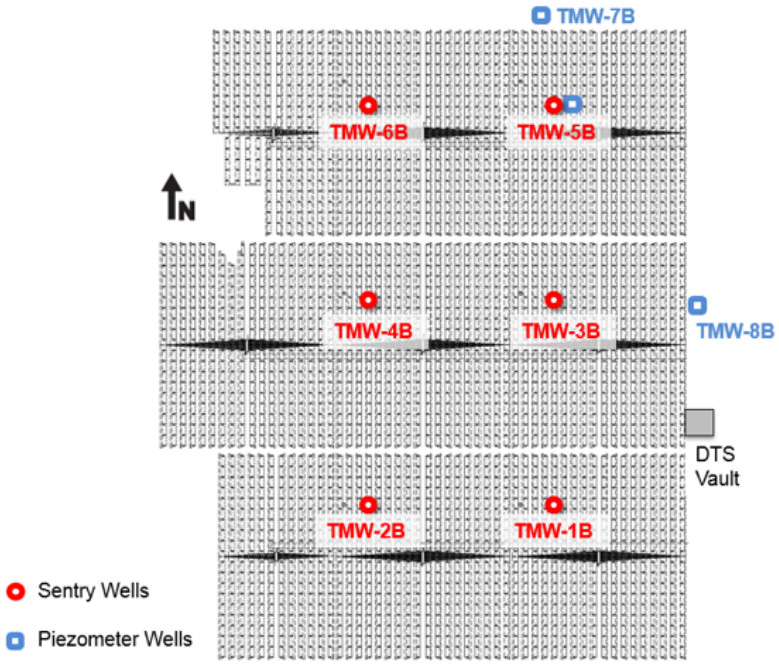

Figure 12. Aerial map of Borefield 4, including locations of Temperature Monitoring Wells 1 through 8 and DTS Vault 14.

A Sensornet Sentinel DTS-LR interrogator with a 16-channel multiplexor is used to collect the fiber optic temperature data, and is located in a vault (Vault 14) on the eastern side of the borefield. Temperatures are calibrated by a dynamic, double-ended, centralized, and remotely accessible manual routine (McDaniel, 2018).

Epic closely monitors and tracks its internal campus heat flows. A centralized data collection network, *Cimplicity*, collects HVAC data and uses it for automatic temperature control. A significant amount of this data is compiled in 15 minute intervals. Useful parameters within these data sets include borefield supply and return temperatures and flow rates for the four borefields and heat sink pond. This data paired with the temperature data allows for borefield energy injection and extraction calculations to be performed. A sample of the script used to interpret this data can be found in Appendix B.

3.4.3 Heat Budget Determination

The heat budget for Borefield 4 is separated into three parameters: heat source (Q_{source}), heat dissipated ($Q_{dissipated}$), and heat storage ($Q_{storage}$). Quantifying these three components is useful when subjectively analyzing borefield heat management and overall borefield design, as it is important to understand how the system's heat load is being distributed. Q_{source} represents the heat injected into or removed from the borefield by the user, $Q_{dissipated}$ is the heat that naturally travels into and out of the bulk volume of the borefield, and $Q_{storage}$ is the heat that is stored in the bulk volume of the borefield. A schematic showing the three heat budget components can be seen in Figure 13.

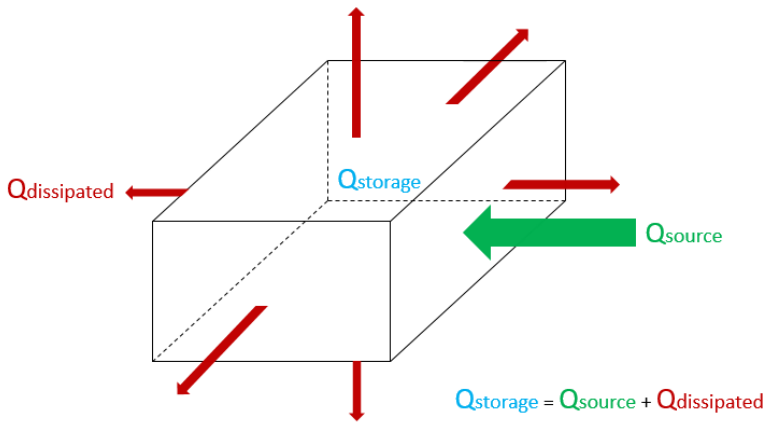

Figure 13. Schematic showing the three parameters that compromise the Borefield 4 heat budget.

The borefield has six faces which heat can travel across. As the temperature gradient across the bulk volume of the borefield and its surroundings fluctuates, heat will either exit the system into the surroundings, or vice versa. The primary control on the temperature of the borefield is Q_{source}, as Epic's heat load varies throughout the year and will contribute to the heat stored within the field. $Q_{dissipated}$ will either add to or decrease the amount of heat stored in the borefield. This means that $\Delta Q_{storage}$ is the sum of Q_{source} and $Q_{dissipated}$, representing the change in heat storage over a period of time . This relationship can also be seen in the form of Equation 1 below.

$$\Delta Q_{storage} = Q_{source} + Q_{dissipated} \qquad \text{[Eq. 1]}$$

where Q_{source}: (+) heat put into borefield, (-) heat removed from borefield
$\Delta Q_{storage}$: (+) heat stored in borefield increases, (-) heat stored in borefield decreases
$Q_{dissipated}$: (+) heat entering borefield from surroundings, (-) heat dissipating out of borefield

Storage is calculated using the long-term borefield temperature data that is collected with the fiber optic technology outlined in the previous section. The change in borefield temperature over time paired with the thermal properties of the subsurface allows us to determine the change in storage, or how much of the storage is affected by Q_{source} versus $Q_{dissipated}$. Borefield 4 is split up into six subsections, with each section corresponding to a certain temperature monitoring well. A map of Borefield 4 with the designated sections can be seen in Figure 14.

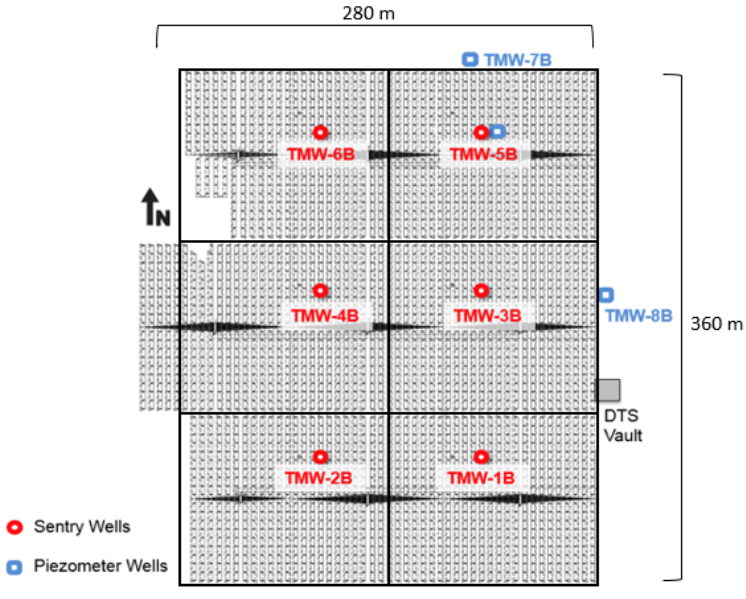

Figure 14. Map of Borefield 4 with the designated sections used for storage calculations boxed.

A storage calculation was done for each of the seven geologic units within each borefield section over monthly time intervals. Parameters needed to calculate storage are change in temperature over time, the thermal properties of the seven geologic units that the borefield interacts with, and the volume of the borefield. The equation used to determine $Q_{storage}$ (Eq. 2) and a table of the necessary thermal and hydrogeological properties (Table 1) of the borefield can be seen below.

$$\Delta Q_{storage} = \Delta T * \rho * C_p * V \qquad \text{[Eq. 2]}$$

where ΔT = change in temperature over one month in one geologic unit [K]

ρ = density of geologic unit [kg m^{-3}]

C_p = specific heat of geologic unit [J kg^{-1} K^{-1}]

V = volume corresponding to certain TMW section [m^3]

Table 1. Thermophysical and hydraulic properties of the geology at Borefield 4 (Walker & Meyer, 2015).

	λ [W m^{-1} K^{-1}]	**C_p** [J kg^{-1} K^{-1}]	**ρ** [kg m^{-3}]	**κ** [mm^2 s^{-1}]	**n** [%]	**K_h** [m day^{-1}]	**K_v** [m day^{-1}]
Gravel and Sand	1.5	800	1800	1.04	15	0.45	0.004
Prairie du Chien	4.14	832	2678	1.86	5	4.115	0.03
Jordan Sandstone	3.3	821	2135	1.88	22	0.091	0.003
St. Lawrence	4.67	872	2678	2	5	18.288	0.003
Tunnel City	2.59	891	2446	1.19	13	0.305	0.5
Wonewoc Sandstone	3.82	900	2650	1.6	10	1.74	0.3
Eau Claire Shale	1.84	795	2477	0.93	5	0.005	0.001

The component Q_{source} is the amount of heat being injected into or removed from the borefield. This value is determined using the *Cimplicity* operational data provided by Epic. This data allows for a calculation of the heat load being transferred into and out of Borefield 4 using Equation 3 below.

$$Q_{source} = Q_w * \Delta T * \rho * C_p \quad \text{[Eq. 3]}$$

where Q_w = volumetric flow rate [m^3 s^{-1}]

ΔT = change in water output temperature and water input temperature [K]

ρ = density of water [kg m^{-3}]

C_p = specific heat of water [J kg^{-1} K^{-1}]

$Q_{dissipated}$ is the amount of heat that is naturally traveling into and out of the borefield. Once $\Delta Q_{storage}$ and Q_{source} are determined using the methods previously outlined, $Q_{dissipated}$ can be estimated using Equation 1 above. While this method only approximates $Q_{dissipated}$ using the other two components of the system, this value could also be roughly estimated to provide partial verification using Equation 4 below.

$$Q_{out} = q * A = -k * \left[\frac{T_{present} - T_0}{dx}\right] * A \quad \text{[Eq. 4]}$$

Because there are only temperature monitoring wells to the north and east of Borefield 4, this calculation would only calculate the heat flux across half of the north and half of the east face of the borefield. The sum of the heat flux calculated across TMW-5B to TMW-7B and TMW-3B to TMW-8B can be multiplied to represent all six faces of the borefield. In this case, the determined heat flux would be multiplied by 12. This method results in an underestimation of the heat flux across the face of the borefield and is only calculating the conductive heat flow, with no consideration of advective heat flow via groundwater flow. The results of the calculations for the heat source (Q_{source}), heat dissipated ($Q_{dissipated}$), and heat storage ($\Delta Q_{storage}$) in Borefield 4 can be found in the following section.

3.5 Results and Discussion

Change in heat storage within the six sections of the borefield varies noticeably over three years, as seen in Figure 15 below. This is due to the fact that Borefield 4 began operation in phases, with Phase 1 consisting of TMW-1&2 and Phase 2 consisting of TMWs 3, 4, 5, and 6. Between 2016 and 2017 there is a large decrease in the storage associated with Phase 2. Because Phase 1 was initiated 11 months before Phase 2, a large temperature gradient was created between the southern third and the northern two-thirds of the borefield. As operation continued, storage in the northern two-thirds of the field increased greatly as a result of the temperature gradient within the borefield. Over time, heat storage within all six sections of the borefield decreased and relative storage between sections leveled out, most likely as a result of the temperature gradient within the borefield decreasing with continued operation.

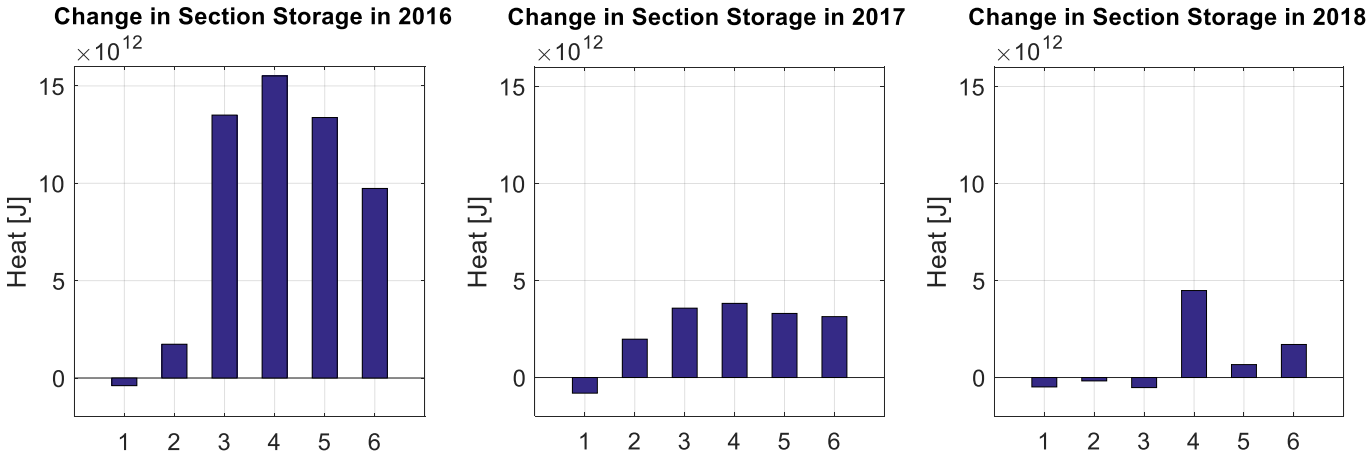

Figure 15. $\Delta Q_{storage}$ within the six sections of Borefield 4 over three years.

Heat storage within Borefield 4 can also be discretized with depth, separated based on geologic unit. Similar to the trend seen in the graphs above, $\Delta Q_{storage}$ in each geologic unit decreases over time (Figure 16). The values for $\Delta Q_{storage}$ that were calculated within each geologic unit are expected, given the known thermophysical properties of the strata. Generally, the shaley

layers with lower thermal conductivity have less storage potential, and the dolomitic and sandy layers have higher storage potential (Clauser & Huenges, 2013).

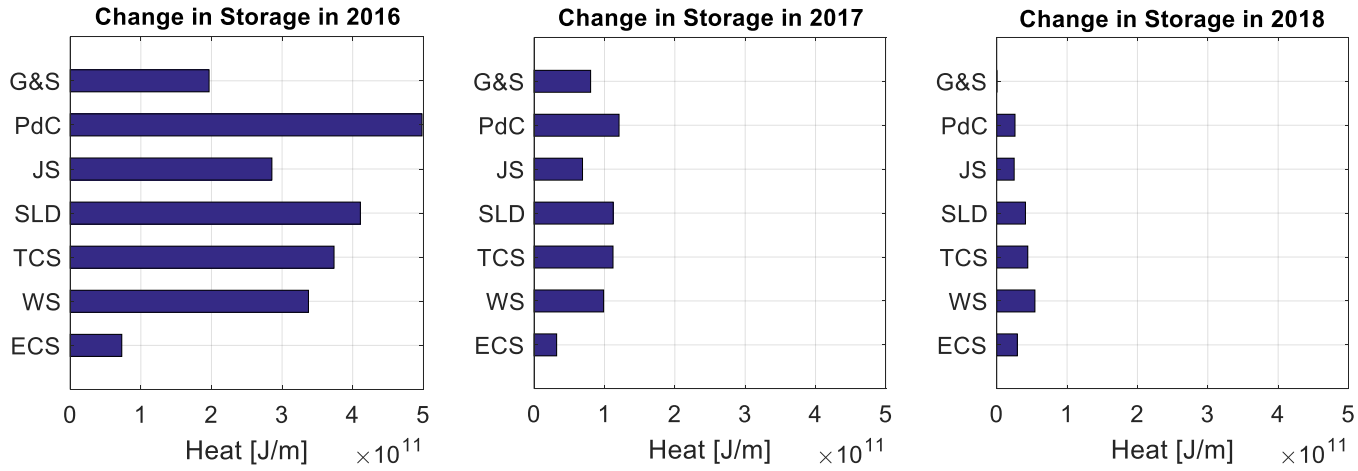

Figure 16. $\Delta Q_{storage}$ within the seven geologic units that Borefield 4 interacts with, normalized by thickness of unit. The thermophysical properties of each unit can be found in Table 1 in the previous section.

The layer of Jordan sandstone has a thermal conductivity of 3.30 W m^{-1} K^{-1} and is surrounded by the Prairie du Chien dolomite above and the St. Lawrence dolomite below, which have a thermal conductivity of 4.14 and 4.67 W m^{-1} K^{-1}, respectively (Walker & Meyer, 2015). In 2016, there is a noticeable difference in change in storage within the Jordan sandstone compared to its surrounding layers, however that difference decreases in 2017 and 2018. This shows that while vertical heterogeneity influences subsurface heat transfer in early operation, heat storage within the borefield and across strata homogenizes over time.

During the initial geotechnical investigation of Borefield 4, it was discovered that the Prairie du Chien formation contains voids and fractures that promote groundwater flow (McDaniel, 2018). These fractures provide a means for heat to be transferred out of the system. Furthermore, as borefield temperatures increase with operation time, there is a higher temperature gradient, which increases heat transport. Compared to the other strata in the borefield, heat storage in the Eau Claire shale at the base of the borefield remains relatively constant. This can be attributed to

the shale layer's low thermal diffusivity (see Table 1), preventing heat from escaping out of the bottom face of Borefield 4. Additionally, the Eau Claire formation is an aquitard that acts as a hydraulic barrier beneath the Wonewoc, and will likely not allow downward advective heat flow.

Overall, monthly heat storage changes ebb and flow in an expected trend, with heat storage increasing in the summer months and decreasing in the winter months. Ideally, change in storage in one year would net zero, however this is not expected at Borefield 4, given that the subsurface temperatures are increasing due to imbalanced heat demand. This effect can also be seen in the supplemental color floods (Appendix A), with temperature in the borefield increasing approximately 2°C over three years. Change in storage in the borefield between December 2015 and December 2018 can be seen below in Figure 17.

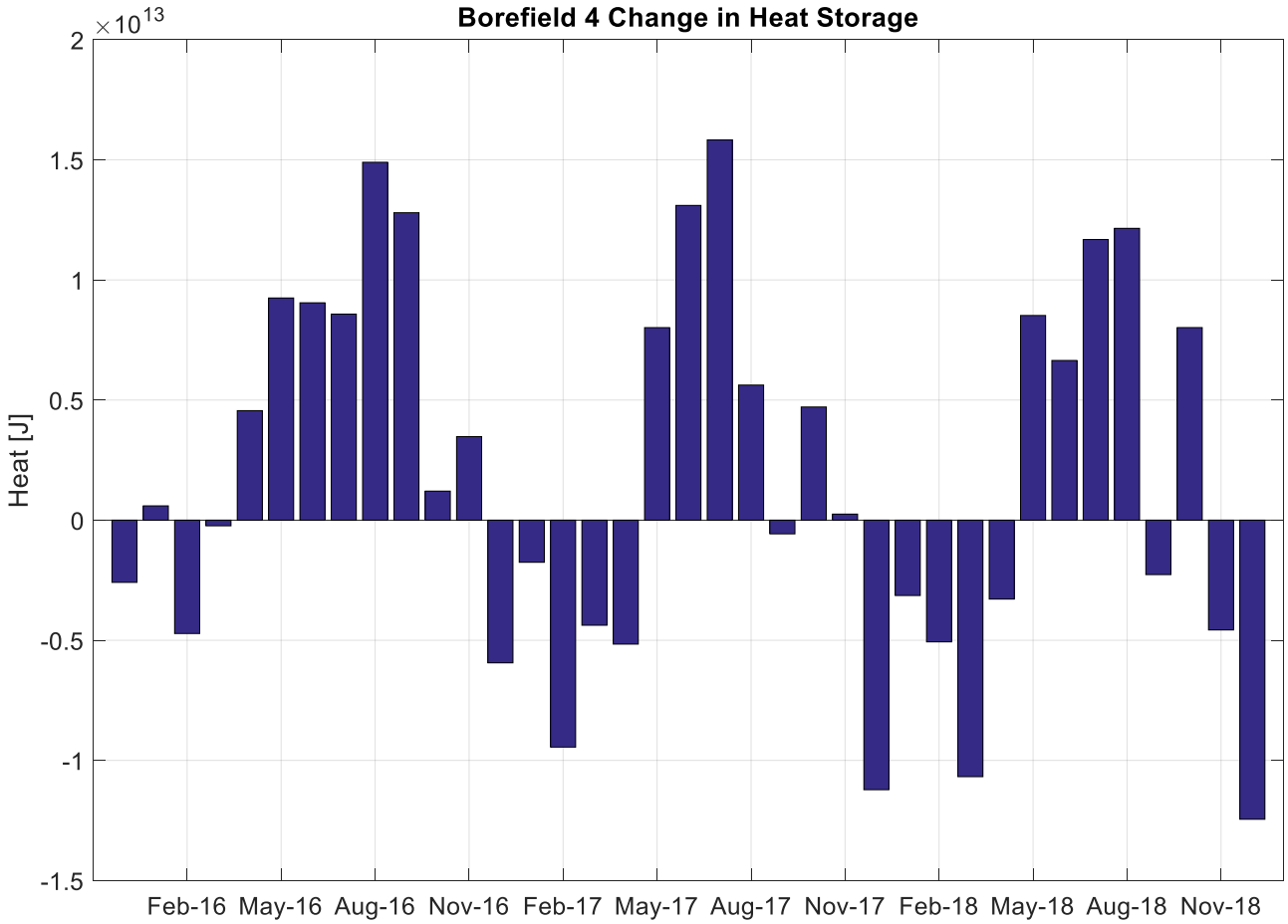

Figure 17. $\Delta Q_{storage}$ for each month between December 2015 and December 2018.

Over time, it appeared that Borefield 4 operation methods evolved, likely with borefield overheating prevention in mind. As seen in Figure 18, Q_{source} in Borefield 4 has decreased with time, showing that some of the campus heat has been redirected to other borefields or the heat sink pond. Long-term conditioning requires $\Delta Q_{storage}$ to not increase dramatically, meaning that Q_{source} needs to be more evenly distributed across borefields. This effort is seen when comparing heat flow into the four borefields and heat sink pond over the three year period. In 2016, a significant heat load was placed in Borefield 4, while a relatively small amount was used in the winter months. In the following years, more heat is removed from Borefield 4 for heating in the winter months, which resulted in a slightly smaller amount of heat being removed from Borefields 1 through 3. Another conditioning method utilized by Epic is to make use of the heat sink pond in the late winter and early spring months as a way to let the borefields prepare for the upcoming heat loads that will be received when outdoor temperatures increase and the heat stored in the field is not needed. These spikes in the pond heat load can be seen in February of 2016 and 2017.

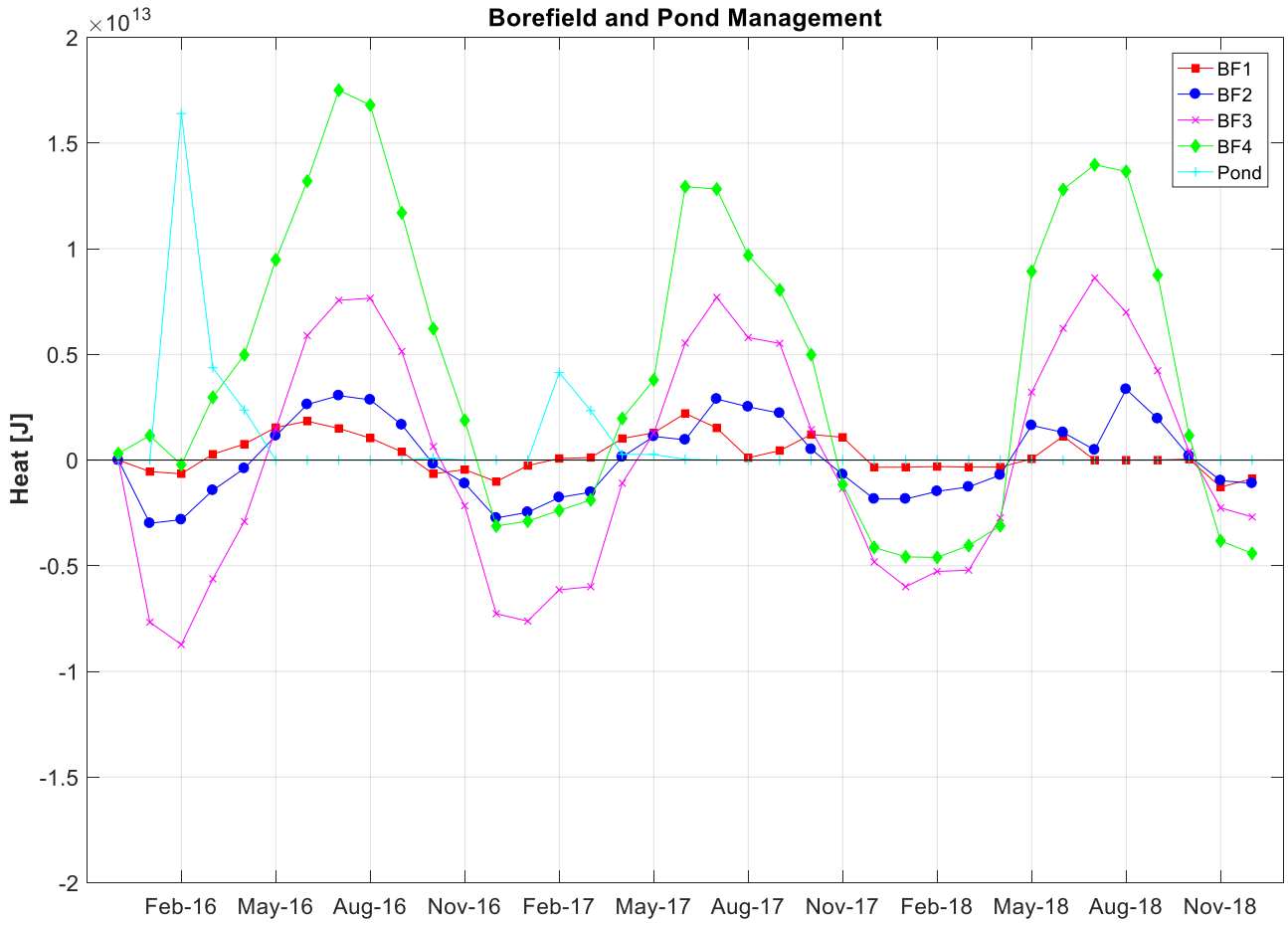

Figure 18. Heat loads carried by the four borefields and heat sink pond. Positive values designate heat placed in the system, and negative values represent heat removed from the system.

Given the known values of Q_{source} and $\Delta Q_{storage}$, $Q_{dissipated}$ was estimated using Equation 1. A summary table of the overall results can be seen in Table 2, and a plot showing the heat budget over three years is presented in Figure 19.

Table 2. Summary table of the three heat budget parameters for three years.

Year	Q_{source} [J]	$\Delta Q_{storage}$ [J]	$Q_{dissipated}$ [J]
2016	8.25E+13	5.35E+13	-2.90E+13
2017	4.18E+13	1.50E+13	-2.68E+13
2018	3.47E+13	5.56E+12	-2.91E+13
Total	1.59E+14	7.41E+13	-8.49E+13

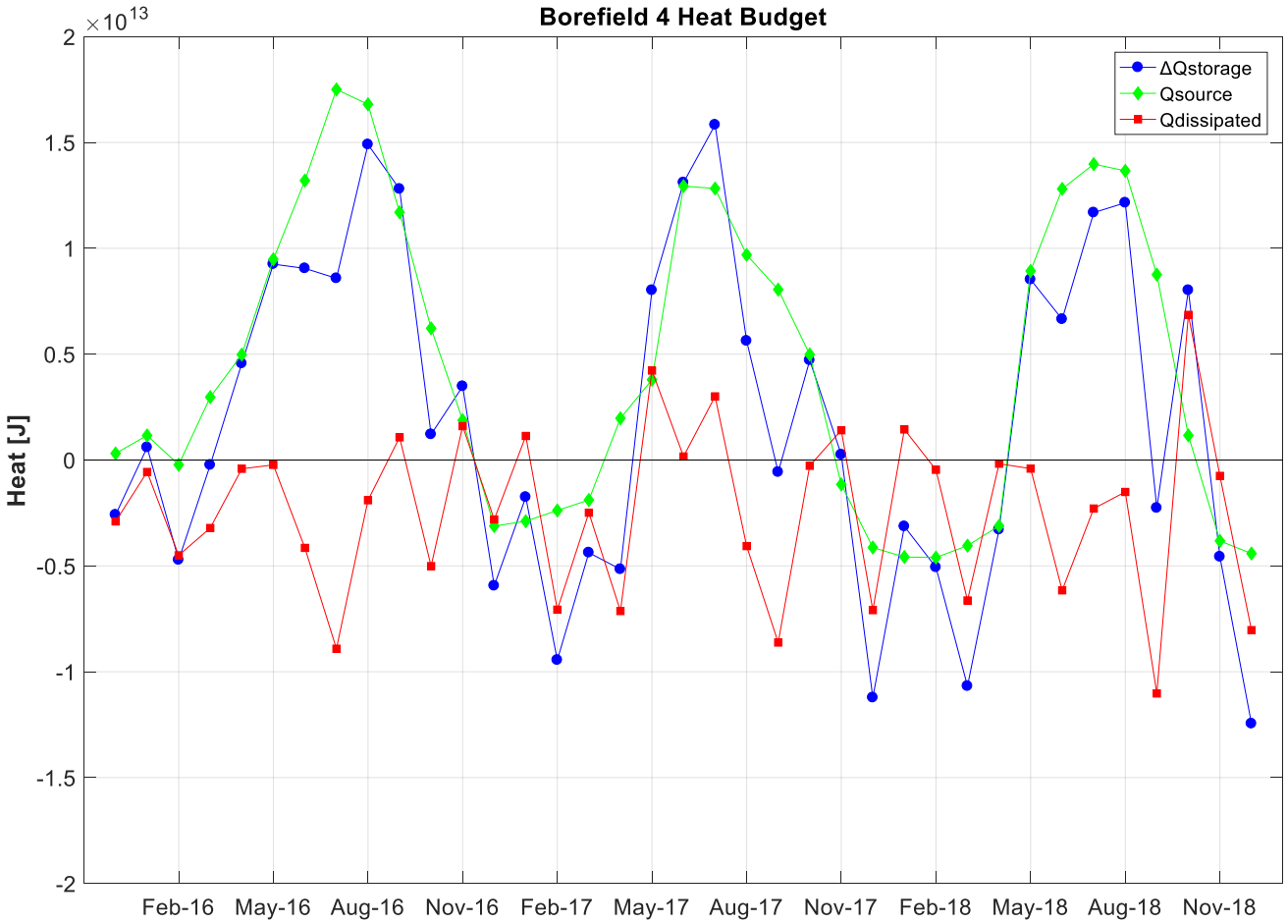

Figure 19. Heat budget in Borefield 4 over three years.

It can be seen that while a large amount of heat being stored in Borefield 4, there is a significant load of heat naturally dissipating out of the borefield. This "leaky reservoir" behavior is beneficial for Epic's imbalanced heat load, as storage values would be higher if heat was unable to escape the field naturally. A lack of storage potential in the borefield would lead to overheating of the borefield, dramatically reducing system efficiency.

A first order estimate of conductive heat flow was made to determine whether or not it was a reasonable mechanism for heat loss from Borefield 4. As seen in Figure 14, TMW-5B is nearly directly south of TMW-7B, and TMW-3B is nearly directly west of TMW-8B. Using Equation 4 presented in the previous section, the amount of heat dissipated via heat conduction was also calculated using the known thermophysical properties of Borefield 4 and the temperature data collected at TMW-7B and TMW-8B. The amount of heat flux to the north (using TMW-5B and TMW-7B) over the three year period was determined to be -2.86E+11 Joules. The amount of heat flux to the east (using TMW-3B and TMW-8B) over the three year period was determined to be -1.79E+11 Joules. As stated in the previous methodology section, these values can be used to predict the total heat flux across all six faces of the borefield, however it is an underestimation. This resulted in a total conductive heat flux of -5.58E+12 Joules. Table 2 shows that the total $Q_{dissipated}$ for the three years is -8.49E+13 Joules. That leaves a portion of the $Q_{dissipated}$ load being controlled by advective heat flow.

Given the known groundwater flow behavior at the site, it is likely that heat is escaping through advective heat transfer and traveling to the southwest out of the borefield. This activity can also be seen in the color flood figures for the piezometer temperature monitoring wells, TMW-7B and 8B (Appendix A), where temperatures just outside the borefield area to the northeast are lower than temperatures recorded within the bulk volume of the borefield. The color flood figures

also display the effects of surface temperatures on the upper 10 meters of the borefield. The significant temperature response to the surface effects can likely be used to justify the months in which $Q_{dissipated}$ is positive, meaning that heat is entering the system through the top face of Borefield 4.

3.6 Conclusion

From the results presented above, it can be seen that Borefield 4 behaves as a leaky reservoir of heat. In a district-scale borefield with the potential to overheat, highly fractured sedimentary units provide a channel for heat removal from the field. Because of Epic's cooling-dominated heat load and Wisconsin's cool climate, having a natural means of heat escape supports borefield longevity and prevents a reduction in system efficiency due to borefield overheating. This understanding of borefield behavior is useful in making better-informed operational decisions, especially on a district-scale, as there is less speculation regarding where heat travels once placed in the borefield. These improvements in district-scale geothermal systems allow for growth in the geothermal sector, and create more reliable and lower-emission alternatives to traditional energy resources.

Chapter 4.0: Life Cycle Assessment and Levelized Cost of Heat Evaluation of a Deep Direct-Use Geothermal System

4.1 Abstract

Deep direct-use (DDU) geothermal energy was assessed for its feasibility as a thermal energy source in district-scale facilities. The primary objective of this project is to investigate the feasibility of implementing a geothermal heat recovery complex in the Illinois Basin on a district-scale. The Illinois Basin is a low-temperature sedimentary basin with multiple potential sources of geothermal energy including the St. Peter Sandstone and Mt. Simon Sandstone. DDU geothermal energy systems are believed to provide lower-emission alternatives compared to traditional heating and cooling methods; however, low-temperature, high-salinity DDU heat sources are less-frequently utilized. A number of system characteristics are investigated, including heat-extraction performance, heat-deployment methods, well design alternatives, challenges of design commercialization, levelized cost of heat, and life cycle environmental impacts. The work in this paper focuses on the preliminary results obtained from a life cycle assessment to quantify the overall environmental impacts of the system. The life cycle assessment was performed using a spreadsheet tool that was simultaneously developed to provide insight into the cradle-to-grave environmental impacts associated with the proposed geothermal system, as well as other deep direct-use systems with similar objectives. This tool allows for a more in-depth analysis of the feasibility of DDU systems with respect to the overall environmental impacts of the system.

4.2 Introduction

The Department of Energy (DOE) has targeted the feasibility of widespread utilization of lower temperature geothermal resources that are shallower than conventional hydrothermal sources, but deeper than geothermal heat pump and other traditional direct-use systems. These reservoirs, referred to as Deep Direct-Use (DDU) resources, are believed to bring valuable returns on geothermal investment in the near-term. Typical geothermal direct-use operations use a flow of geothermal fluid that can deliver heating and cooling potential to buildings. The DDU systems investigated in this project utilize a similar range of fluid temperatures, but on a larger scale (GTO, 2018). The overall objective of this work is to determine the feasibility of designing a district-scale geothermal heating and cooling system for a district-scale campus in the Illinois Basin utilizing DDU.

Two geologic formations in the Illinois Basin (ILB) region were determined to have potential as a geothermal energy source based on initial temperatures and flow rates of fluids. These formations are the St. Peter and Mt. Simon sandstones, where the top of those formations lie at depths of approximately 630 and 1280-m, respectively. The geothermal energy extracted from these formations within the ILB may be considered for heating and cooling of the facilities on a district-scale campus. For the assessment herein, a doublet (two-well) system is analyzed. The results from this study will also allow geothermal resources from the full footprint of the ILB to be assessed, and allow the technology to potenitally be extended to other areas with similar low-temperature sedimentary basins (Stumpf, et al., 2018).

This paper presents the preliminary results obtained from a Life Cycle Assessment (LCA) spreadsheet tool that was developed to analyze a DDU system in the ILB. The LCA spreadsheet tool provides further insight into the cradle-to-grave environmental impacts associated with the

system over the lifetime of the project, as well as other deep direct-use systems with similar objectives. This tool allows for a more in-depth analysis of the feasibility of DDU systems with respect to the overall environmental impacts of the system. Additionally, this tool allows for comparison between baseline and alternate systems to be made, which provides the user with an opportunity to further maximize system efficiency with the needs of the end-user in mind.

4.3 Background

4.3.1 Direct-Use Geothermal Energy

The direct use of geothermal energy refers to the thermal utilization of geothermal heat in residential, commercial, and industrial facilities that have a need for a reliable supply of heat. Most direct-use applications require low-to-moderate temperature geothermal fluids, between 20°C and 150°C, which are typically found at depths shallower (between 10 and 150 m) than those required for the traditional high-temperature power generation methods. Deep direct-use systems have the potential to increase the distribution of geothermal heat in areas with relatively lower heat flow that rely on traditional, high-emission sources of heat by drilling thousands of meters into the subsurface. According to data reported by the U.S. Energy Information Administration, the total thermal energy from 0 to 260°C used in 2008 was 33.5 EJ, which is approximately one-third of the entire U.S. demand. Space heating and water heating, which have end-use temperatures ranging from 40 to 60°C, are responsible for 38% of the total thermal energy demand below 260°C. Utilizing geothermal direct-use through the implementation of DDU projects would offer a relatively sustainable and low-emission alternative to the conventional heat sources supplied by fossil fuels (GTO, 2018).

The figure presented below (Figure 20) illustrates the concept of utilizing hot water from a subsurface aquifer formation and delivering that heat to a surface application. Once the heat is

used on the surface, the cooler water is returned to the aquifer through an injection well, where it is mixed with the warm water in the aquifer. The temperature of the aquifer can decrease over time due to the injection of used water through the system. The thermal drawdown rate is dependent on a number of factors, such as the size of the aquifer and the production and injection water temperatures.

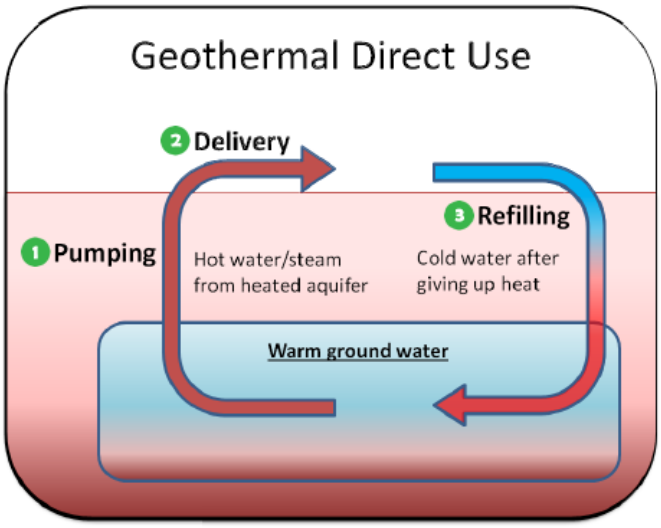

Figure 20. Schematic showing concept of deep direct-use geothermal energy from an aquifer (EPA, n.d.).

4.3.2 Life Cycle Assessments

Life Cycle Assessment (LCA) is a technique for assessing the potential environmental aspects and potential aspects associated with a product or service by compiling an inventory of relevant inputs and outputs, evaluating the potential environmental impacts associated with those inputs and outputs, and interpreting the results of the inventory and impact phases in relation to the objectives of the study (ISO, 2006). LCAs can be performed on a variety of products and services, ranging from wind farms, to recycled concrete aggregate, other geothermal systems, and everything in between.

For example, an LCA of the Glacier Hills Wind Park in south-central Wisconsin was performed in order to highlight the significant areas of energy consumption and emissions associated with wind energy development (Rajaei & Tinjum, 2013). A quantitative analysis of the life cycle emissions and environmental impact associated with wind development from construction through operation revealed that transportation of large components from overseas led to significant consumption of fossil fuels, responsible for nearly a quarter of the total greenhouse gas emissions due to transportation. Energy payback time and total equivalent grams of CO_2 per kWh of energy were also calculated over the lifetime of the wind farm. LCA methodology was also applied to a non-conventional deep insulated single-hole ground source heat pump to compare its impacts with conventional heating, ventilation, and cooling methods (Woods-Robinson, 2013). The results of the LCA show that top contributors to CO_2 equivalent emissions are heat-exchanger operation, borehole drilling, and circulation pump operation. The sustainability of construction with recycled materials was also evaluated using life cycle assessment methodology (Lee, 2010). This work involved developing a rating system called the Building Environmentally and

Economically Sustainable Transportation-Infrastructure-Highways (BE^2ST-in-Highways^{TM}). This system compares the environmental and economic life cycle impacts between different construction material methods. Furthermore, this paper developed an Amoeba diagram to compare the impacts between various construction material alternatives and how they reach certain sustainability goals. A similar concept was applied in this LCA methodology for the DDU system in the ILB, which is herein referred to as a spider diagram.

4.4 Methods and Materials

4.4.1 Field Site

The geology on site was characterized by using data obtained from drilling records and petrophysical analysis of core samples. The bedrock surface is masked by Pleistocene glacial sediments, ranging from less than 40-m to more than 120-m thick. Cambrian through Pennsylvanian aged sedimentary rocks are below, with an approximate thickness between 1525-m and 1830-m. Precambrian metamorphic and igneous rocks underlie the sedimentary units (Stumpf, et al., 2018). A detailed table of the stratigraphy on site can be found in Appendix D. The St. Peter Sandstone is found at depths of 618 to 677-m within the 90 km^2 assessment area, and the Mt. Simon Sandstone is found at depths of 1329 to 2031-m within the assessment area. Based on bottomhole temperatures from well logs, formation water temperature of the St. Peter Sandstone ranged between 23.1 to 25.9°C, and temperatures in the Mt. Simon ranged from 36.9 to 49.8°C (Stumpf, et al., 2018).

4.4.2 DDU System Design

The system will be comprised of both subsurface and surface components. The subsurface components include two wells, an extraction and injection well, and downhole pumps. The surface equipment includes possible heat pumps and exchangers, as well as fluid transport and monitoring systems. A concept diagram of the proposed DDU system can be seen in Figure 21.

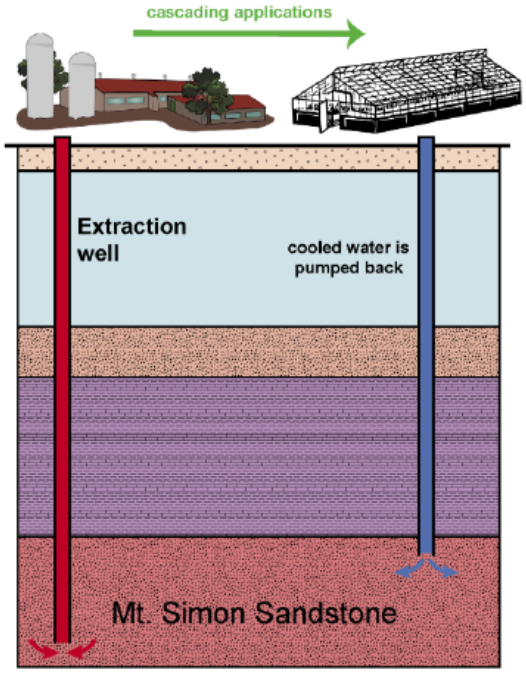

Figure 21. Conceptual diagram of a proposed DDU system (Stumpf, et al., 2018).

A schematic of a typical DDU well design can be found in Figure 22. Both wells would be drilled to reach the Mt. Simon Sandstone, with the production well drilled to a total depth of 1981-m (6500 ft.), and the injection well drilled to a total depth of 1676-m (5500 ft.). The production zone perforations are proposed between 1860 and 1905-m (6100 to 6250 ft.) and the injection zone ranges from 1555 to 1615-m (5100 to 5300 ft.). The production well is comprised of three casings – a surface casing, an intermediate casing, and a long string casing. The injection well design varies slightly and is comprised of a surface, intermediate, and production casing. A more detailed breakdown of the individual well components and parts can be found in the following sections.

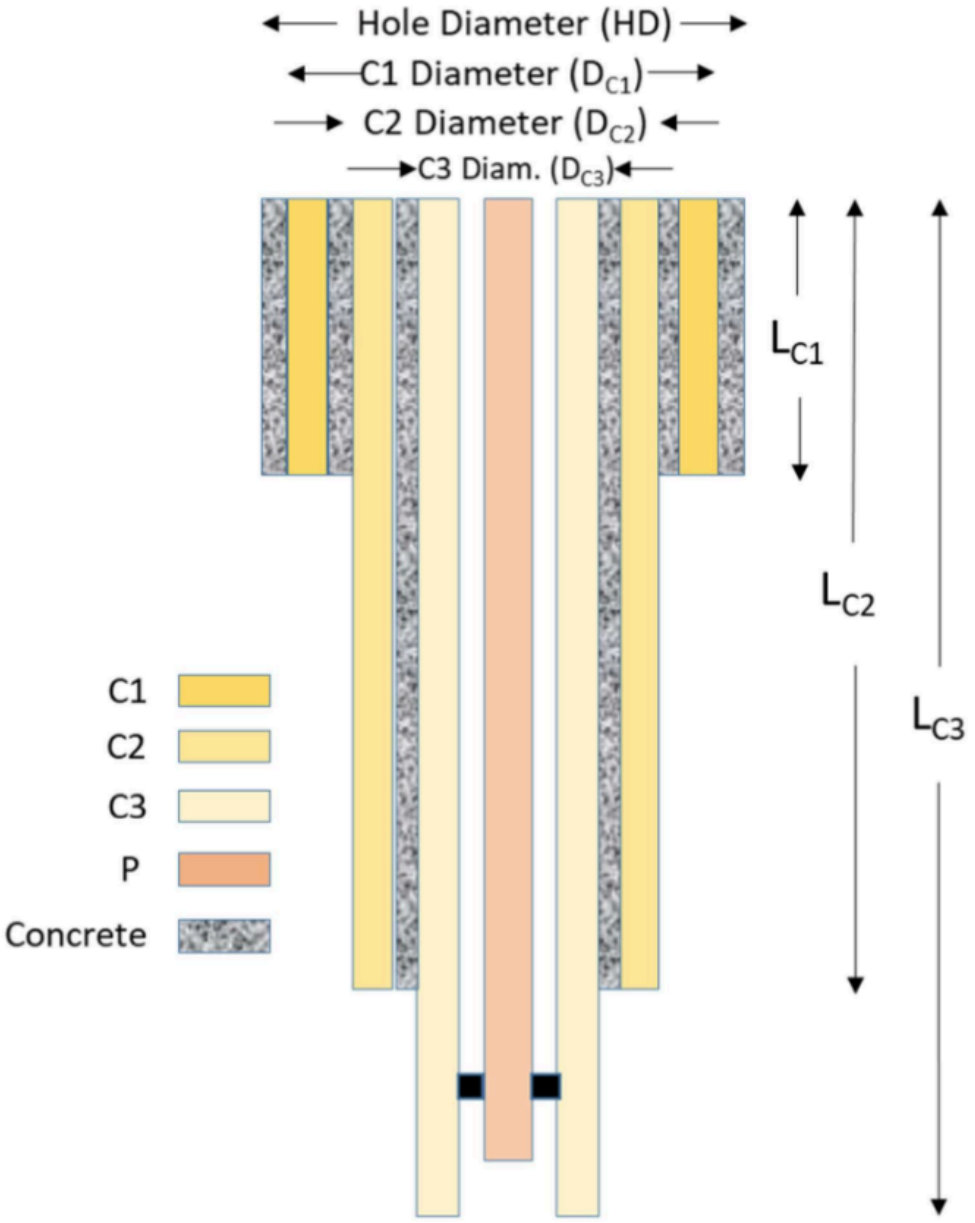

Figure 22. Typical well design for a DDU system .

The production and injection wells would be located approximately 150 m away from the main building on site. High-density polyethylene (HDPE) pipes will be laid underground to transport the heated supply water to the facilities, and a return line will be placed to discharge the cooler water away from the facilities.

4.4.3 Methodology

A Life Cycle Assessment was performed to assess the environmental impacts associated with the project, including raw material extraction, materials processing, manufacture, distribution, use, disposal, and recycling. The goal of this assessment is to quantify the environmental impacts of the project in order to provide information to assist in evaluating design alternatives. The framework of this LCA is based on four life cycle stages: (1) material production, (2) material transport and construction, (3) use of system, and (4) end of life. The material production stage involves the acquisition of raw materials and manufacturing of materials. Material transport and construction includes a number of parameters including the distance to the project site, the methods used to transport materials, the installation of the production and injection wells, as well as the installation of certain surface components (e.g., heat exchangers, generators, pumps, and pipelines). The use of system stage involves the use of electricity, heat transfer to and from the subsurface, operation of a chiller, as well as other operation and maintenance activities. Finally, the end of life stage is focused on deconstruction and sealing of the production and injection wells, well sealing, waste, and transportation of waste. Figure 23 shows a schematic of the four life cycle stages.

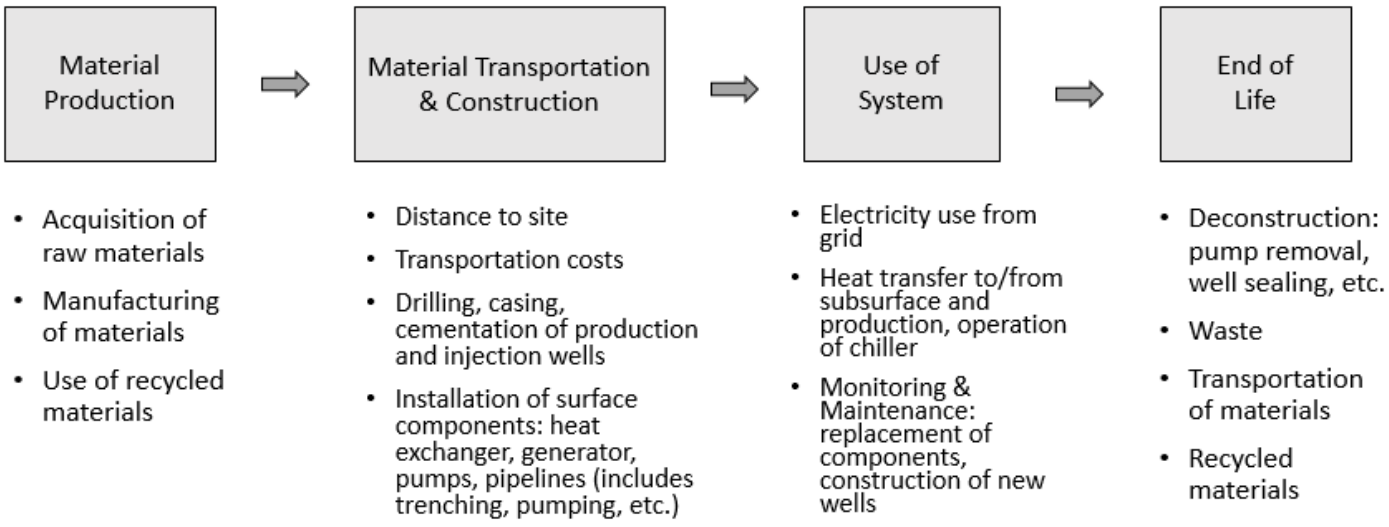

Figure 23. Schematic summarizing the four life cycle stages for a geothermal system.

Within the four stages of the life cycle, the goal, scope, and system boundary of the life cycle assessment was structured to focus on the materials and processes that have the largest environmental impacts. Because typical LCAs of geothermal systems identify the material acquisition and installation of the wells as the top contributor to the environmental impacts of the system, the components of the production and injection wells were investigated in great detail (Tomasini-Montenegro, 2017). An inventory flow diagram showing a breakdown of the scope of the construction and use of the geothermal system is conveyed in Figure 24.

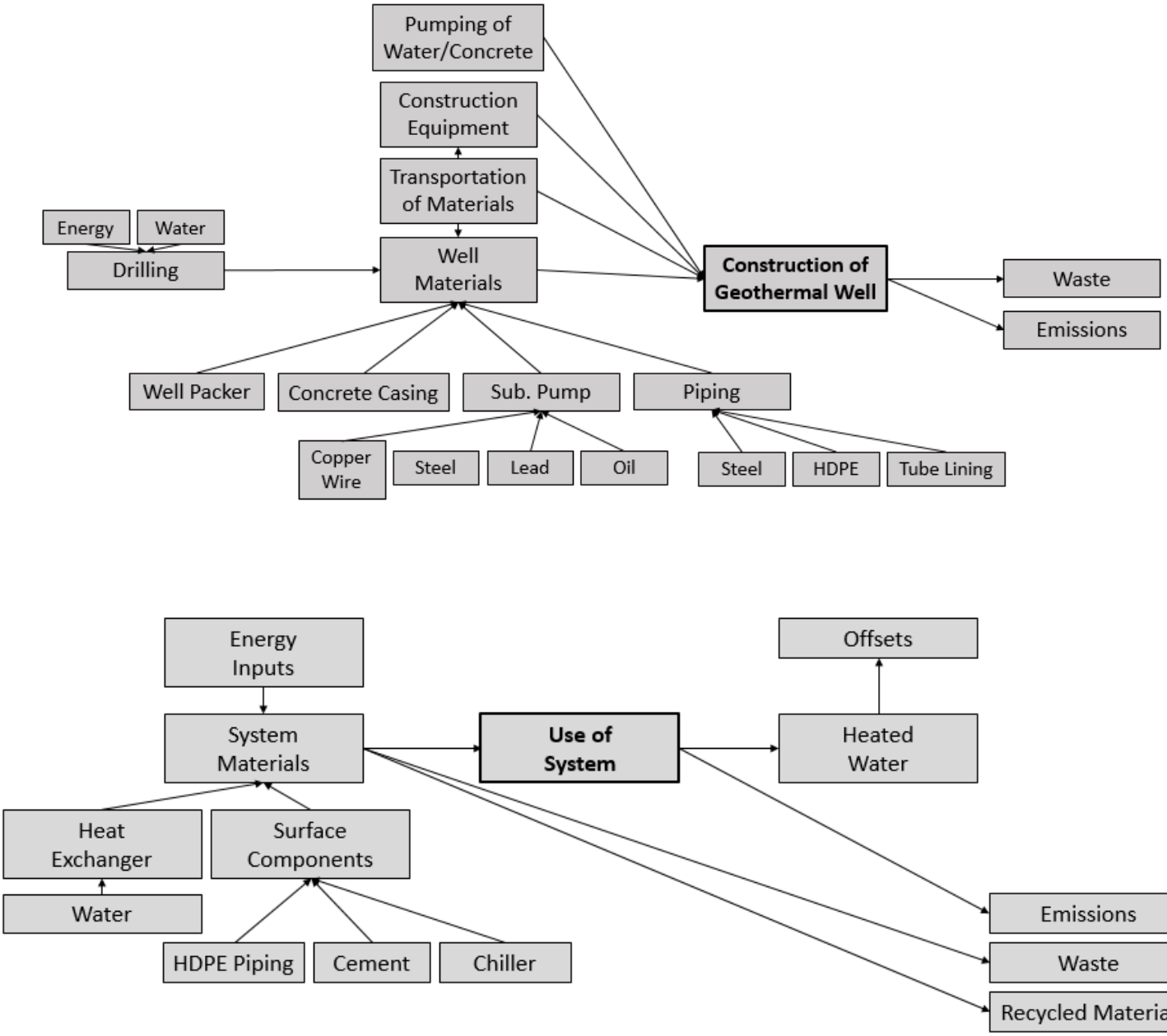

Figure 24. Schematic representing the scope of the life cycle assessment, including the components that comprise the well design and operation of system.

The inventory of impacts for the LCA spreadsheet tool was collected using SimaPro version 8.5.2 and the TRACI version 2.1 Impact Assessment Methodology. SimaPro is a commercial life cycle assessment tool used to collect, analyze, and monitor the sustainability performance of a product or service. It measures the environmental impact of products across all life cycle stages, from raw material extraction, to manufacturing, distribution, use, and disposal (SimaPro, n.d.). Using the scope diagrams in Figure 24 above, an inventory of individual component impacts were gathered within SimaPro. Several assumptions were made regarding components of parts, a summary table of these assumptions can be found in Appendix D.

The impact categories that are evaluated within this LCA tool are ozone depletion, global warming potential, smog, acidification, eutrophication, and fossil fuel depletion, which are all of the relevant impact categories available within the SimaPro software. Ozone depletion measures the levels of chlorofluorocarbons (CFCs), which are ozone depleting substances. High concentrations of CFCs lead to more harmful UV radiation reaching the earth's surface and has negative human health risks as well as poses threats to terrestrial and aquatic ecosystems (Solomon, 1999). Global warming potential is a measure of carbon dioxide (CO_2) levels in the atmosphere, which absorbs sunlight and solar radiation, leading to elevated global temperatures (Eckaus, 1992). Smog is a measure of O_3, a reaction product of NO_x and VOCs in the atmosphere, which has associated human health risks and reductions in air quality. Acidification relates to SO_2 concentrations, which is an acidifying compound with potential groundwater and surface water impacts, including threats to soil and aquatic organisms. Eutrophication quantifies levels of nitrogen, which is a limiting nutrient. Eutrophication causes dense growth of plant life and death of animal life in aquatic bodies due to a lack of oxygen. This issue is particularly important in areas with significant agriculture markets, as fertilizer collects in surface water runoff and deposits

nitrogen in surrounding lakes, rivers, and streams (Harris, et al., 2017). Lastly, fossil fuel depletion is measured in terms of MJ surplus, which is defined as the total additional future cost to the global society due to the production of one unit of resource. It is related to future global production, specifically resource extraction cost and recycling rate (Ponsioen, 2013). These impact categories are meant to guide a user in evaluation of the overall environmental impacts of a product or service. Because consumptive water of the materials was not an available impact category within SimaPro, embodied water was estimated through an external calculation using values from literature. This analysis can be found in the following results section.

The unit lifecycle impact for the proposed DDU system were compiled for each of the six impact categories were compiled. Each individual impact was gathered from the SimaPro database as a singular unit quantity so that the user of the spreadsheet can adjust the value of the material to fit the specific design being analyzed. The only inventory item not obtained from the SimaPro database was the electricity source, as information from a local electricity provider was used instead. In this location in 2017, it was reported that 49% of the overall electricity was sourced from coal-fired power (ICC, 2017). Using this information, the carbon dioxide emissions for 1 kWh of electricity were estimated and used for this LCA. A table showing the unit impacts for the proposed geothermal system within the ILB can be found in Tables 4 and 5 below.

Table 4. Inventory table showing the unit impacts of the material production phase of the system, with the impact values gathered from SimaPro.

Lifecycle Stage, Components & Processes		Impact Categories					
Material Production		Impact Inventory					
Injection Well (IW)	**SimaPro Process and Unit**	**Total kg CFC eq**	**Total kg CO_2 eq**	**Total kg O_3 eq**	**Total kg SO_2 eq**	**Total kg N eq**	**Total MJ surplus**
Casing 1 (surface)	1 kg Steel, unalloyed {RoW}| steel production, converter, unalloyed | Alloc Def, U	9.76E-08	1.82E+00	8.99E-02	7.36E-03	6.23E-03	7.45E-01
Casing 2 (int.)	1 kg Steel, unalloyed {RoW}| steel production, converter, unalloyed | Alloc Def, U	9.76E-08	1.82E+00	8.99E-02	7.36E-03	6.23E-03	7.45E-01
Casing 3 (prod.)	1 kg Steel, unalloyed {RoW}| steel production, converter, unalloyed | Alloc Def, U	9.76E-08	1.82E+00	8.99E-02	7.36E-03	6.23E-03	7.45E-01
Concrete 1 (surface)	1 m^3 Concrete, normal {RoW}| market for | Alloc Def, U	1.85E-05	2.24E+02	1.38E+01	7.22E-01	2.68E-01	1.69E+02
Concrete 2 (int.)	1 m^3 Concrete, normal {RoW}| market for | Alloc Def, U	1.85E-05	2.24E+02	1.38E+01	7.22E-01	2.68E-01	1.69E+02
Concrete 3 (prod.)	1 m^3 Concrete, normal {RoW}| market for | Alloc Def, U	1.85E-05	2.24E+02	1.38E+01	7.22E-01	2.68E-01	1.69E+02
Tubing	1 kg Steel, unalloyed {RoW}| steel production, converter, unalloyed | Alloc Def, U	9.76E-08	1.82E+00	8.99E-02	7.36E-03	6.23E-03	7.45E-01
Tube lining	1 kg Tetrafluoroethylene {GLO}| market for | Alloc Def, U	9.42E-03	3.23E+02	6.41E-01	1.03E-01	4.66E-02	1.77E+01
Injection packer insulation	1 kg Polymer foaming {RoW}| processing | Alloc Def, U	4.73E-08	9.51E-01	6.90E-02	5.43E-03	3.27E-03	5.01E-01
Drilling (prod. of fuel)	1 kg Diesel, low-sulfur {RoW}| production	9.20E-07	5.76E-01	4.60E-02	5.53E-03	1.83E-03	8.15E+00
Drilling (water)	1 kg Tap water {RoW}| tap water production, underground water without treatment	1.96E-11	3.07E-04	1.58E-05	1.55E-06	1.28E-06	2.04E-04
Production Well (PW)	**SimaPro Process and Unit**	**Total kg CFC eq**	**Total kg CO_2 eq**	**Total kg O_3 eq**	**Total kg SO_2 eq**	**Total kg N eq**	**Total MJ surplus**
Casing 1 (surface)	1 kg Steel, unalloyed {RoW}| steel production, converter, unalloyed | Alloc Def, U	9.76E-08	1.82E+00	8.99E-02	7.36E-03	6.23E-03	7.45E-01
Casing 2 (int.)	1 kg Steel, unalloyed {RoW}| steel production, converter, unalloyed | Alloc Def, U	9.76E-08	1.82E+00	8.99E-02	7.36E-03	6.23E-03	7.45E-01
Casing 3 (long string)	1 kg Steel, unalloyed {RoW}| steel production, converter, unalloyed | Alloc Def, U	9.76E-08	1.82E+00	8.99E-02	7.36E-03	6.23E-03	7.45E-01
Concrete 1 (surface)	1 m^3 Concrete, normal {RoW}| market for | Alloc Def, U	1.85E-05	2.24E+02	1.38E+01	7.22E-01	2.68E-01	1.69E+02
Concrete 2 (int.)	1 m^3 Concrete, normal {RoW}| market for | Alloc Def, U	1.85E-05	2.24E+02	1.38E+01	7.22E-01	2.68E-01	1.69E+02
Concrete 3 (long string)	1 m^3 Concrete, normal {RoW}| market for | Alloc Def, U	1.85E-05	2.24E+02	1.38E+01	7.22E-01	2.68E-01	1.69E+02
Tubing	1 kg Steel, unalloyed {RoW}| steel production, converter, unalloyed | Alloc Def, U	9.76E-08	1.82E+00	8.99E-02	7.36E-03	6.23E-03	7.45E-01
Tube lining	1 kg Tetrafluoroethylene {GLO}| market for | Alloc Def, U	9.42E-03	3.23E+02	6.41E-01	1.03E-01	4.66E-02	1.77E+01
Production packer insulation	Polymer foaming {RoW}| processing | Alloc Def, U	4.73E-08	9.51E-01	6.90E-02	5.43E-03	3.27E-03	5.01E-01
Drilling (prod. of fuel)	1 kg Diesel, low-sulfur {RoW}| production	9.20E-07	5.76E-01	4.60E-02	5.53E-03	1.83E-03	8.15E+00
Drilling (water)	1 kg Tap water {RoW}| tap water production, underground water without treatment	1.96E-11	3.07E-04	1.58E-05	1.55E-06	1.28E-06	2.04E-04
Submersible Pump	**SimaPro Process and Unit**	**Total kg CFC eq**	**Total kg CO_2 eq**	**Total kg O_3 eq**	**Total kg SO_2 eq**	**Total kg N eq**	**Total MJ surplus**
Copper wire	1 kg Copper wire, technology mix, consumption mix, at plant, cross section 1 mm^2 EU-15 S	1.11E-07	7.89E-01	3.89E-02	3.60E-03	2.41E-04	7.48E-01
Steel	1 kg Steel, low-alloyed {GLO}| market for	1.12E-07	1.64E+00	1.02E-01	8.08E-03	1.23E-02	1.04E+00
Lead	1 kg Lead {GLO}| market for | Alloc Def, U	1.27E-07	1.36E+00	1.38E-01	1.90E-02	1.30E-02	1.40E+00
Lubricant oil	1 kg Lubricating oil {RER}| production | Alloc Def, U	1.26E-06	1.00E+00	6.98E-02	8.27E-03	4.09E-03	1.11E+01
Chiller	**SimaPro Process and Unit**	**Total kg CFC eq**	**Total kg CO_2 eq**	**Total kg O_3 eq**	**Total kg SO_2 eq**	**Total kg N eq**	**Total MJ surplus**
Refrigerant	1 kg Refrigerant R134a {RoW}| production | Alloc Def, U	1.04E-02	1.03E+02	7.87E-01	8.98E-02	2.44E-02	1.53E+01
Steel	1 kg Steel, low-alloyed {GLO}| market for	1.12E-07	1.64E+00	1.02E-01	8.08E-03	1.23E-02	1.04E+00
Aluminum							
Copper	1 kg Copper wire, technology mix, consumption mix, at plant, cross section 1 mm^2 EU-15 S	1.11E-07	7.89E-01	3.89E-02	3.60E-03	2.41E-04	7.48E-01
Surface Components	**SimaPro Process and Unit**	**Total kg CFC eq**	**Total kg CO_2 eq**	**Total kg O_3 eq**	**Total kg SO_2 eq**	**Total kg N eq**	**Total MJ surplus**
Heat Exchanger	1 kg Steel, unalloyed {RoW}| steel production, converter, unalloyed | Alloc Def, U	9.76E-08	1.82E+00	8.99E-02	7.36E-03	6.23E-03	7.45E-01
HDPE	1 kg HDPE pipes E	0.00E+00	2.48E+00	1.12E-01	9.46E-03	2.16E-04	1.11E+01

Table 5. Inventory table showing the unit impacts of the construction, use of system, and end of life phases of the system, with impact values gathered from SimaPro. Electricity use impacts were calculated using information external from SimaPro.

Material Transport & Construction							
Transportation of Materials	**SimaPro Process and Unit**	**Total kg CFC eq**	**Total kg CO_2 eq**	**Total kg O_3 eq**	**Total kg SO_2 eq**	**Total kg N eq**	**Total MJ surplus**
Transport of concrete	1 tkm Transport, freight, lorry >32 metric ton, EURO5 {GLO}| market for | Alloc Def, U	2.30E-08	9.13E-02	7.14E-03	3.43E-04	9.74E-05	2.04E-01
Transport of steel	1 tkm Transport, freight, lorry >32 metric ton, EURO5 {GLO}| market for | Alloc Def, U	2.30E-08	9.13E-02	7.14E-03	3.43E-04	9.74E-05	2.04E-01
Transport of construction equip.	1 tkm Transport, freight, lorry >32 metric ton, EURO5 {GLO}| market for | Alloc Def, U	2.30E-08	9.13E-02	7.14E-03	3.43E-04	9.74E-05	2.04E-01
Construction of Wells	**SimaPro Process and Unit**	**Total kg CFC eq**	**Total kg CO_2 eq**	**Total kg O_3 eq**	**Total kg SO_2 eq**	**Total kg N eq**	**Total MJ surplus**
Drilling IW (comb. of fuel)	1 m Deep well, drilled, for geothermal power {RoW}| deep well drilling, for deep geothermal power | Alloc Def, U	2.51E-04	3.92E+03	2.04E+02	1.89E+01	1.67E+01	2.67E+03
Pumping cement IW (comb. of fuel)	1 hr Machine operation, diesel, < 18.64 kW, generators {GLO}| machine operation, diesel, < 18.64 kW, generators | Alloc Def, U	1.06E-06	4.37E+00	7.25E-01	2.57E-02	4.13E-03	9.35E+00
Pumping water IW (comb. of fuel)	1 hr Machine operation, diesel, < 18.64 kW, generators {GLO}| machine operation, diesel, < 18.64 kW, generators | Alloc Def, U	1.06E-06	4.37E+00	7.25E-01	2.57E-02	4.13E-03	9.35E+00
Drilling PW (comb. of fuel)	1 m Deep well, drilled, for geothermal power {RoW}| deep well drilling, for deep geothermal power | Alloc Def, U	2.51E-04	3.92E+03	2.04E+02	1.89E+01	1.67E+01	2.67E+03
Pumping cement PW (comb. of fuel)	1 hr Machine operation, diesel, < 18.64 kW, generators {GLO}| machine operation, diesel, < 18.64 kW, generators | Alloc Def, U	1.06E-06	4.37E+00	7.25E-01	2.57E-02	4.13E-03	9.35E+00
Pumping water PW (comb. of fuel)	1 hr Machine operation, diesel, < 18.64 kW, generators {GLO}| machine operation, diesel, < 18.64 kW, generators | Alloc Def, U	1.06E-06	4.37E+00	7.25E-01	2.57E-02	4.13E-03	9.35E+00
Trenching	**SimaPro Process and Unit**	**Total kg CFC eq**	**Total kg CO_2 eq**	**Total kg O_3 eq**	**Total kg SO_2 eq**	**Total kg N eq**	**Total MJ surplus**
Excavating	1 hr Excavator, technology mix, 100 kW, Construction GLO	4.39E-12	2.00E-03	2.00E-04	9.49E-06	5.40E-07	4.02E-03
Use of System							
Operation of Wells	**SimaPro Process and Unit**	**Total kg CFC eq**	**Total kg CO_2 eq**	**Total kg O_3 eq**	**Total kg SO_2 eq**	**Total kg N eq**	**Total MJ surplus**
Electricity for pumps	1 kWh from Ameren		6.23E-01				
Operation of chiller	1 kWh from Ameren		6.23E-01				
Operation of heat exchanger	1 kWh from Ameren		6.23E-01				
Maintenance	Maintenance, heat and power co-generation unit, 160kW electrical {GLO}| market for | Alloc Def, U	2.69E-03	3.98E+03	2.07E+03	2.28E+02	1.33E+02	2.22E+04
End of Life							
Deconstruction	**SimaPro Process and Unit**	**Total kg CFC eq**	**Total kg CO_2 eq**	**Total kg O_3 eq**	**Total kg SO_2 eq**	**Total kg N eq**	**Total MJ surplus**
Pump removal	1 hr Machine operation, diesel, < 18.64 kW, generators {GLO}| machine operation, diesel, < 18.64 kW, generators | Alloc Def, U	1.06E-06	4.37E+00	7.25E-01	2.57E-02	4.13E-03	9.35E+00
Surface equip. removal	1 hr Machine operation, diesel, < 18.64 kW, generators {GLO}| machine operation, diesel, < 18.64 kW, generators | Alloc Def, U	1.06E-06	4.37E+00	7.25E-01	2.57E-02	4.13E-03	9.35E+00
Sealing IW	1 m^3 Concrete, sole plate and foundation {RoW}| concrete production, for civil engineering, with cement CEM I | Alloc Def, U	1.80E-05	3.55E+02	1.63E+01	9.15E-01	3.66E-01	1.68E+02
Sealing PW	1 m^3 Concrete, sole plate and foundation {RoW}| concrete production, for civil engineering, with cement CEM I | Alloc Def, U	1.80E-05	3.55E+02	1.63E+01	9.15E-01	3.66E-01	1.68E+02
Waste	1 kg _48 Recycling of concrete, asphalt and other mineral products, DK	0.00E+00	4.81E-03	2.37E-04	2.54E-05	7.42E-07	7.98E-03
Transport of waste	1 tkm Transport, freight, lorry 3.5-7.5 metric ton, EURO3 {RoW}| transport, freight, lorry 3.5-7.5 metric ton, EURO3	1.20E-07	5.22E-01	7.55E-02	3.01E-03	7.20E-04	1.08E+00

To compare the potential DDU system in the ILB with an existing system that also produces thermal energy, a spider diagram template was created. This diagram allows the user to compare two systems based on five categories: annual energy use, global warming potential, water consumption, waste production, and annual heat production. These categories were chosen to allow the user to investigate common impact categories of interest that are not as heavily emphasized by the SimaPro analysis. The user can also weight the importance of performance improvement for each of the five categories using a point system. In the case of a proposed DDU system in the ILB, the system was compared against the current usage on a similar campus.

4.5 Results and Discussion

Using the inventory of unit impacts shown in Tables 4 and 5 of the previous section, the life cycle impacts of the proposed system were calculated. Overall, one of the components of the project with a significantly large impact is the material production of the two wells, specifically with regard to the use of steel and concrete. These impacts could change noticeably depending on the selected inventory from the SimaPro database, and should be adjusted if more information about the raw material sourcing is known for the specific project. A table showing the overall lifecycle totals for each impact category is below in Table 6.

Table 6. Impact totals for each lifecycle stage as well as total lifecycle impacts of the project.

Stages	Total kg CFC eq	Total kg CO_2 eq	Total kg O_3 eq	Total kg SO_2 eq	Total kg N eq	Total MJ surplus
Material Production	1.25E+01	1.32E+06	6.28E+04	5.12E+03	4.02E+03	1.16E+06
Material Transport/Cons.	2.46E-01	3.78E+06	1.98E+05	1.82E+04	1.60E+04	2.60E+06
Operation	0.00E+00	5.41E+06	0.00E+00	0.00E+00	0.00E+00	0.00E+00
End of Life	3.36E-03	6.53E+04	3.03E+03	1.69E+02	6.74E+01	3.13E+04
TOTAL	1.28E+01	1.06E+07	2.64E+05	2.35E+04	2.01E+04	3.79E+06

As seen in Table 6, operation of the system contributes the most to Global Warming Potential (kg CO_2 eq.) of the four lifecycle phases. This is also seen in Figure 25, where the four lifecycle stages are compared. The high emissions associated with operation are attributed to the electricity used to run the pumps, heat exchangers, etc. Altering the design to implement instrumentation with lower electricity use would assist in decreasing the GWP associated with operating the system.

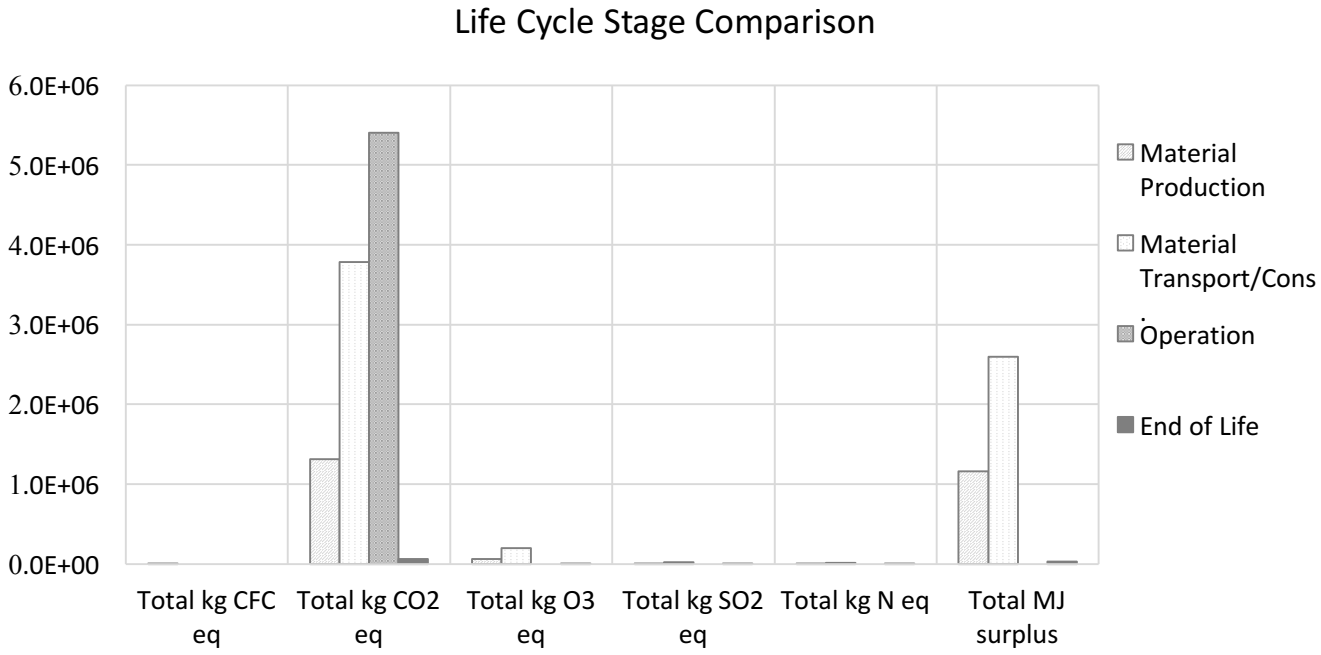

Figure 25. Impact comparison of the four lifecycle stages.

The figure above also shows the high impacts associated with the material production and material transport and construction phases. Specifically, the GWP and fossil fuel depletion impacts. When investigating those impacts further, it is seen that concrete and steel are the top contributors to these impacts. Figure 26 shows the significant CO_2 emissions associated with the use of steel, totaling to an order or magnitude higher than the other materials. The use of diesel, primarily during the material transport and construction phase of the project, is the primary contributor to the fossil fuel depletion associated with the project.

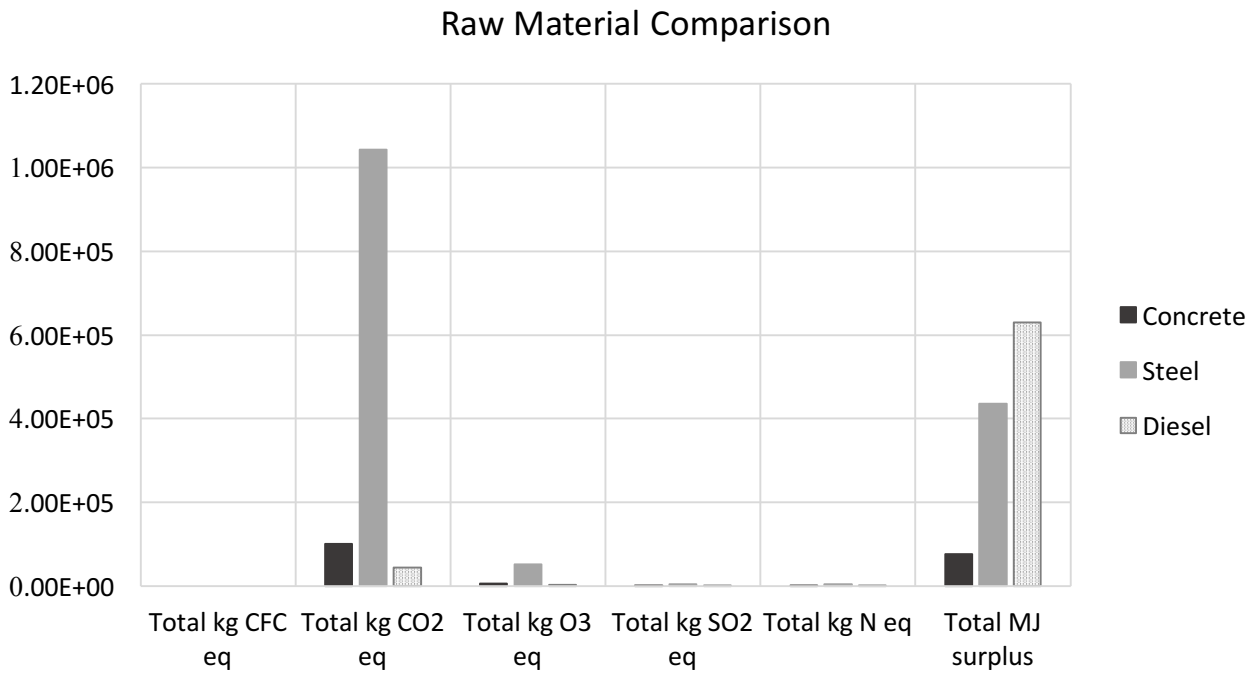

Figure 26. Impacts associated with the use of concrete, steel, and diesel for a DDU project. These three materials comprise the top contributors to the overall environmental impacts of the project.

There are a number of reasons for the high impacts associated with the use of steel. First, the depth of the production and injection wells requires a significant amount of steel for the well casings, with the deepest casing reaching a depth of 1,981-m (6,500 ft.). This is likely the explanation for why the steel impacts are higher than the concrete impacts. In many life cycle assessments of geothermal systems, concrete is commonly the top contributor to the overall GWP

of the system. This is due to the fact that concrete has an embodied energy of 12.5 MJ kg^{-1}, whereas steel has 10.5 MJ kg^{-1} (Hsu, 2010). Because of the depth of the wells associated with a deep direct-use system in the ILB, the amount of steel is higher than that of a typical geothermal system. This can also been seen when looking at the impacts from the production and injection wells (Figure 27), where the GWP of the production well is higher than that of the injection well, because it is about 300 m (1000 feet) deeper.

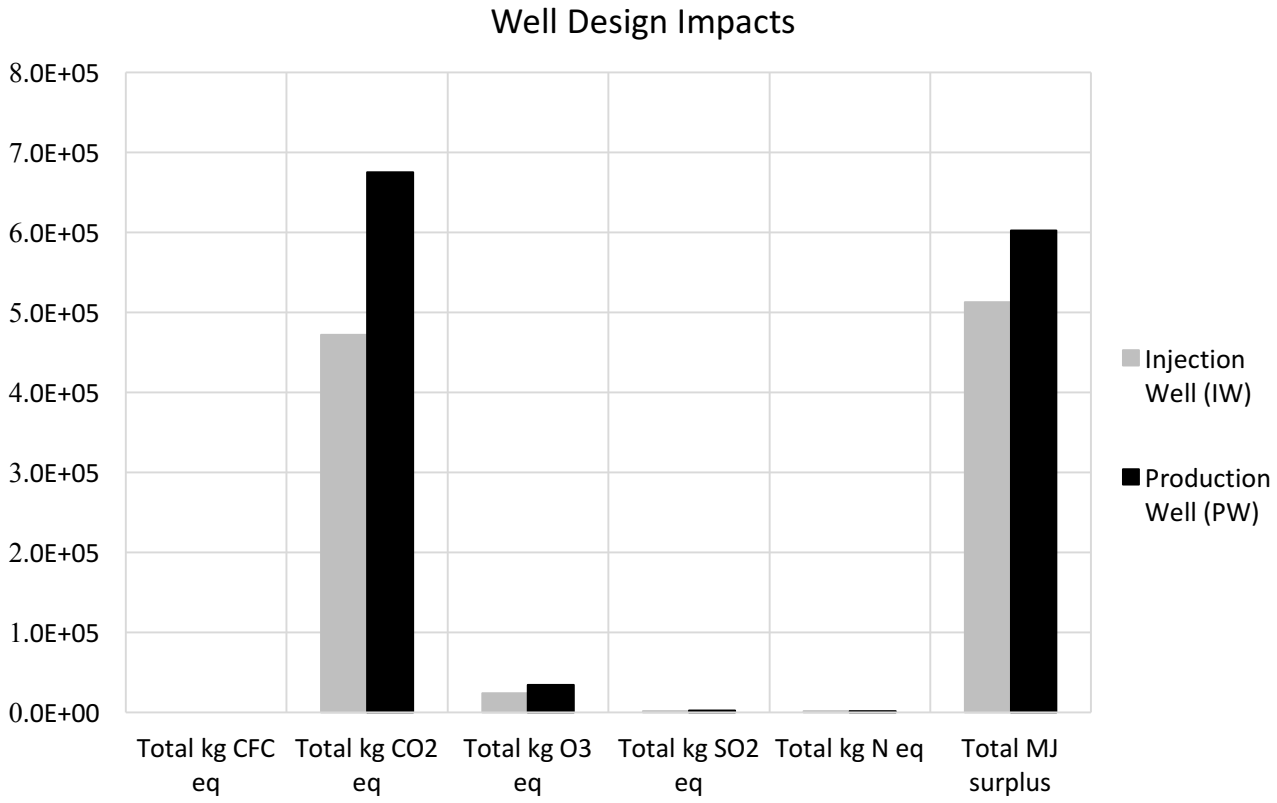

Figure 27. Comparison of the impacts associated with production and injection wells designed for a potential system in the ILB.

The embodied water of concrete and steel was also calculated using available information in literature. The blue water footprint of unalloyed steel is approximately 7.6 L/kg of steel (Bosman, 2016). This resulted in a total embodied water value of 8,605,044 L of water from the use of unalloyed steel for a DDU system. The embodied water within concrete was estimated using a blue water footprint of 987 L/ton of concrete (Netz & Sundin, 2015). This resulted in a total embodied water value of 1,061,798 L of water from the use of concrete for the DDU system. This consumptive water estimate reveals a sizable water footprint associated with the construction of the DDU system; however, the use of water during operation of the system is relatively small, as the cooler water is returned to the Mt. Simon after use. This is uncommon for most energy sources, where the typical trend is to see a significant consumptive water footprint associated with the operation of the system compared to the construction of the system (Mekonnen, 2015).

While there are significant CO_2 emissions associated with a DDU system, it still has the potential to offset the environmental impacts associated with common alternative heat options. Using available emissions data for propane and natural gas, the carbon dioxide emissions associated with heating facilities of similar size were calculated (EIA, 2016). This information is presented in Table 7.

Table 7. Emissions associated with existing heating operations using standard fuel sources.

Facility Emissions	
Annual NG Use (MMBtu/yr)	5638
Emissions from NG (kg CO2/MMBtu)	53.07
Annual Propane Use (MMBtu/yr)	3814
Emissions from Propane (kg CO2/MMBtu)	63.07
Existing Emissions (kg CO2/yr)	5.40E+05
Years until DDU emissions offset	10.02

Table 7 shows that the annual emissions associated with the heating of multiple buildings with propane and natural gas to be 539,758 kg CO_2 per year. If these facilities were instead heated through the use of the proposed deep direct-use system, the emissions associated with the use of traditional fuels could be offset in approximately 10 years of operation.

A DDU system in the ILB can also be compared to the operations of a steam power plant. Using available data collected from a typical power plant, the heat production and associated emissions were calculated. This information is presented in Tables 8 and 9.

Table 8. Heat production data at a typical steam power plant.

Power Plant Production	
Hourly Steam Production (lb/hr)	8.00E+05
Annual Steam Production (lb/yr)	7.01E+09
% Steam Used	0.60
Heat in 1 lb of 100 C Steam (Btu/lb)	1112
Hourly Heat Production (MMBtu/hr)	8.90E+02
Daily Heat Production (MMBtu/day)	2.14E+04
Annual Heat Production (MMBtu/yr)	7.79E+06

Table 9. Calculated CO_2 emissions associated with the use of steam.

Power Plant Emissions	
Co-generated steam emissions, 2016 (kg CO_2)	112714860
Annual Steam Production at capacity (lb/yr)	4.20E+09
Emissions from Steam (kg CO_2/lb)	0.0268

As stated in Table 9, approximately 0.0268 kg of CO_2 are emitted per pound of steam used, assuming conservatively that only half of the total steam produced is used for energy (Lowe, 2011). With this information, it is possible to compare the emissions associated with the power plant to the emissions associated with the a DDU alternative. The CO_2 emissions related to operation of a DDU system total to 5.41E+06 kg CO_2 equivalent. As a result, it will take an estimated 24 years for the DDU emissions to offset the emissions of the power plant alternative. Table 10 summarizes this information below.

Table 10. CO_2 emissions offset by a DDU system in the ILB to replace an existing power plant.

Facility Steam Usage & DDU Offsets	
Annual Steam Usage (lb/yr)	8500000
Annual CO_2 emissions offset by DDU (kg)	2.28E+05
Years until DDU emissions offset	23.7

Performance of a potential DDU system in the ILB was also compared to the current impacts of an existing facility using a Spider diagram. The results show that a DDU system is a comparable alternative to help improve campus performance in annual energy use, global warming potential, water consumption, waste production, and especially in annual heat production. Using the estimated low end of heat production estimated for the system, a DDU system could produce 2053% more heat than what is currently being used by the existing facility. That equates to heating 14 buildings at maximum monthly heat use. If the analysis was done using the estimated high-end of the DDU heat production, the number of possible buildings heated would increase to a total of 23 buildings. These results show that while there are still notable impacts associated with geothermal systems like the DDU system proposed here, there are still tangible benefits that should be considered. Table 11 shows the criteria categories and the associated points assigned to that target performance. These target improvements and corresponding point values were set using a combination of common goals set in publicly published climate action plans and general societal trends, such as the University of Illinois Climate Action Plan (UIUC, Illinois Climate Action Plan, 2015). The climate action plan stated a goal of 30% reduction in in total campus building energy use by FY20. Because of this goal, one point was assigned for a 25% reduction, and 2 points for a 40% reduction. Campus emissions goals stated a 30% reduction by 2020 and 100% reduction by 2050, reflected by one point assigned for a 30% reduction, and 2 points for a 70% reduction. Campus water use goals were set with a percent reduction from 2008, where a 30% reduction is predicted by 2020, and 60% reduction by 2050, which is reflected by one point assigned for a 30% reduction, and 2 points for a 70% reduction in Table 12. The facility has taken actions to achieve zero waste since FY08. As zero waste is the overall goal, one point was assigned for 70% reduction, two points for 100% reduction. Lastly, current heat production on campus (through the

use of steam power plant) was compared to the proposed DDU system. One point was assigned for a 50% improvement in heat production, and two points were assigned for a 100% improvement. Table 12 shows the performance calculation for each of the five categories, and Figure 28 shows the resulting Spider diagram.

Table 11. Points assigned for each of the criteria with respect to the desired performance.

Criteria	Target Improvement	Points
Energy Use (MBTU)	25%	1
	40%	2
GWP (kg CO2 eq)	30%	1
	70%	2
Water Consumption (kg)	30%	1
	70%	2
Waste Production (kg)	70%	1
	100%	2
Annual Heat Production (MBTU)	50%	1
	100%	2

Table 12. Performance comparison of typical existing site to the proposed system in the ILB.

Criteria	Reference	Strategy	Performance	Points
Annual Energy Use (MBTU)	9.5E+03	7.0E+03	25%	1
GWP (kg CO2 eq)	1.1E+08	1.1E+07	91%	2
Water Consumption (kg)	8.0E+06	2.5E+05	97%	2
Waste Production (kg)	1.0E+04	9.0E+02	91%	1
Annual Heat Production (MBTU)	1.6E+04	3.5E+05	2053%	2

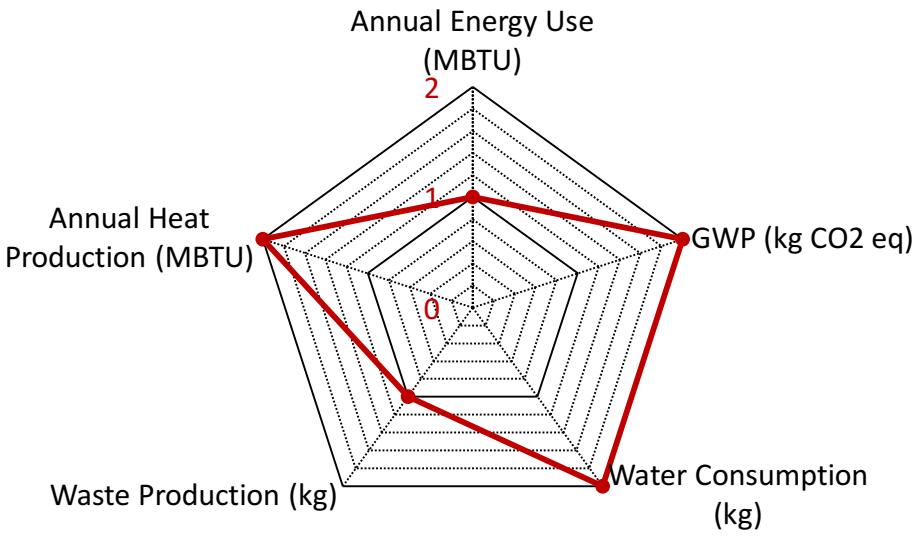

Figure 28. Spider diagram showing how a DDU system in the ILB would improve the overall waste production, water consumption, global warming potential, annual energy use, and annual heat production at an existing facility.

All of the LCA results presented above can be manipulated to represent other DDU systems using the spreadsheet tool that was developed simultaneously to produce these results. Because a significant portion of a DDU system is still in development and design parameters are subject to change, it is suggested that the inputs presented here are reviewed as designs are updated. A guide to using the spreadsheet tool can be found as a separate supplemental document in Appendix D.

4.6 Conclusion

Deep direct-use geothermal systems are low-emission heat source alternatives that have the potential to increase the distribution of geothermal heat in areas with lower heat flow that rely on traditional, high-emission sources of heat. While these systems are often considered truly sustainable energy sources, further investigation into the environmental performance of the system reveal that there are significant impacts associated with various components of DDU systems throughout the lifecycle of the system. A number of the high-impact components of DDU systems

come from the electricity required to power external supplements to the system. Sourcing the electricity used for these components from low-emission sources, rather than a facility that sources ~50% of its electricity from coal-fired sources, could assist in reducing the environmental impacts of the system. Furthermore, carefully considering the amount of raw material used to construct the system could reduce any unnecessary impacts from material sourcing and transport. In the case of a DDU system in the ILB, the results of the LCA show that the system can serve as promising alternative source of heat to replace heat provided from existing power plants. To truly quantify the total environmental impacts associated with the DDU system, a full design of the system is required. Once the design is completed, using the developed LCA spreadsheet tool will assist the project team with understanding the benefits and drawbacks of implementing a system of this nature. Furthermore, using the tool while finalizing the design of the system could provide further insight into areas of the system that produce a large amount of emissions.

Chapter 5.0: Recommendations for Future Work

As mentioned in Chapter 2, lifetime performance of GSHP systems has proven difficult to predict, and this lack of confidence when sizing systems has led to poor economic and environmental outcomes. While a number of predictive models have been developed to size GSHP systems, these models often focus on the performance of mechanical components of the system, without dedicating much focus on the subsurface response to heat. Subsurface heat transfer is typically estimated under the assumption of one homogenous unit, rather than with a system interacting with a variety of thermophysical parameters. As the work in Chapter 3 shows, thermophysical parameters of the subsurface vary with depth and location within the borefield, and vary in their response to large loads of heat. Geothermal heat system models that ignore the heterogeneity of the subsurface often oversize GSHP systems, and do not take into account certain controls on subsurface heat flow. The continuation of the homogenous "grey box" subsurface assumptions does not allow for improving future GSHP designs that interact with a heterogeneous subsurface.

The ability to understand, monitor, and predict GSHP performance throughout the lifetime of the system can be improved by investigating the variability of the subsurface and how it affects long-term performance of GSHP systems. This has been done at Borefield 4 using fiber optic distributed temperature sensing. The DTS system has provided over three years of quasi-continuous temperature data with sufficient spatial and temporal resolution to describe heat transfer within and around a ground heat exchanger. This effort alone provided significant information to guide long-term field-monitored data to further validate the district-scale borefield design method so that water movement and long-term heat storage are more properly addressed. This effort can also be improved by further understanding the difficulties of field-

monitoring of district-scale borefields. Long-term or permanent distributed temperature sensing introduces a variety of challenges that are not seen in temporary or short-term setups. An investigation into permanent calibration configurations is performed in Appendix A, where suggestions for improved permanent field monitoring are made.

Chapter 3 builds upon the work done at Borefield 4 by quantifying heat storage in the field, as well as estimating the amount of heat traveling out of the borefield. The results presented in Chapter 3 show that Borefield 4 behaves as a leaky reservoir of heat, with a sizable portion of the heat load interacting with the borefield independently traveling outside of the bulk borefield volume. Because of Epic's cooling-dominated heat load and Wisconsin's cool climate, having a natural means of heat escape supports borefield longevity and prevents a reduction in system efficiency due to borefield overheating. This understanding of borefield behavior is useful in making better-informed operational decisions, especially on a district-scale, as there is less speculation regarding where heat travels once placed in the borefield.

To continue this work, it would be beneficial to have additional monitoring at Borefield 4 that would assist in quantifying the amount of heat being transferred via groundwater advection. While the piezometers to the north and east of the borefield provide useful information regarding temperature response outside of the borefield, it does not offer any information about how the groundwater flowing generally to the south and west carries heat. If additional piezometer temperature monitoring wells are installed to the southwest of Borefield 4, the load of heat dissipated via advective heat flow could be quantified. Furthermore, the combination of the thermophysical properites of the subsurface, three plus years of temperature data in the borefield, and the heat loads interacting with the system could inform a model that could potentially be used for district-scale borefield design. Developing a design manual that

better incorporates the effects of groundwater behavior and long-term subsurface heat response could reduce the over-design of district-scale geothermal systems.

Appendix A: Improvements and Adjustments to Long-term FO DTS Calibration Setup at Borefield 4

Borefield 4, a district-scale geothermal exchange borefield that serves Epic Systems, has been instrumented with temperature monitoring wells (TMW) with fiber optic loops down to the base of the borefield. There are six sentry wells within the bulk volume of the borefield, and two piezometer wells along the outside perimeter of the borefield. The piezometer wells are screened in the shallow aquifer, the deep aquifer, and have a fiber optic loop installed to the base of the borefield. A map of the borefield can be seen in Figure 29.

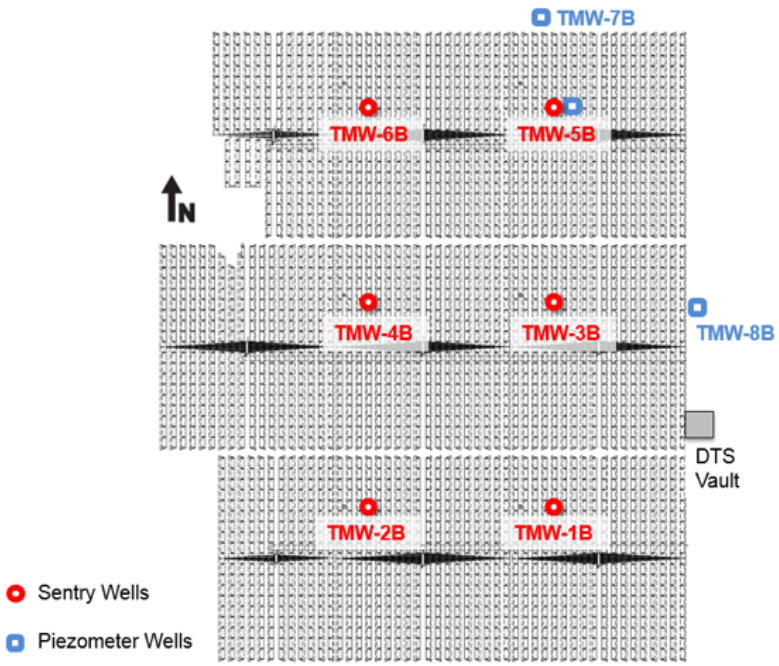

Figure 29. Aerial map of Borefield 4, including locations of Temperature Monitoring Wells 1 through 8 and Vault 14.

A Sensornet Sentinel DTS-LR interrogator with a 16-channel multiplexor is used to collect the fiber optic temperature data. Temperatures are calibrated by a dynamic, double-ended, centralized, and remotely accessible manual routine (McDaniel, 2018).

As part of the calibration routine developed, the temperature of the fiber is calculated using Equation 1, shown below, and also presented in Chapter 2 of this thesis. At position z (m), the Raman Stokes, $P_s(z)$, and anti-Stokes, $P_{aS}(z)$, signals are used to calculate temperatures.

$$T(z,t) = \frac{\gamma}{ln\frac{P_S(z,t)}{P_{aS}(z,t)} + C - \int_0^z \Delta\alpha(z')dz'} \qquad [1]$$

where γ (K) represents the change in energy between the photon at the laser and the scattered Raman photon, C is a parameter that encompasses laser and DTS properties, and $\Delta\alpha$ (m^{-1}) is the differential attenuation between the Stokes and anti-Stokes signals (Hausner, 2011). This integral in the denominator of the equation can be referred to as the "cumulative differential attenuation," and is a product of signal loss down the length of the fiber. When gathering data in a double-ended measurement, pulses of light are sent both ways down the loop of fiber, resulting in a "forward" and "reverse" measurement. In addition a small reference section of the cable remains a constant temperature through the use of temperature controlled calibration baths. With the reference temperature gathered at those baths, Equation 2 can be used to solve for differential attenuation, $\Delta\alpha$.

$$\int_z^{z+\Delta z} \Delta\alpha(z')dz' = \frac{ln\left(\frac{P_S(z+\Delta z)}{P_{aS}(z+\Delta z)}\right)_{\Rightarrow} - ln\left(\frac{P_S(z)}{P_{aS}(z)}\right)_{\Rightarrow} + ln\left(\frac{P_S(z)}{P_{aS}(z)}\right)_{\Leftarrow} - ln\left(\frac{P_S(z+\Delta z)}{P_{aS}(z+\Delta z)}\right)_{\Leftarrow}}{2} \qquad [2]$$

Where the arrows indicate whether the measurement is forward (⇒) or reverse (⇐). If the value for attenuation for every Δz is summed, starting at z=0, an average differential attenuation along the cable for each section can be determined (Giesen, 2012).

Once $\Delta\alpha$ is determined for each section of the fiber, it is possible to further calibrate this temperature data to provide a smoother plot with less fluctuation in temperature between time

steps. This is done by finding an average γ value across the length of fiber. This fixed gamma value will then be used to let the constant C be variable through the cable (McDaniel, 2018). Once the values of constants γ and C are found, they can be substituted into Equation 1 to determine temperature down the length of the cable.

Using the data collection and calibration methods outlined above, data has been collected and calibrated for the eight temperature monitoring wells for over three years. As part of that calibration method, an overall average γ value (for approximately 1.5 years of data) is applied to all of the data, and a variable C is used. It is rare to have continuous and/or permanent calibration setups like the one at Epic. Setups of this nature are typically temporary, especially when working with calibration baths. Over the years, maintaining constant calibration bath temperatures has proven to be difficult, resulting in fluctuations of the physical parameters, γ and C, used to calibrate the temperatures of the subsurface. The original setup comprised of two calibration baths, one hot and one ambient, of water in coolers. The hot bath is heated using a submersible aquarium pump, as the excess heat from running the pump raises the temperature of the water sufficiently enough to serve as the upper bracket of temperatures that the fiber experiences in the field. The ambient bath was originally a sealed cooler with room temperature water. Temperature variation in the vault, due to seasonal temperature variation at the surface, led the ambient bath temperatures to fluctuate slightly over time. The color floods below (Figures 30 – 37) show the results using this original calibration method. One feature that is apparent in many of the color floods presented below is the presence of streaks that break up the continuity of the plot. These streaks potentially represent rapid subsurface response to a heat load, or they could represent noise in the collected data.

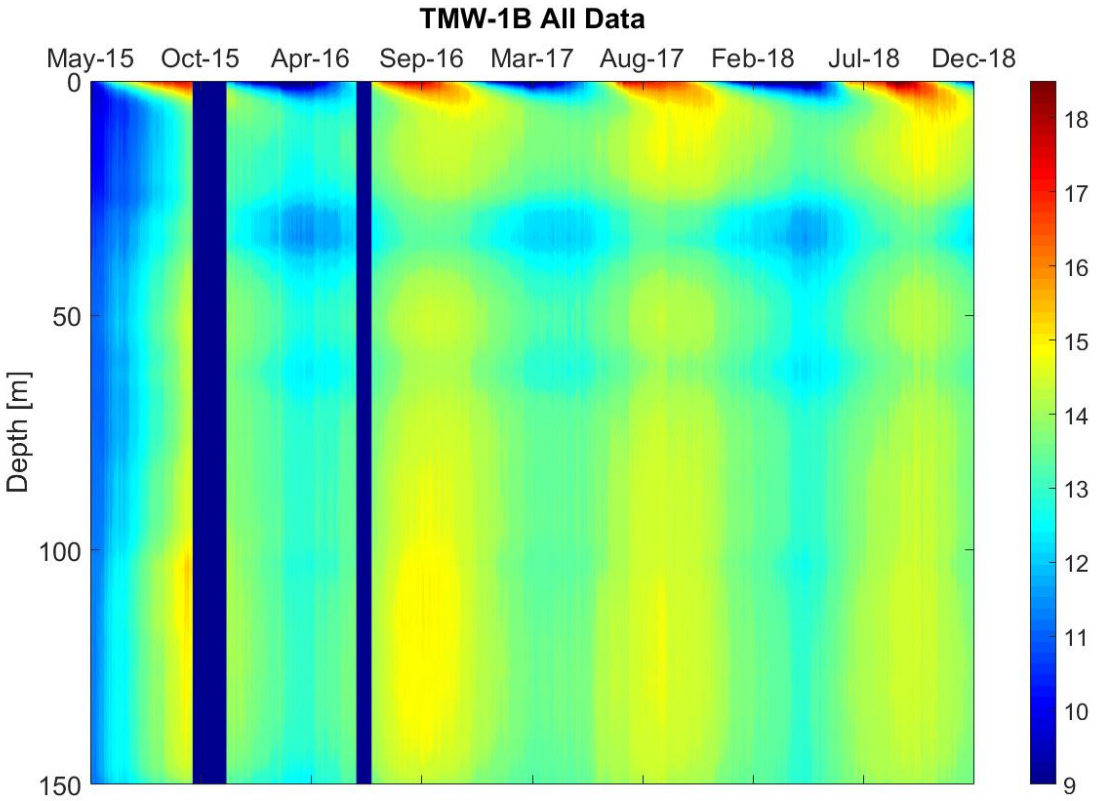

Figure 30. Results from original overall average gamma calibration for TMW-1B.

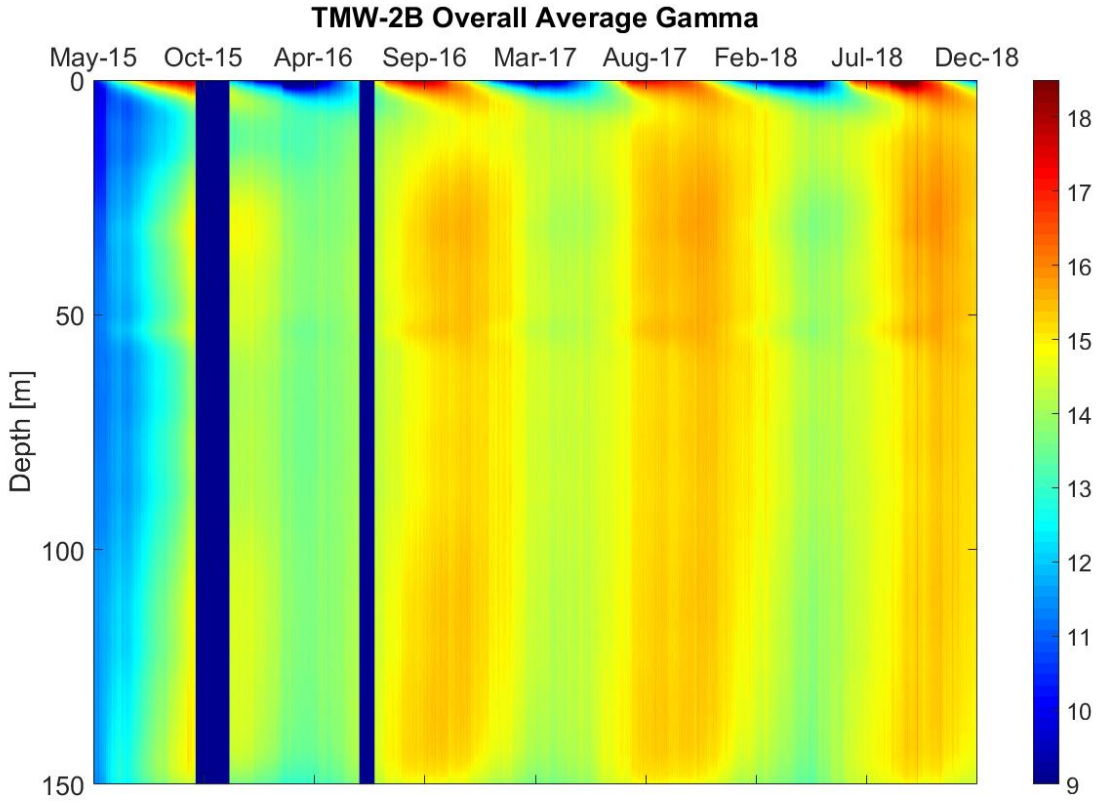

Figure 31. Results from original overall average gamma calibration for TMW-2B.

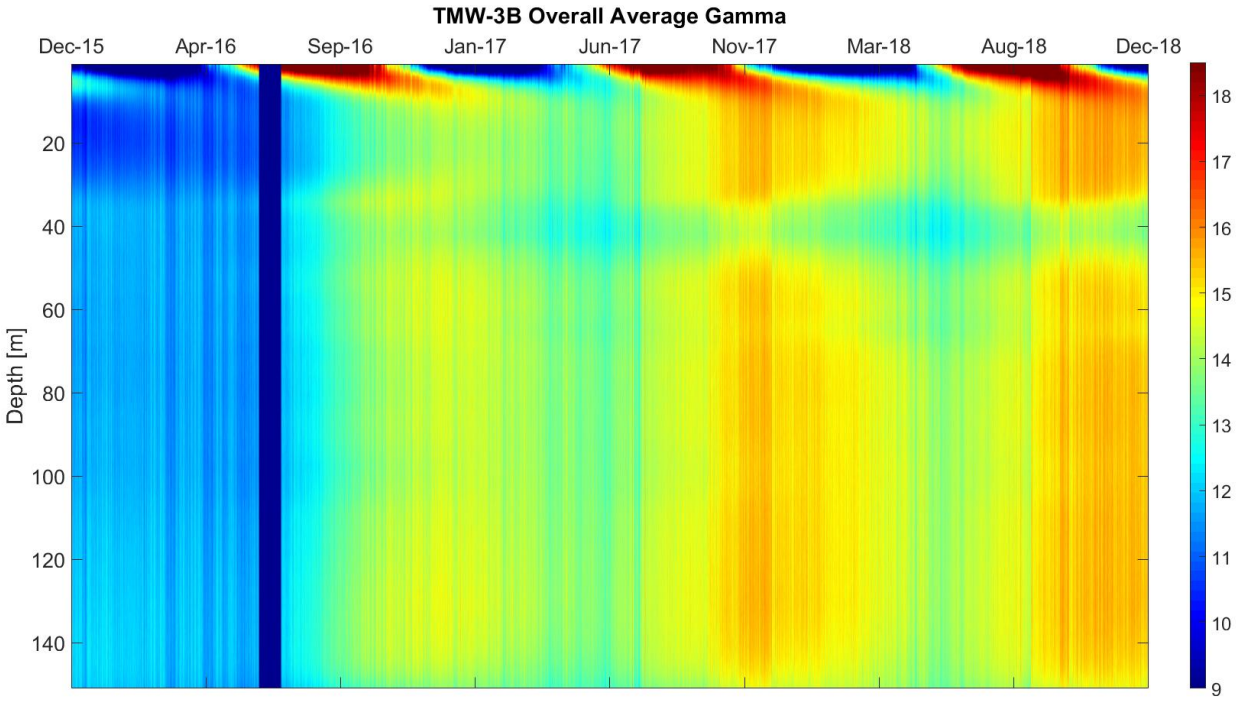

Figure 32. Results from original overall average gamma calibration for TMW-3B.

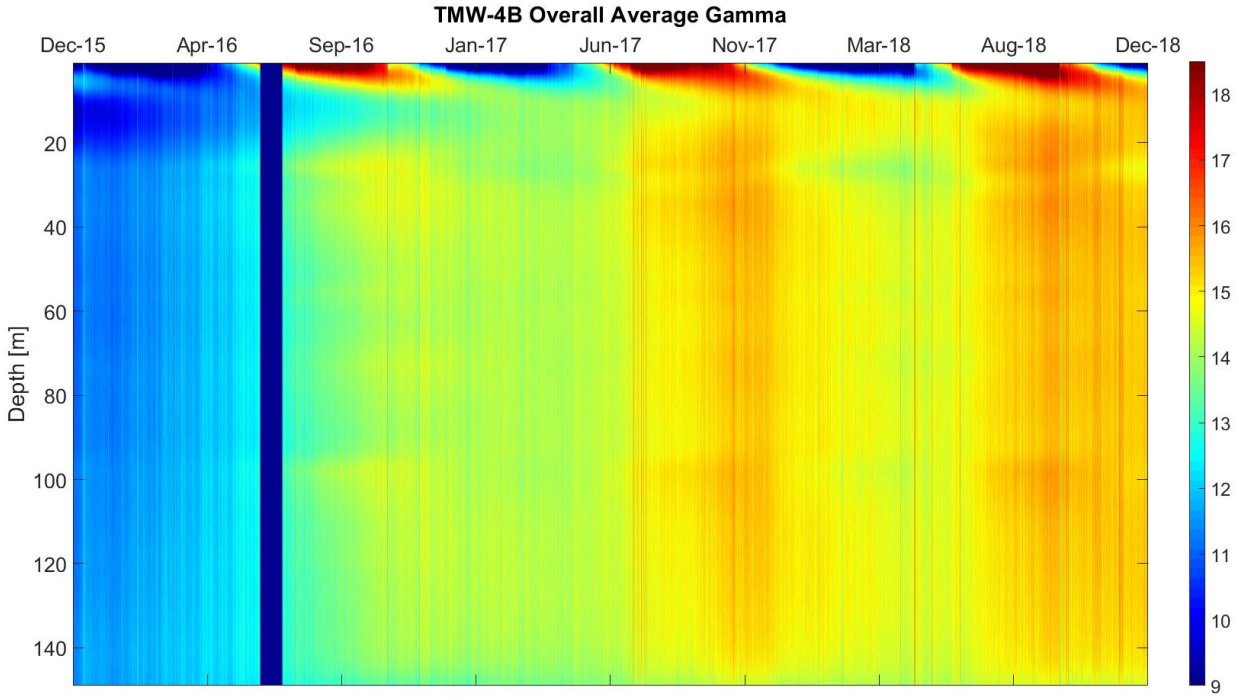

Figure 33. Results from original overall average gamma calibration for TMW-4B.

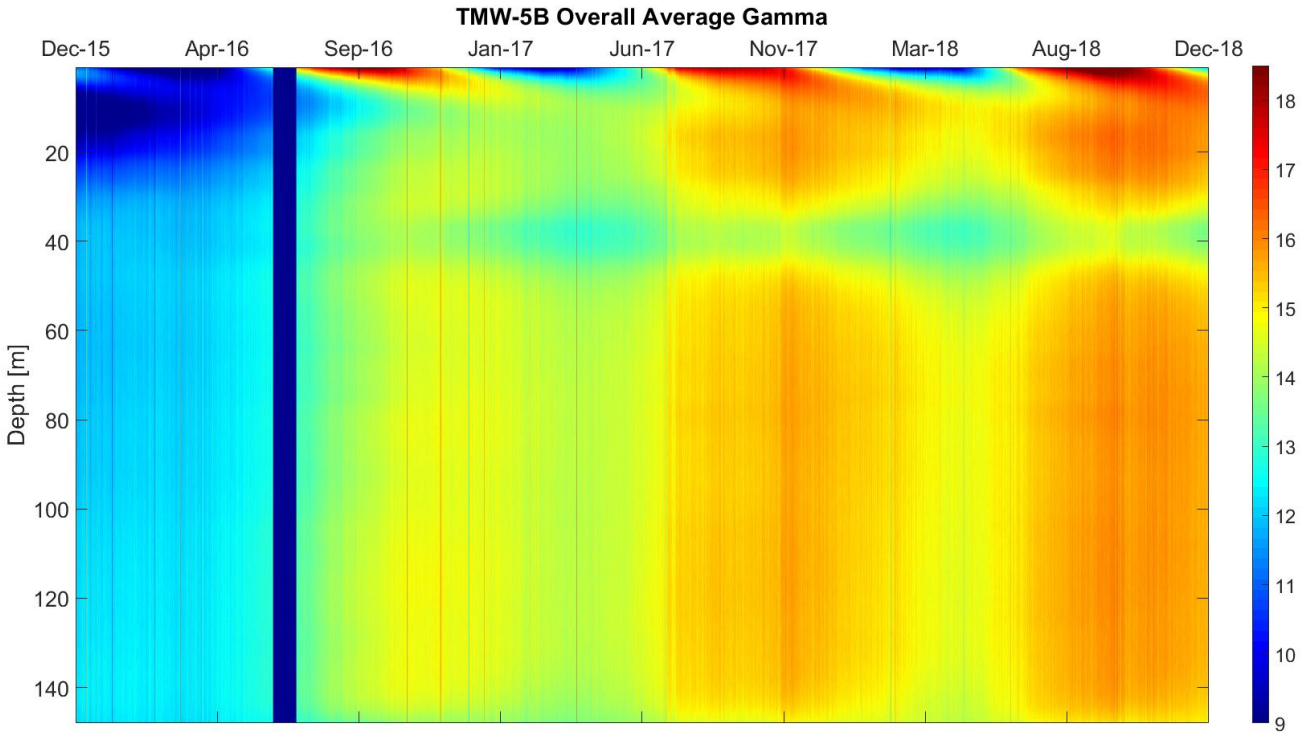

Figure 34. Results from original overall average gamma calibration for TMW-5B.

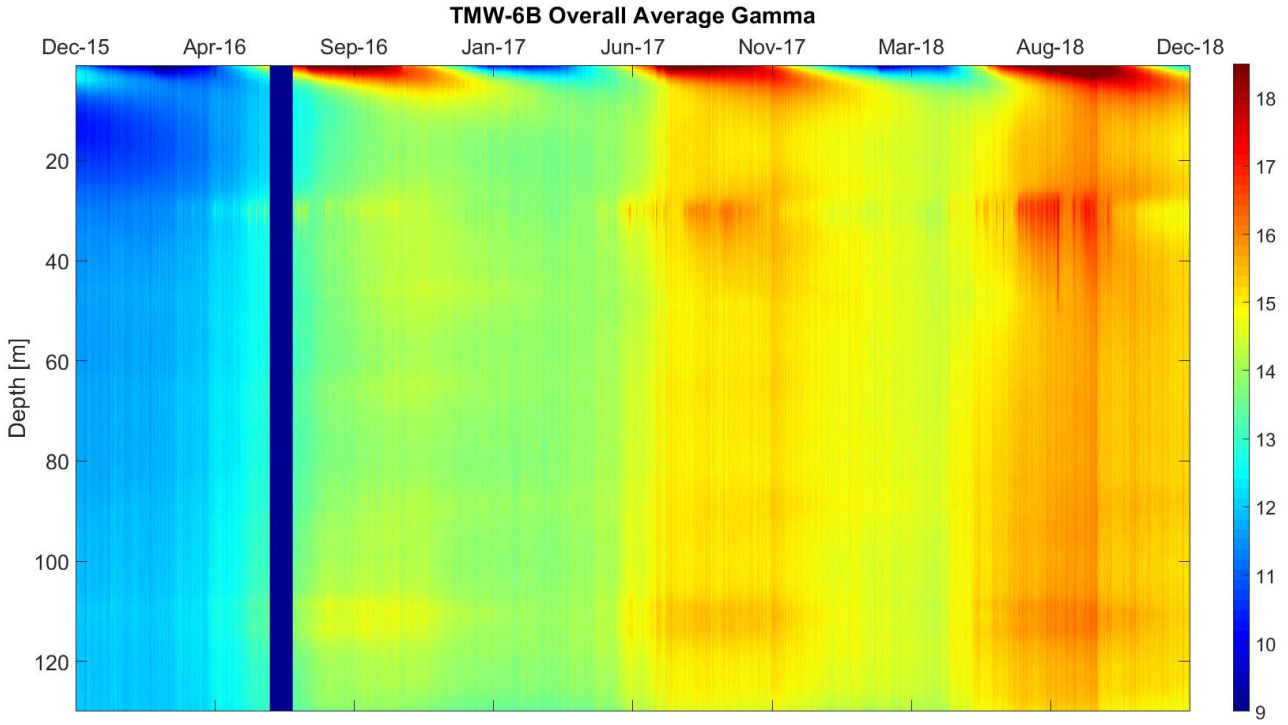

Figure 35. Results from original overall gamma calibration for TMW-6B.

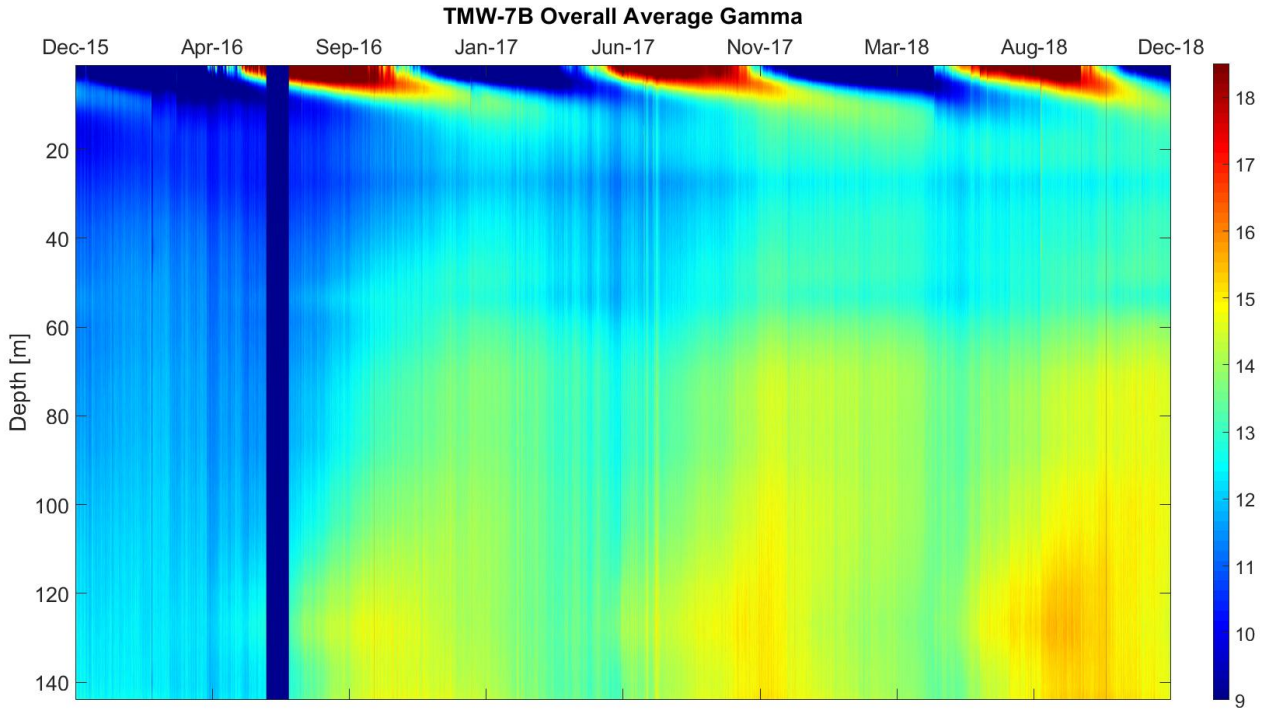

Figure 36. Results from original overall gamma calibration for TMW-7B.

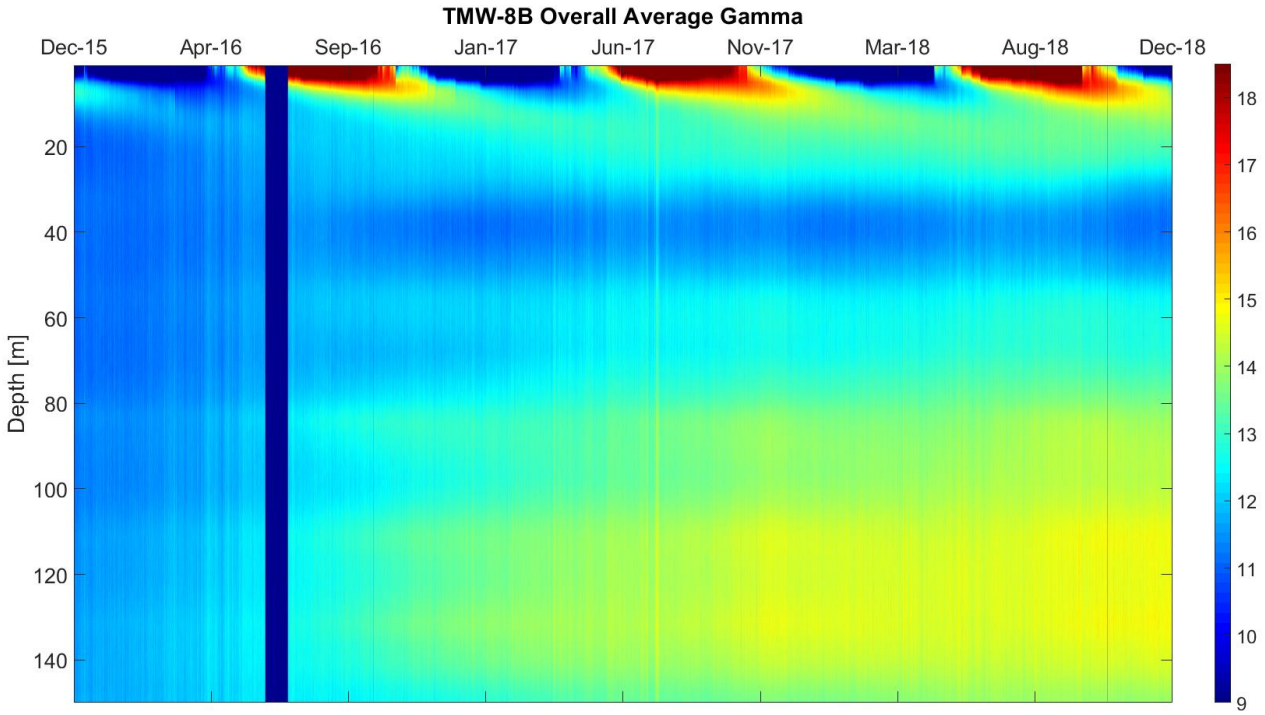

Figure 37. Results from original overall gamma calibration for TMW-8B.

In addition to the inherent noise associated with fiber optic DTS data due to temperature variation in the ambient calibration bath, there were also multiple known disturbances to the calibration baths over time that likely contribute to periods of particularly erratic (represented by data streaks) calibrated temperatures. In July 2017, there was a series of rainfall events that led to water accumulation in the subsurface vault where the calibration baths are housed. After further investigation, it was revealed that the sump pumps used to divert water from the vault were not functioning properly, causing a flood in Vault 14. Due to the high water levels, the calibration baths were overturned. Once the sump pumps were fixed, the calibration baths remained knocked over and empty. This lead to the submersible pump running on air, and the reference sections of fiber being left in ambient air temperature. This can be seen in the calibration bath temperatures, shown in Figure 38 below.

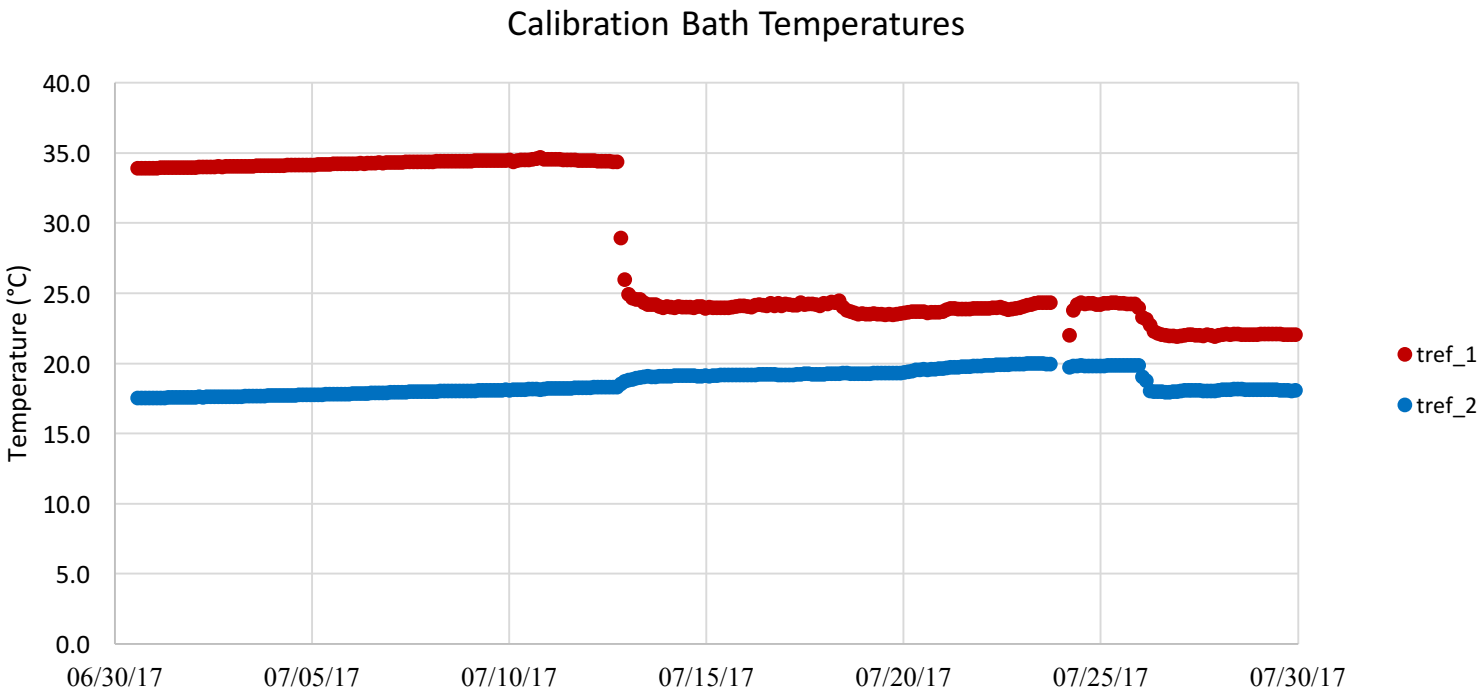

Figure 38. Calibration bath temperatures in July 2017, measured using thermistors placed in each bath. The hot bath is represented by tref_1, and the ambient bath is represented by t_ref2.

In October of 2018, there was an intentional disruption of the calibration baths to replace the previously ambient bath with a cold bath. This was done to assist with better bracketing the temperatures that the fiber experiences in the field. Prior to this date, the ambient bath was fluctuating between 15 and 20 °C, which is higher than some of the temperatures that the fiber collects in Borefield 4. Placing the lower-bracket bath in a refrigerator would simultaneously reduce as well as maintain the cold bath at a temperature of approximately 6 °C. This change is seen in Figure 39.

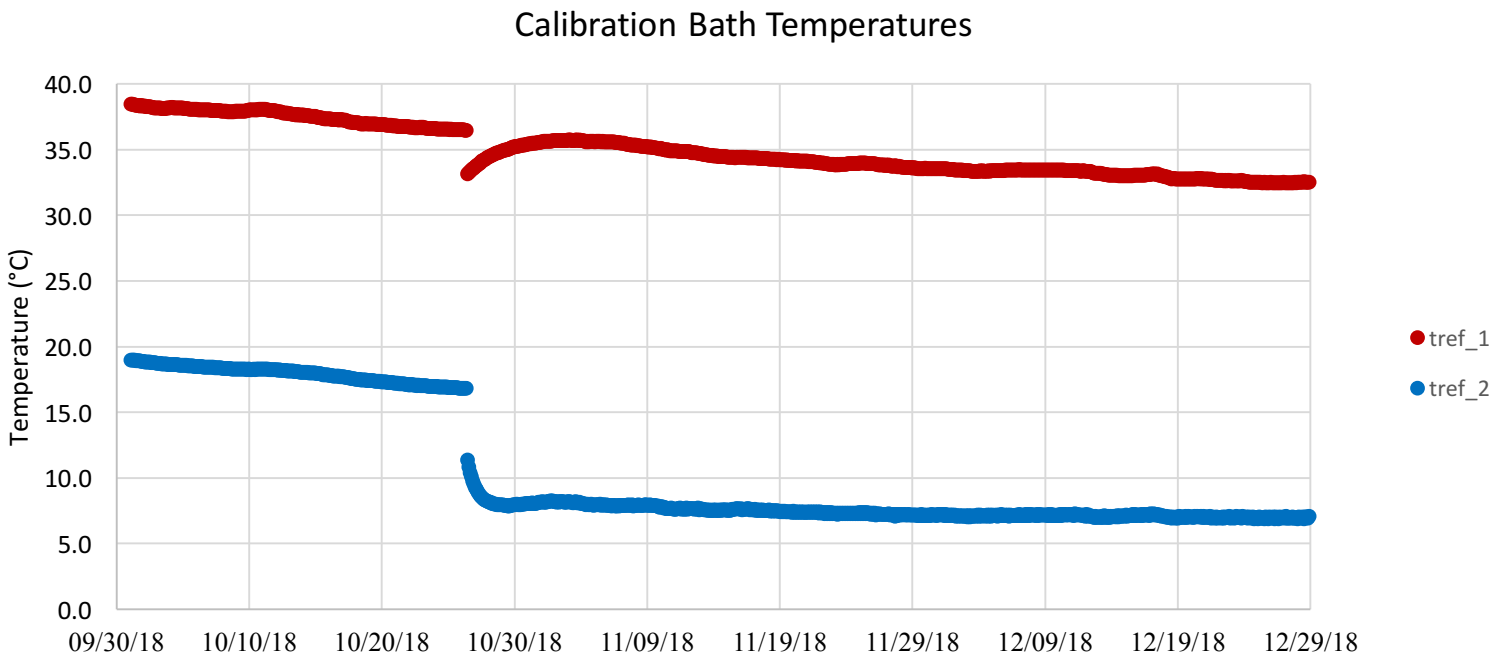

Figure 39. Calibration bath temperatures from September through December 2018, showing the transition from an ambient bath to cold bath in order to better bracket field temperatures. The hot bath is shown by t_ref1, and the cold bath is represented by t_ref2.

The fluctuations in calibration bath temperatures resulted in dramatic changes in the physical calibration parameters, gamma (γ) and C. Because the original calibration method involved applying an overall average gamma, rather than using an individual gamma value for each iteration, the fluctuating calibration parameters contributed to the noise observed in the calibrated temperature data. This is seen in the color floods presented above (Figures 33-40), where there is significant noise in July 2017, October 2018, as well as in other time periods.

To investigate the noise seen in the color floods, temperatures were calibrated using an average monthly gamma rather than an overall average gamma. This provided further insight into where the calibration parameters are fluctuating, and if there are trends associated with how the calibration parameters change. It was determined that there were three primary shifts in gamma that corresponded to shifts in calibration bath temperature: July – October 2017, November 2017 – October 2018, and November 2018 – present. This can be seen in the eight color floods, shown in Figures 40 through 57, below.

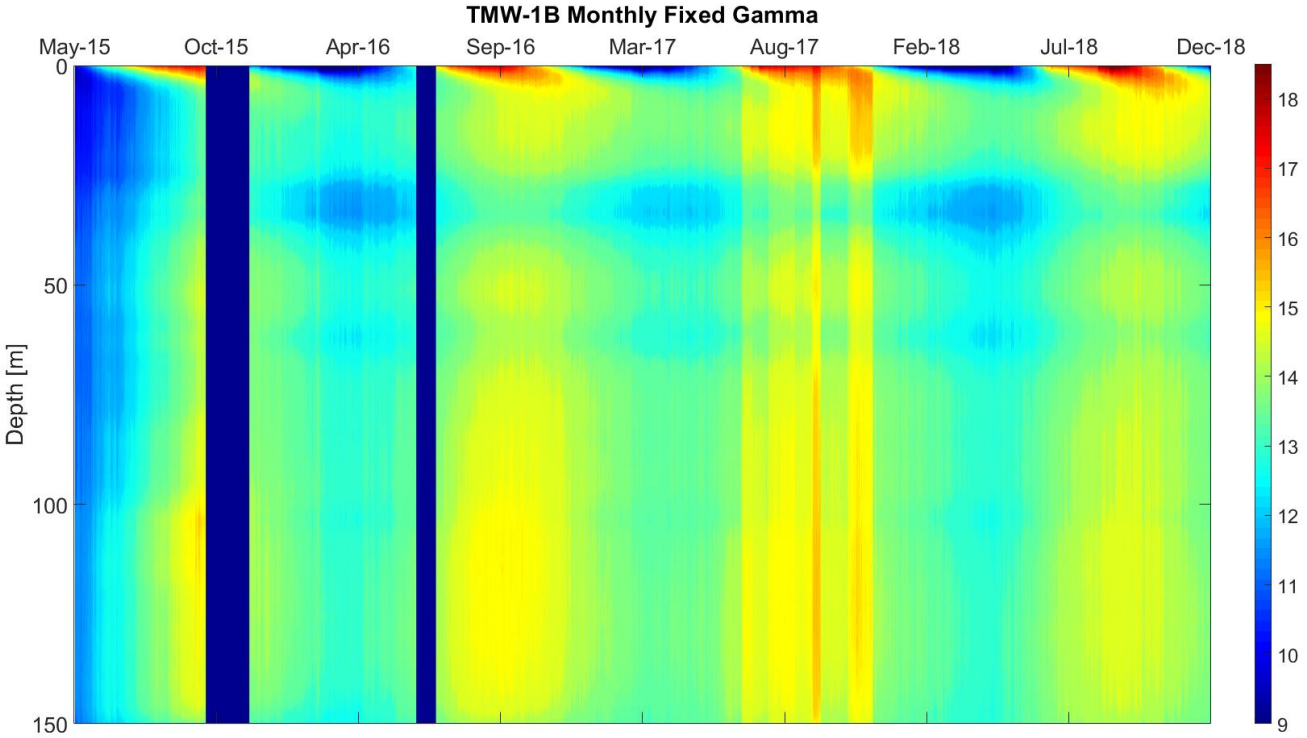

Figure 40. Results from monthly average gamma calibration for TMW-1B. Note the various jumps in temperature from month-to-month, due fluctuations in the calibration bath temperatures and resulting calibration parameters.

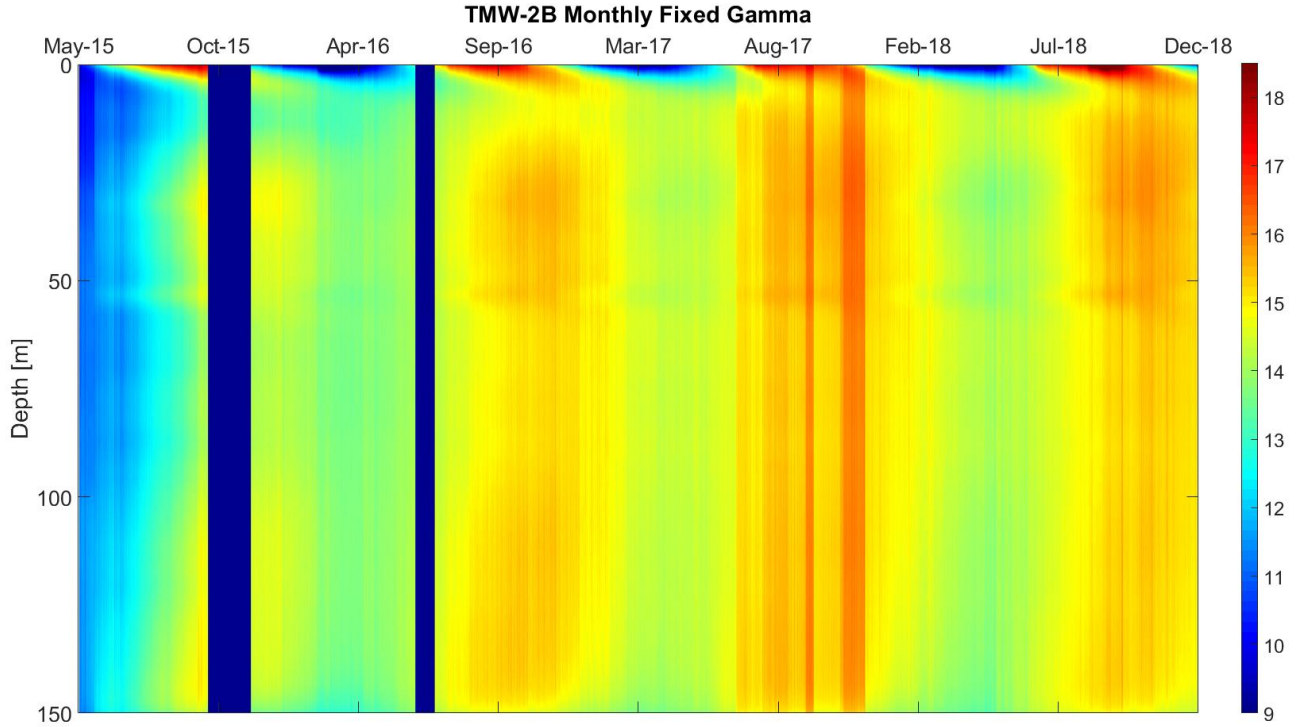

Figure 41. Results from monthly average gamma calibration for TMW-2B. Note the various jumps in temperature from month-to-month, due fluctuations in the calibration bath temperatures and resulting calibration parameters.

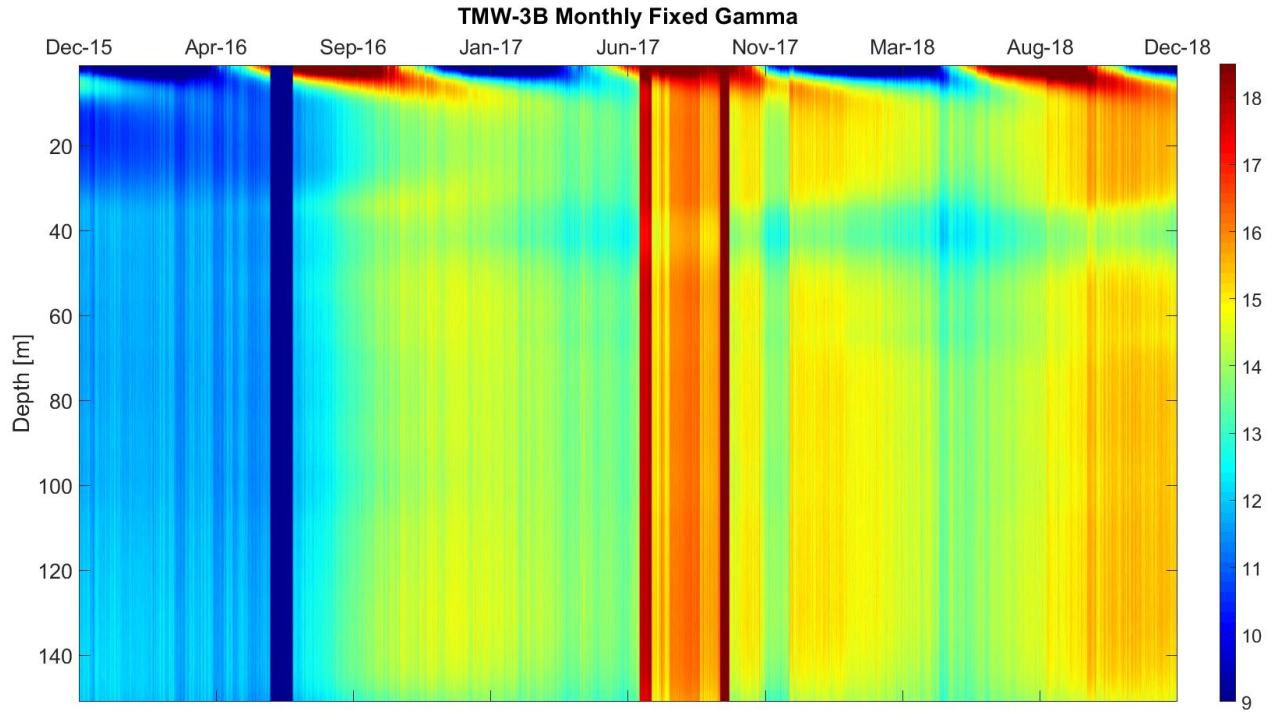

Figure 42. Results from monthly average gamma calibration for TMW-3B. Note the various jumps in temperature from month-to-month, due fluctuations in the calibration bath temperatures and resulting calibration parameters.

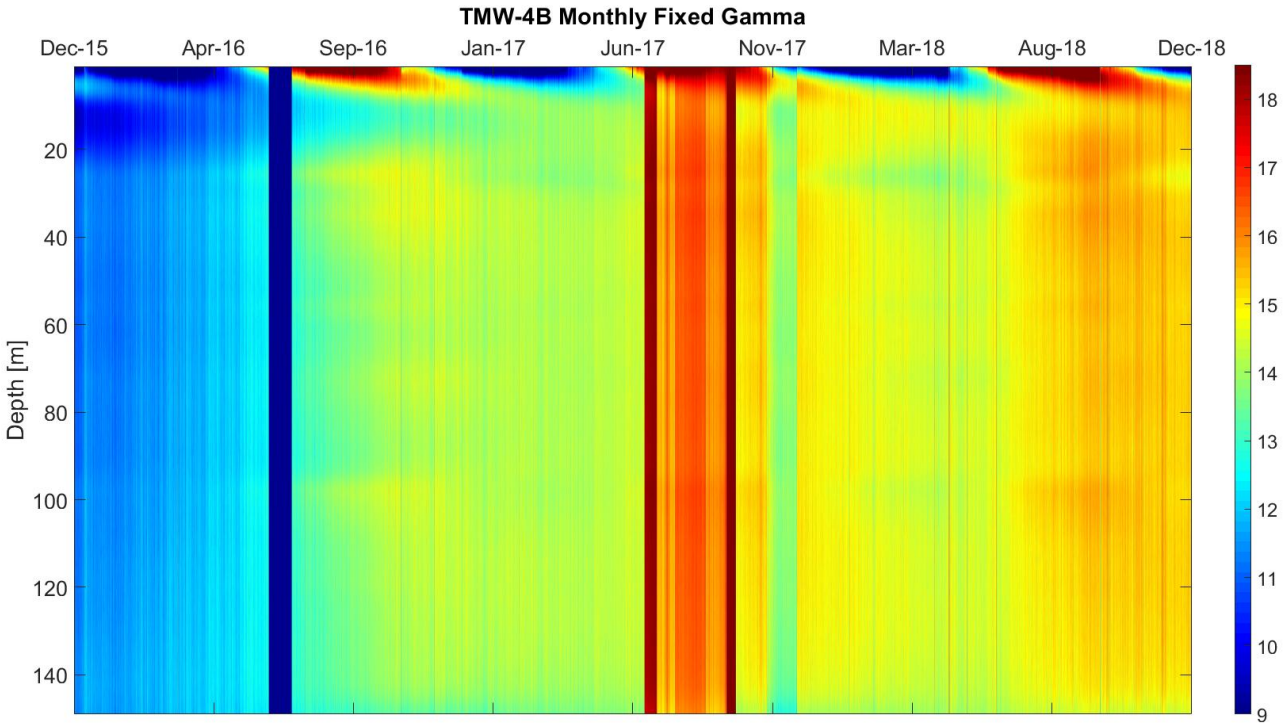

Figure 43. Results from monthly average gamma calibration for TMW-4B. Note the various jumps in temperature from month-to-month, due fluctuations in the calibration bath temperatures and resulting calibration parameters.

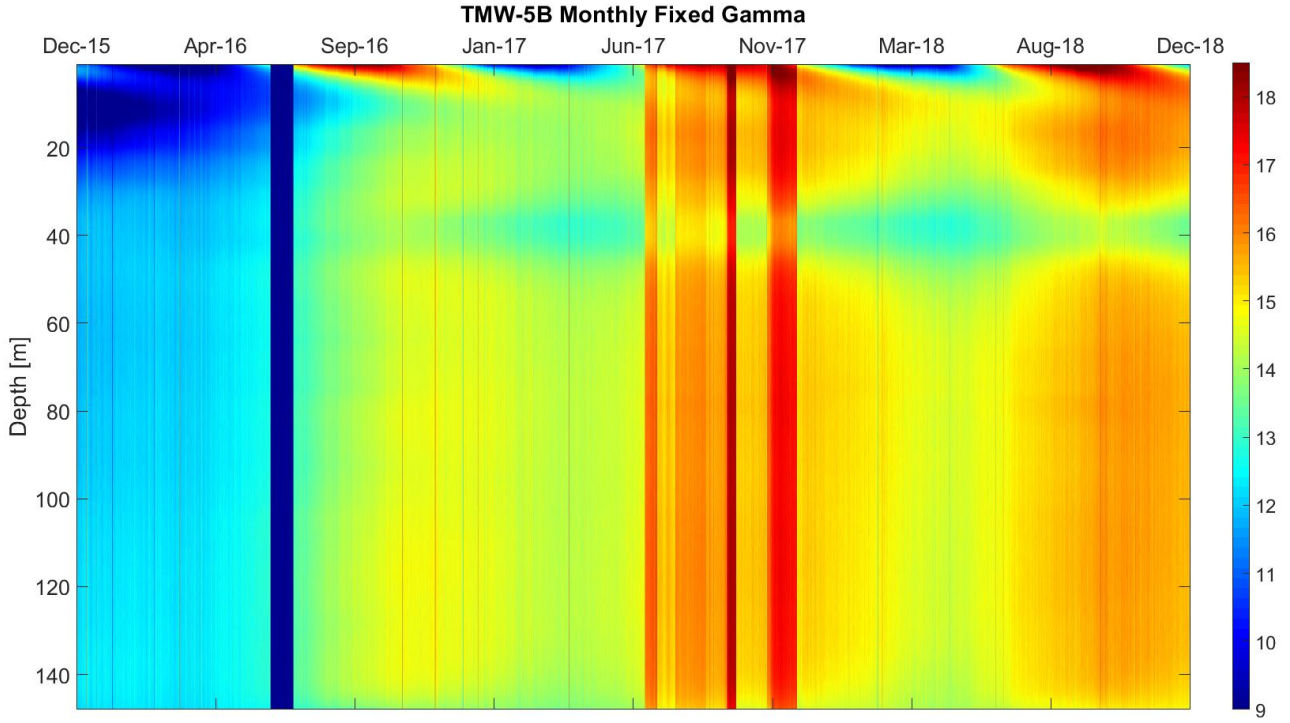

Figure 44. Results from monthly average gamma calibration for TMW-5B. Note the various jumps in temperature from month-to-month, due fluctuations in the calibration bath temperatures and resulting calibration parameters.

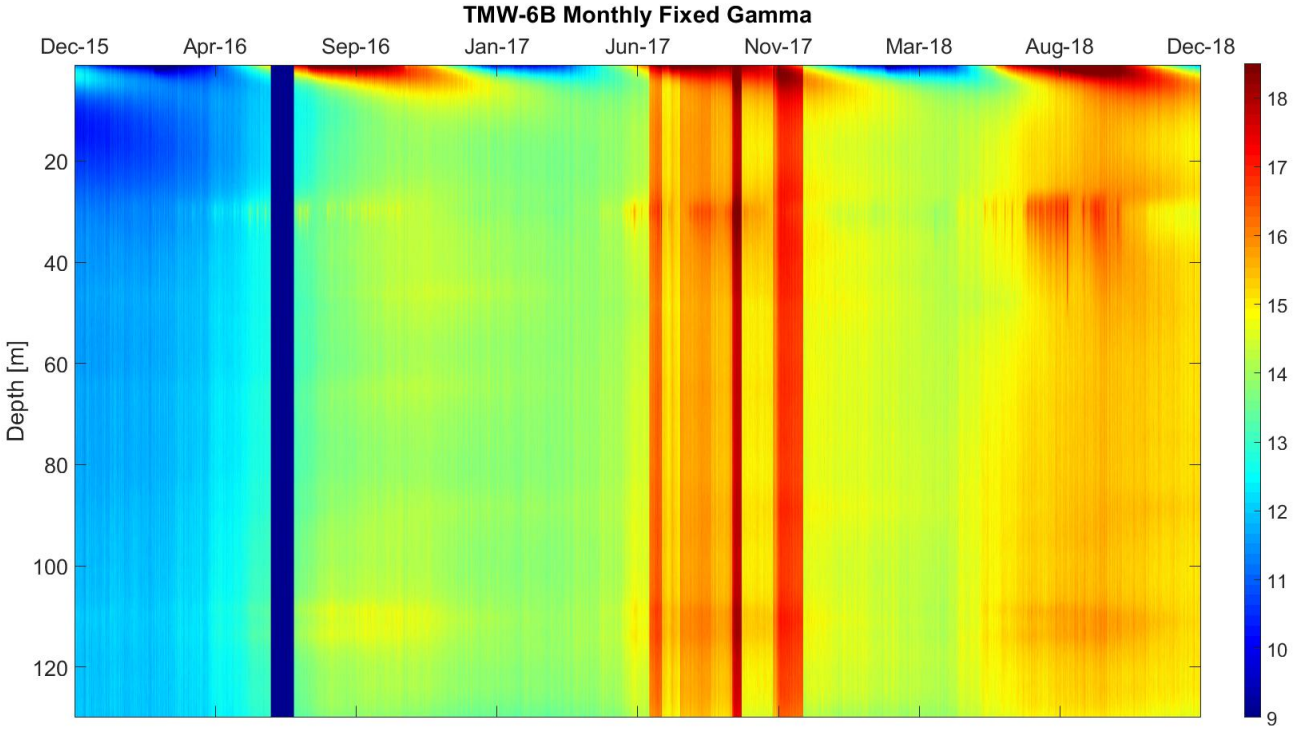

Figure 45. Results from monthly average gamma calibration for TMW-6B. Note the various jumps in temperature from month-to-month, due fluctuations in the calibration bath temperatures and resulting calibration parameters.

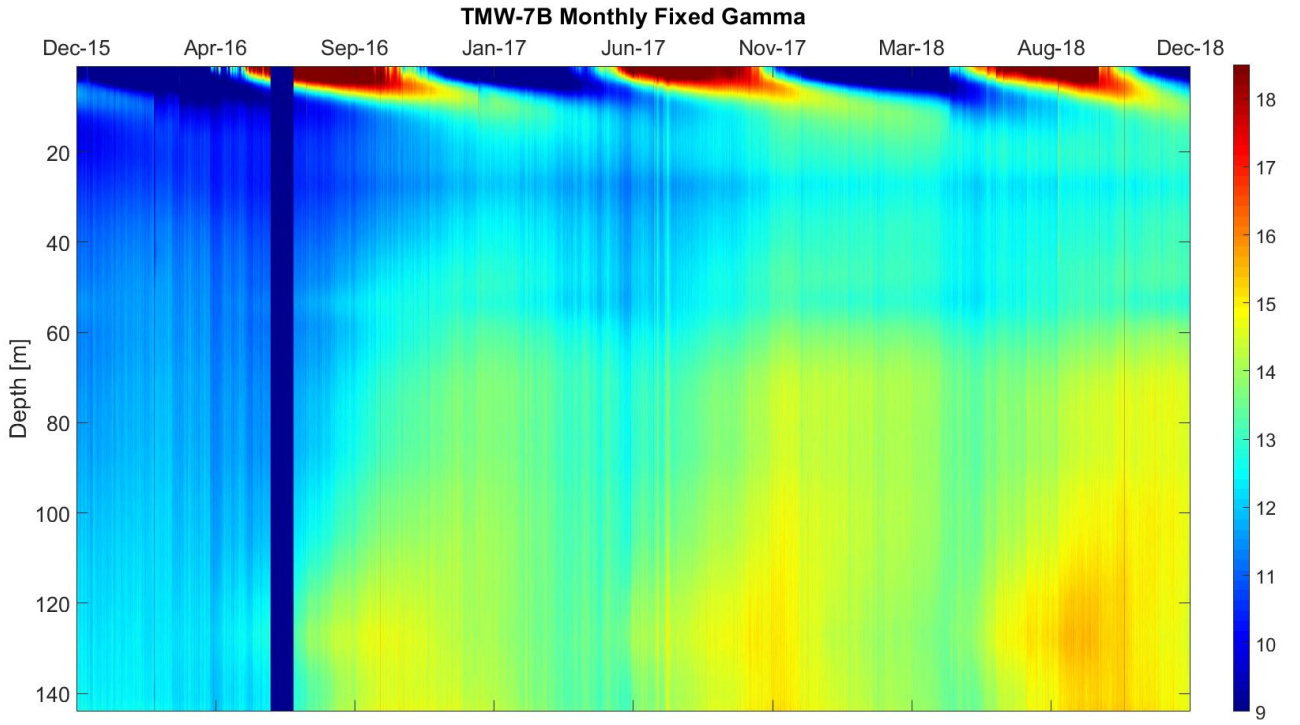

Figure 46. Results from monthly average gamma calibration for TMW-7B. Note the various jumps in temperature from month-to-month, due fluctuations in the calibration bath temperatures and resulting calibration parameters.

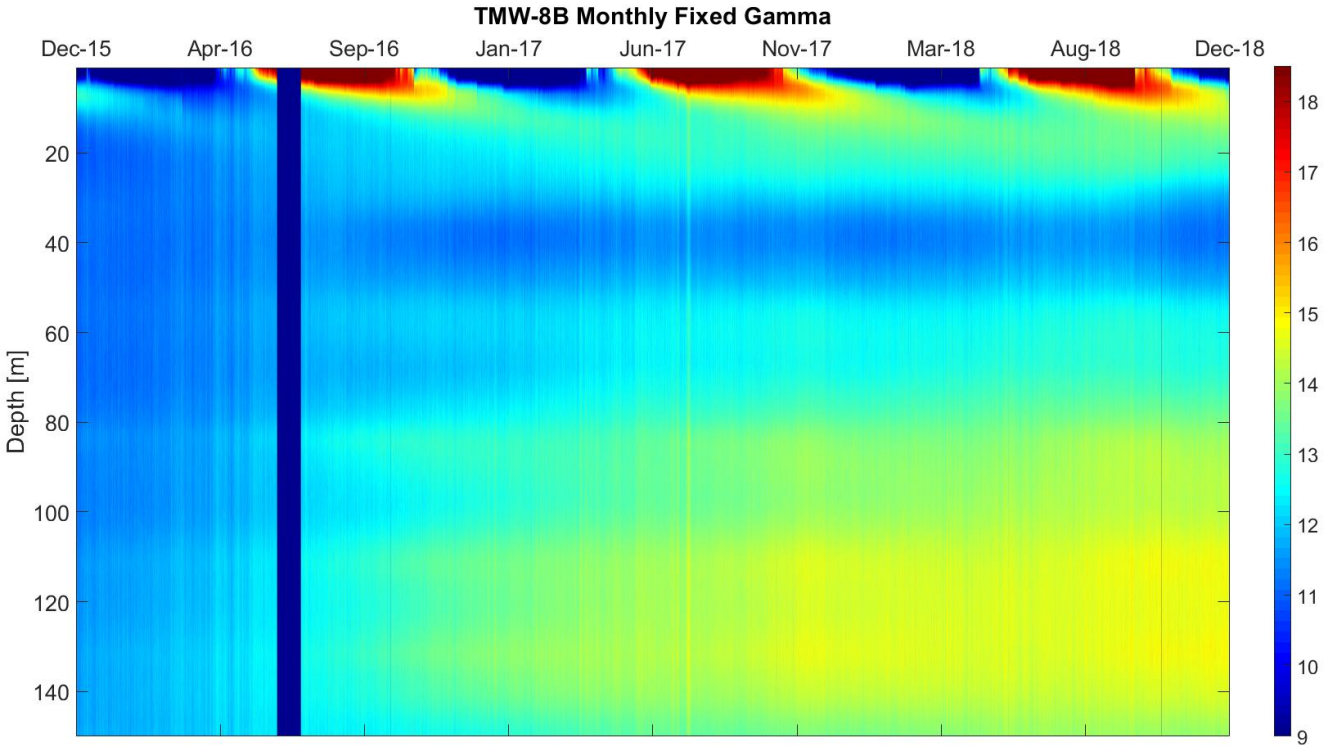

Figure 47. Results from monthly average gamma calibration for TMW-8B. Note the various jumps in temperature from month-to-month, due fluctuations in the calibration bath temperatures and resulting calibration parameters.

After determining where the primary gamma shifts were located, temperatures were calibrated using different average gamma values for the three main shifts: July – October 2017, November 2017 – October 2018, and November 2018 – present. Once that was completed, outliers in temperature data, as well as other seemingly random pockets of noise or error, were manually corrected using interpolation of calibrated temperatures. The final step was to apply a moving average across the calibrated temperatures in order to further reduce noise in the data. The average was applied across nine data points, or one day of data. The figures below (Figures 48-63) show the discretized average gamma calibration and followed by the moving average for each temperature monitoring well.

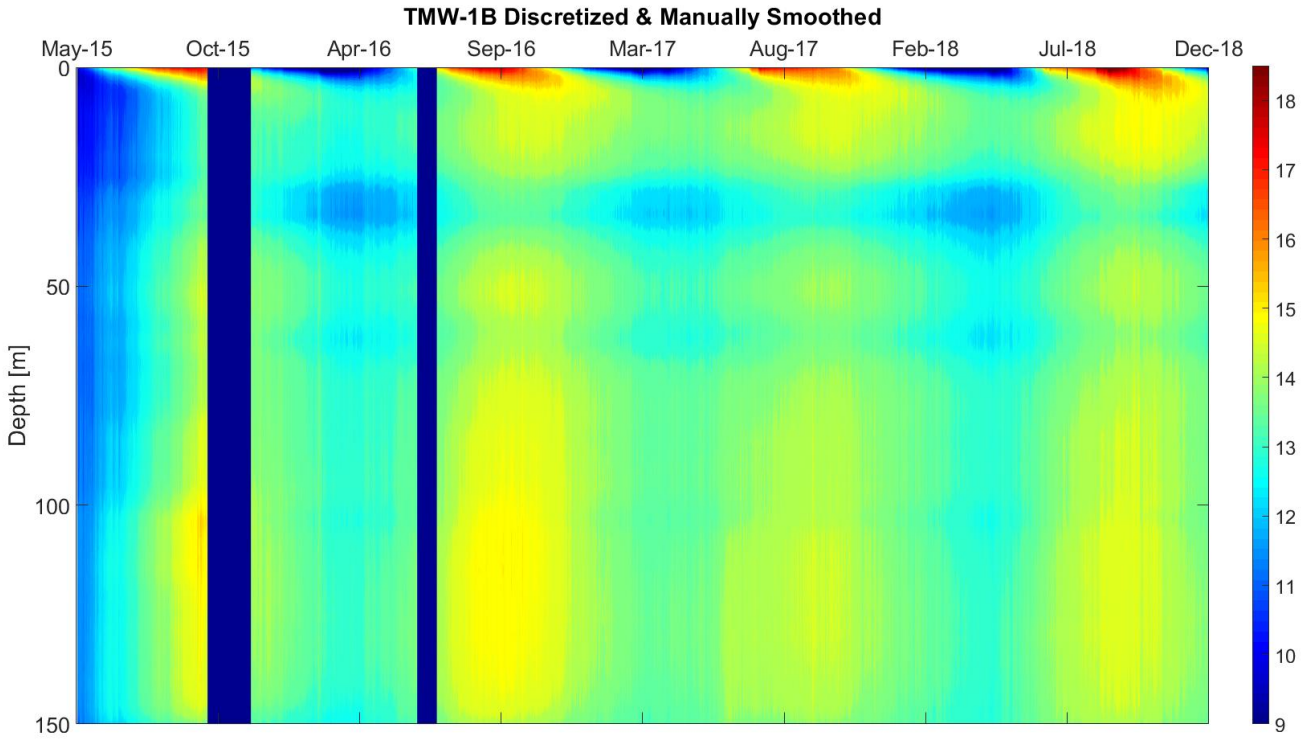

Figure 48. Discretized average gamma calibration and manual smoothing using interpolation of calibrated temperatures for TMW-1B.

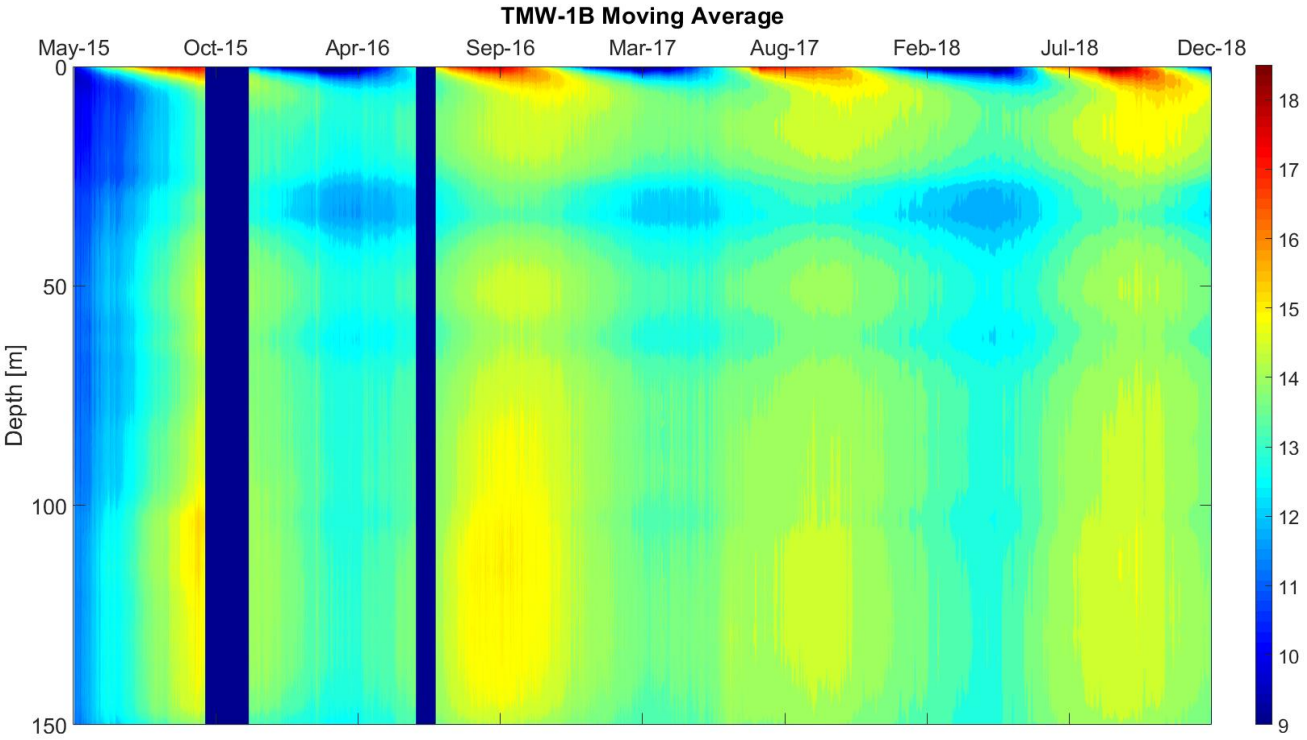

Figure 49. Discretized average gamma calibration figure with moving average applied for TMW-1B.

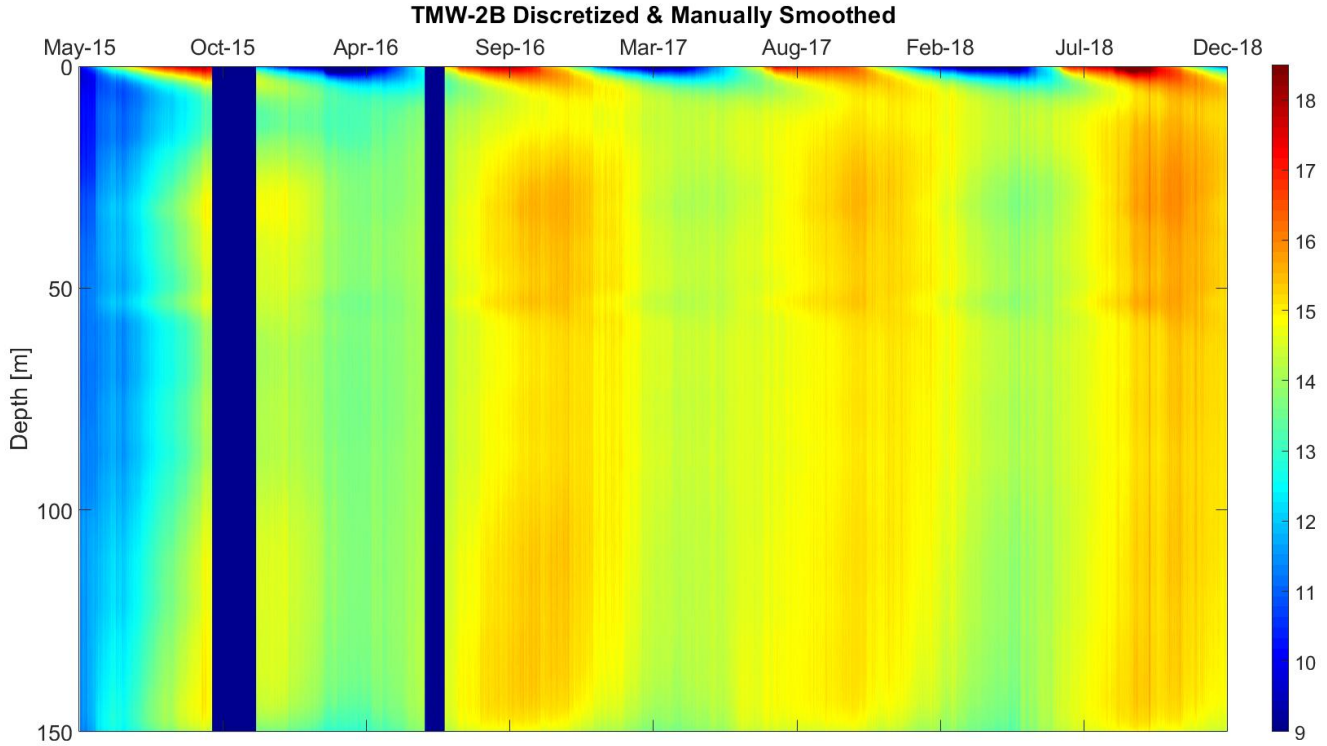

Figure 50. Discretized average gamma calibration and manual smoothing using interpolation of calibrated temperatures for TMW-2B.

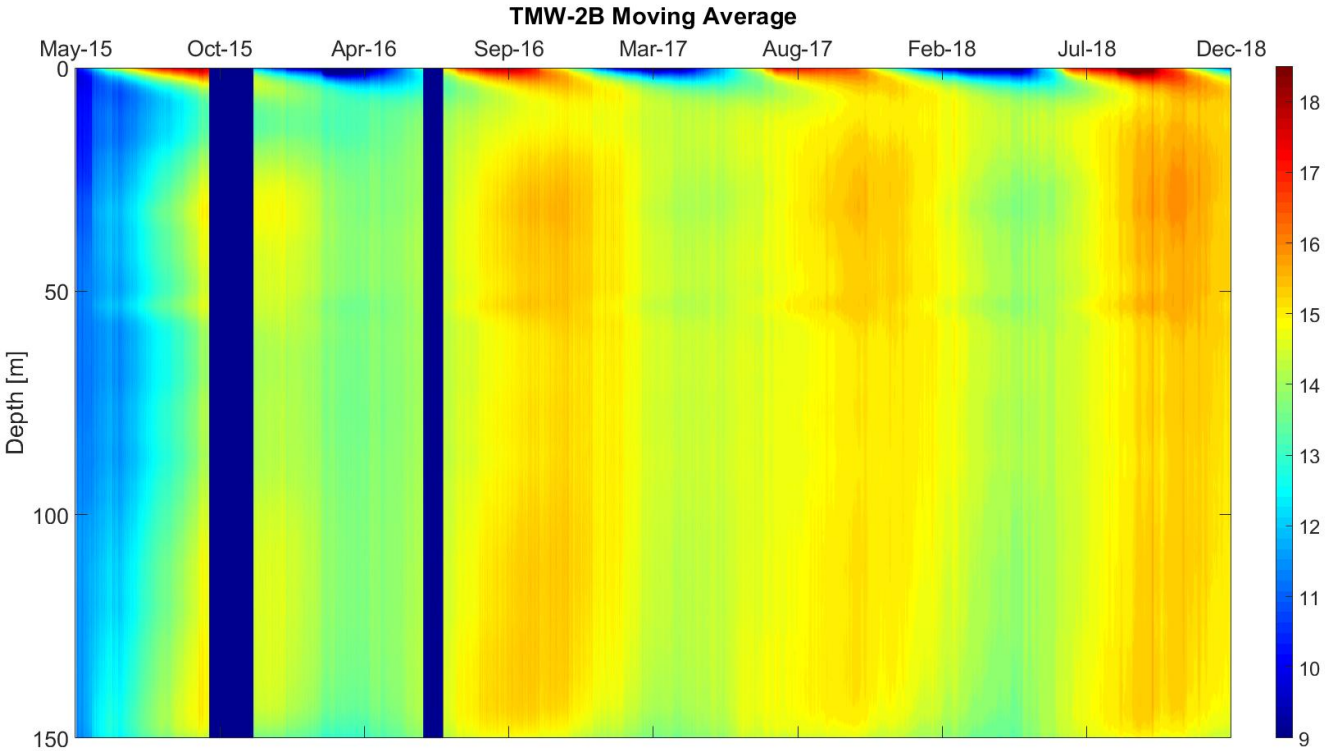

Figure 51. Discretized average gamma calibration figure with moving average applied for TMW-2B.

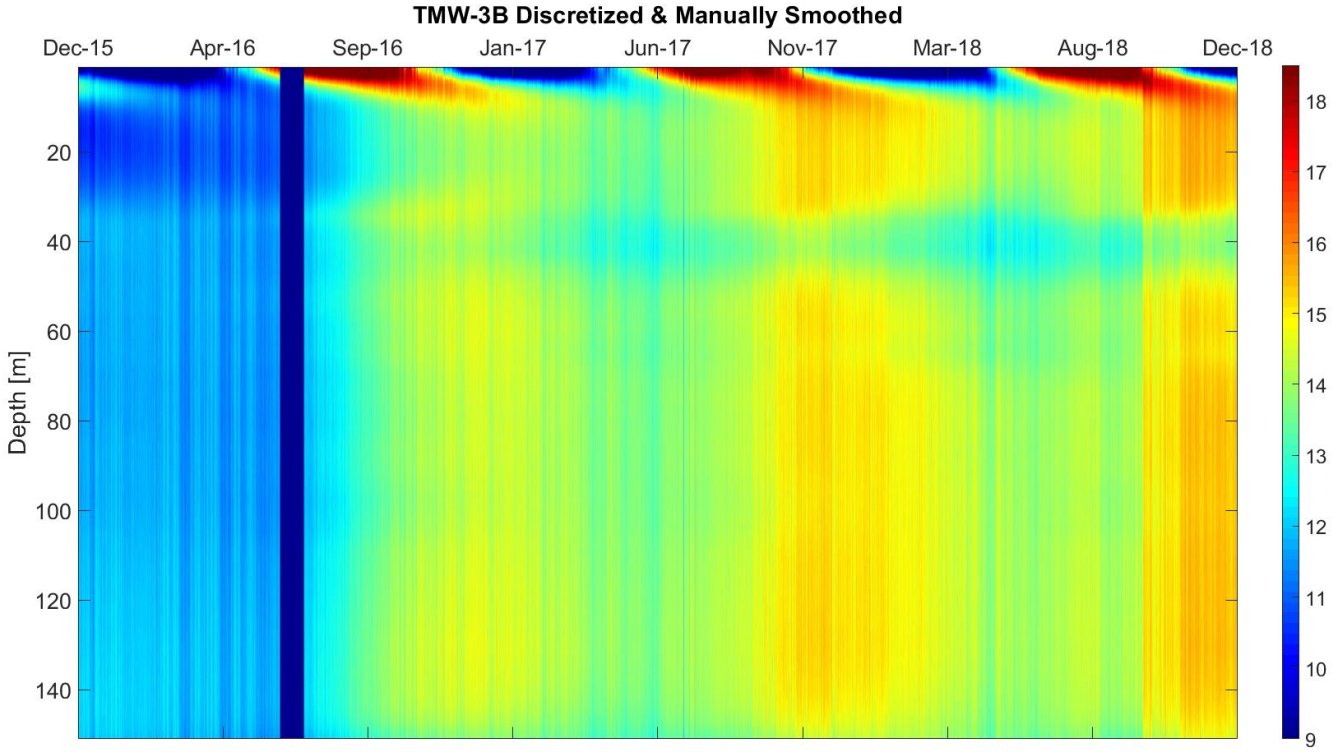

Figure 52. Discretized average gamma calibration and manual smoothing using interpolation of calibrated temperatures for TMW-3B.

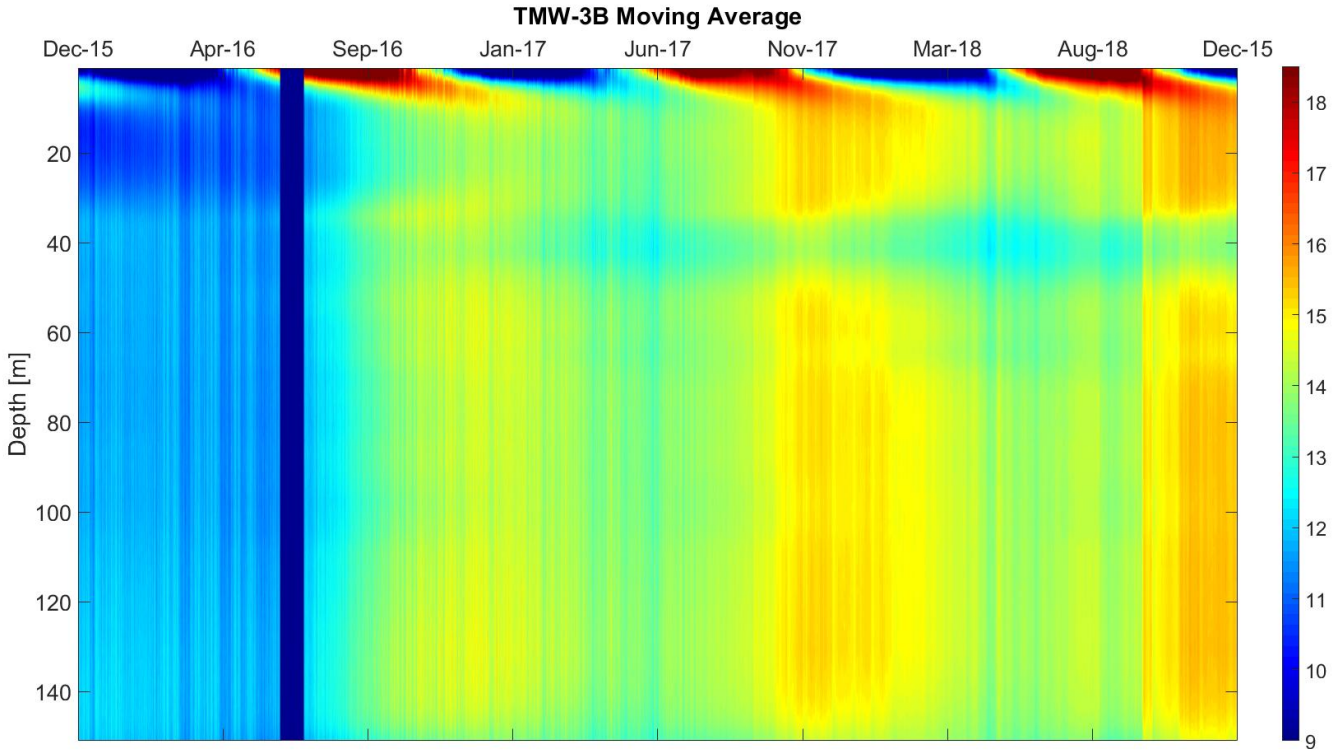

Figure 53. Discretized average gamma calibration figure with moving average applied for TMW-3B.

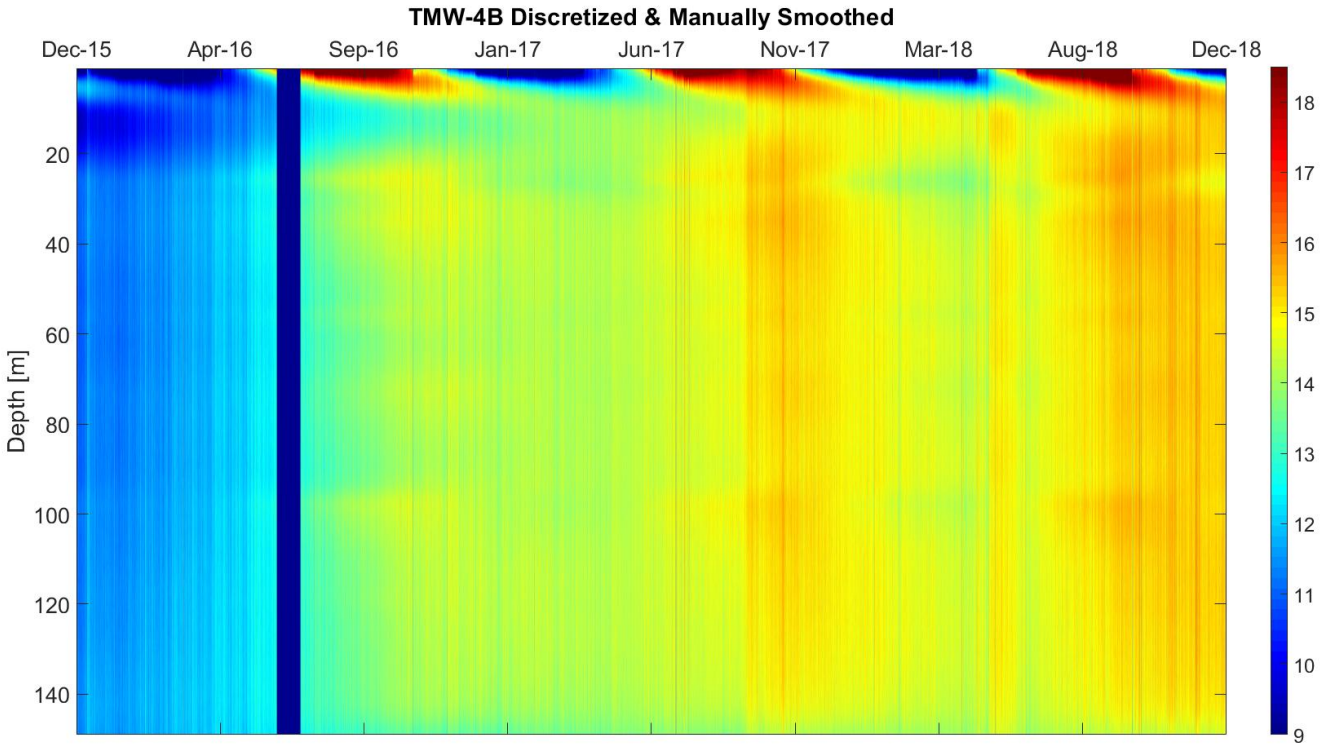

Figure 54. Discretized average gamma calibration and manual smoothing using interpolation of calibrated temperatures for TMW-4B.

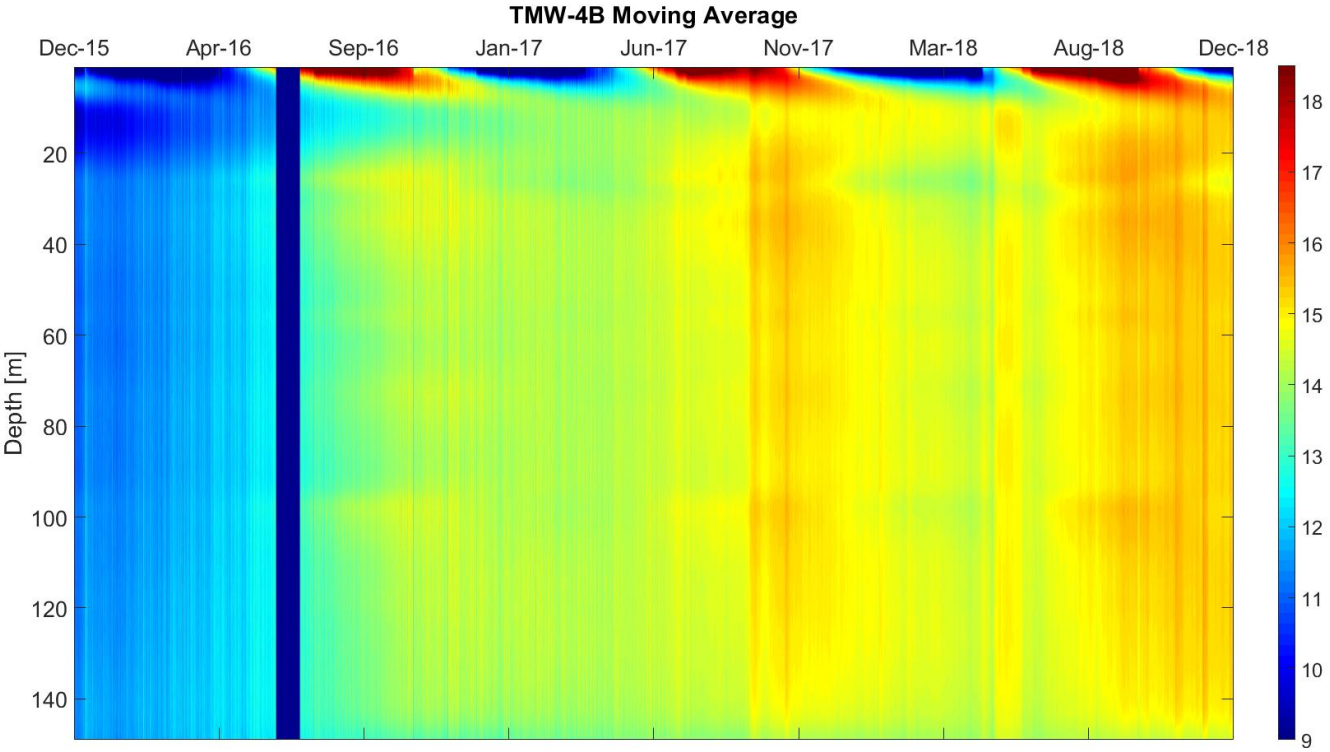

Figure 55. Discretized average gamma calibration figure with moving average applied for TMW-4B.

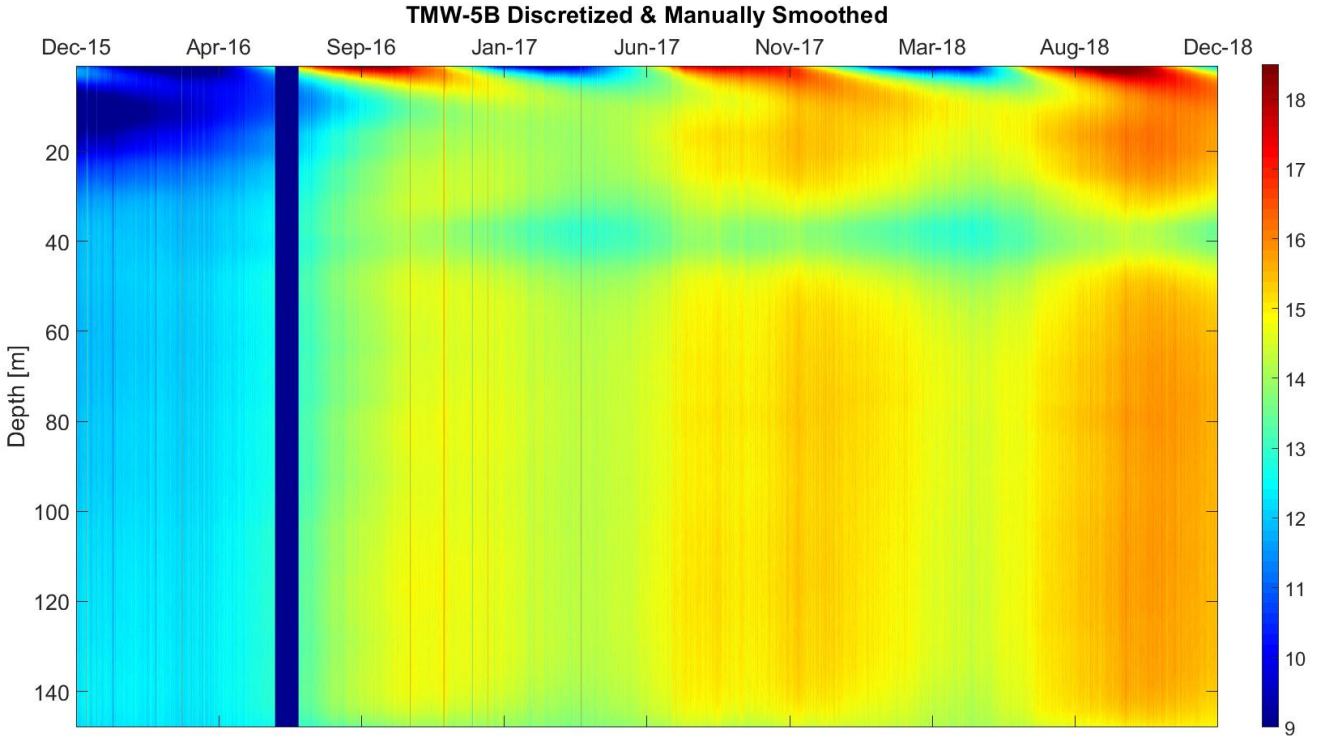

Figure 56. Discretized average gamma calibration and manual smoothing using interpolation of calibrated temperatures for TMW-5B.

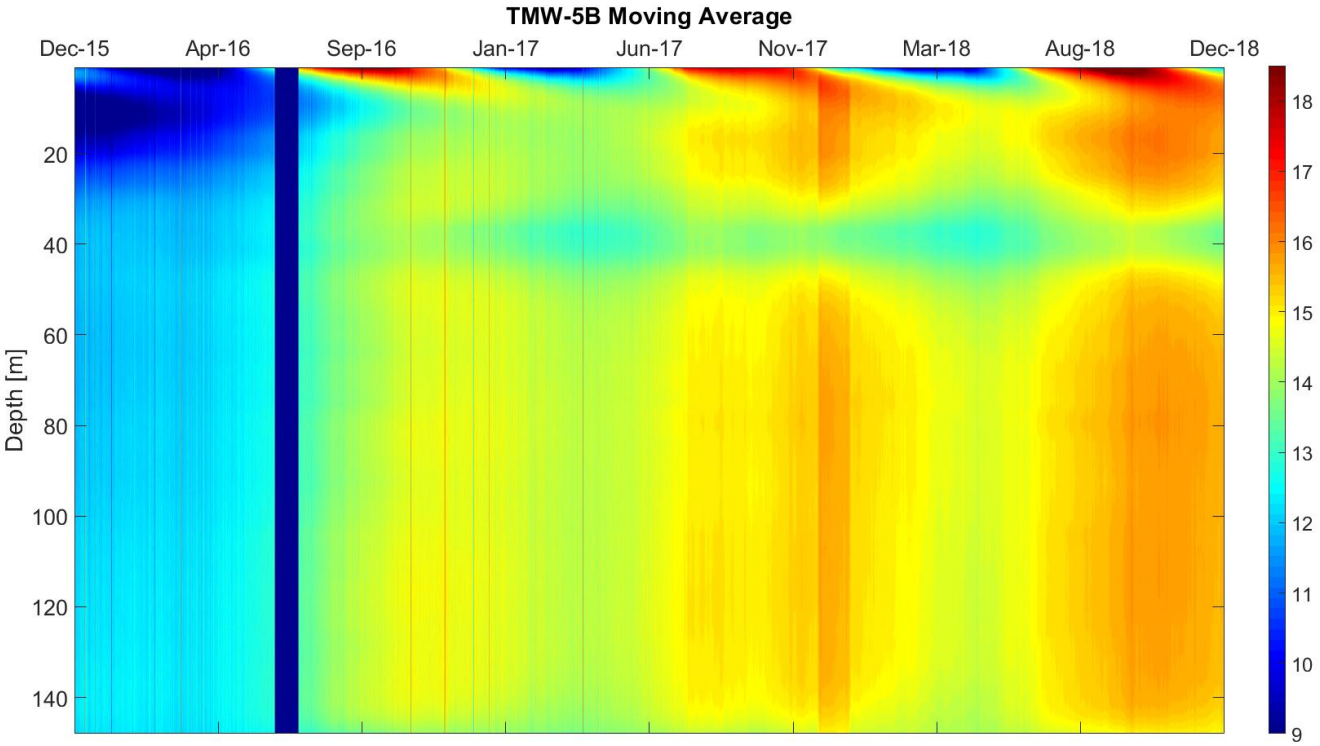

Figure 57. Discretized average gamma calibration figure with moving average applied for TMW-5B.

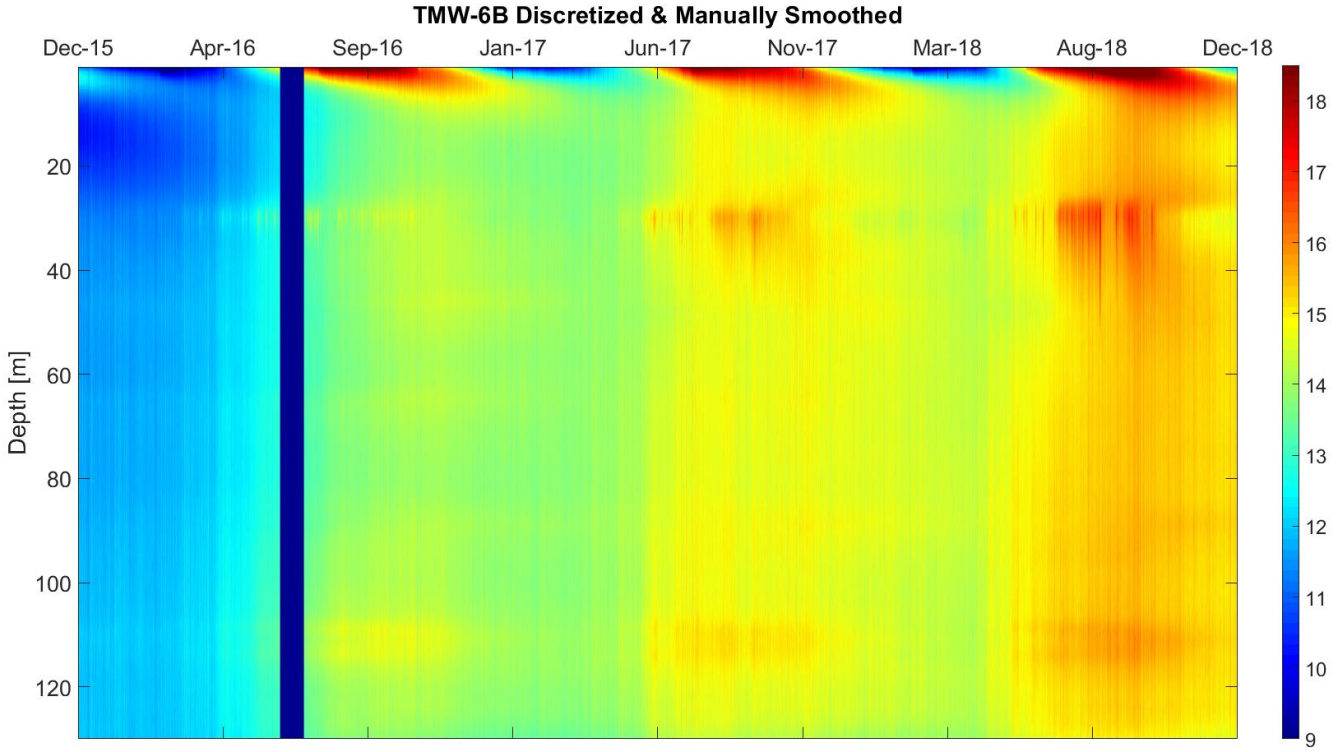

Figure 58. Discretized average gamma calibration and manual smoothing using interpolation of calibrated temperatures for TMW-6B.

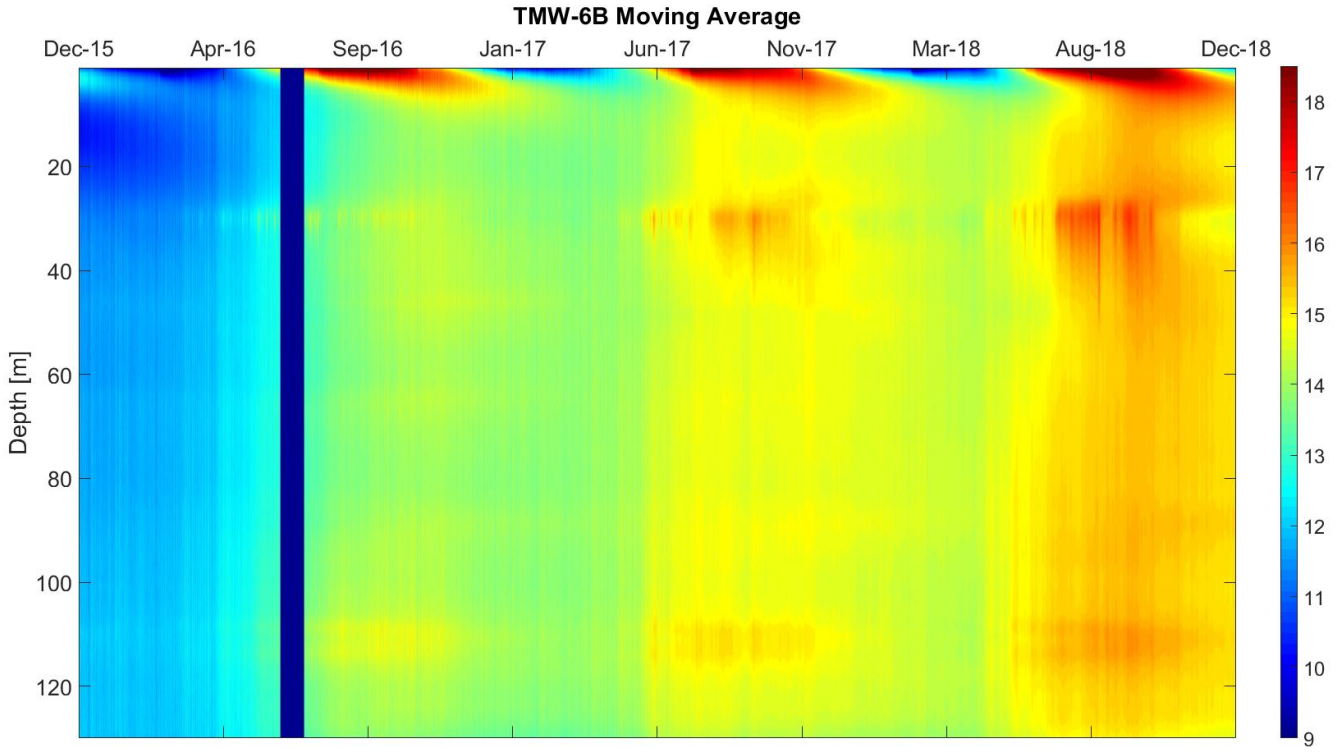

Figure 59. Discretized average gamma calibration figure with moving average applied for TMW-6B.

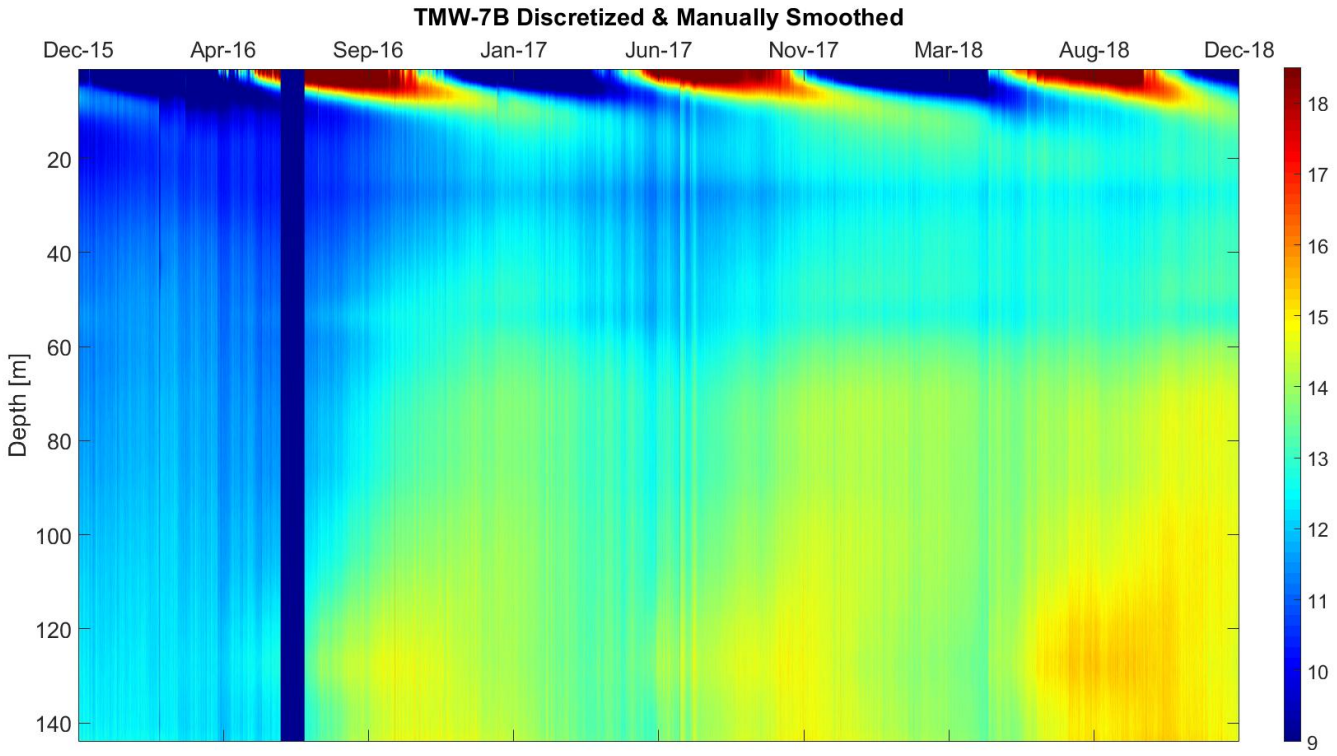

Figure 60. Discretized average gamma calibration and manual smoothing using interpolation of calibrated temperatures for TMW-7B.

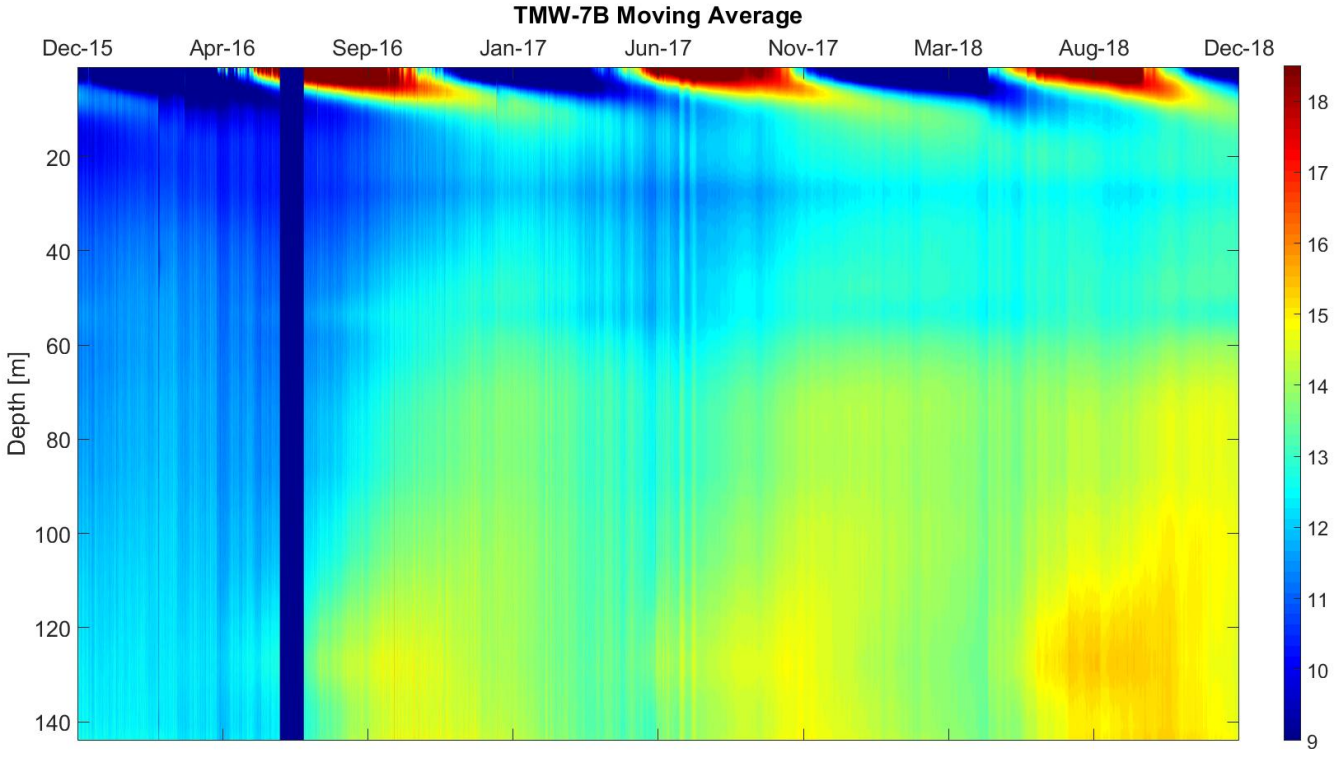

Figure 61. Discretized average gamma calibration figure with moving average applied for TMW-7B.

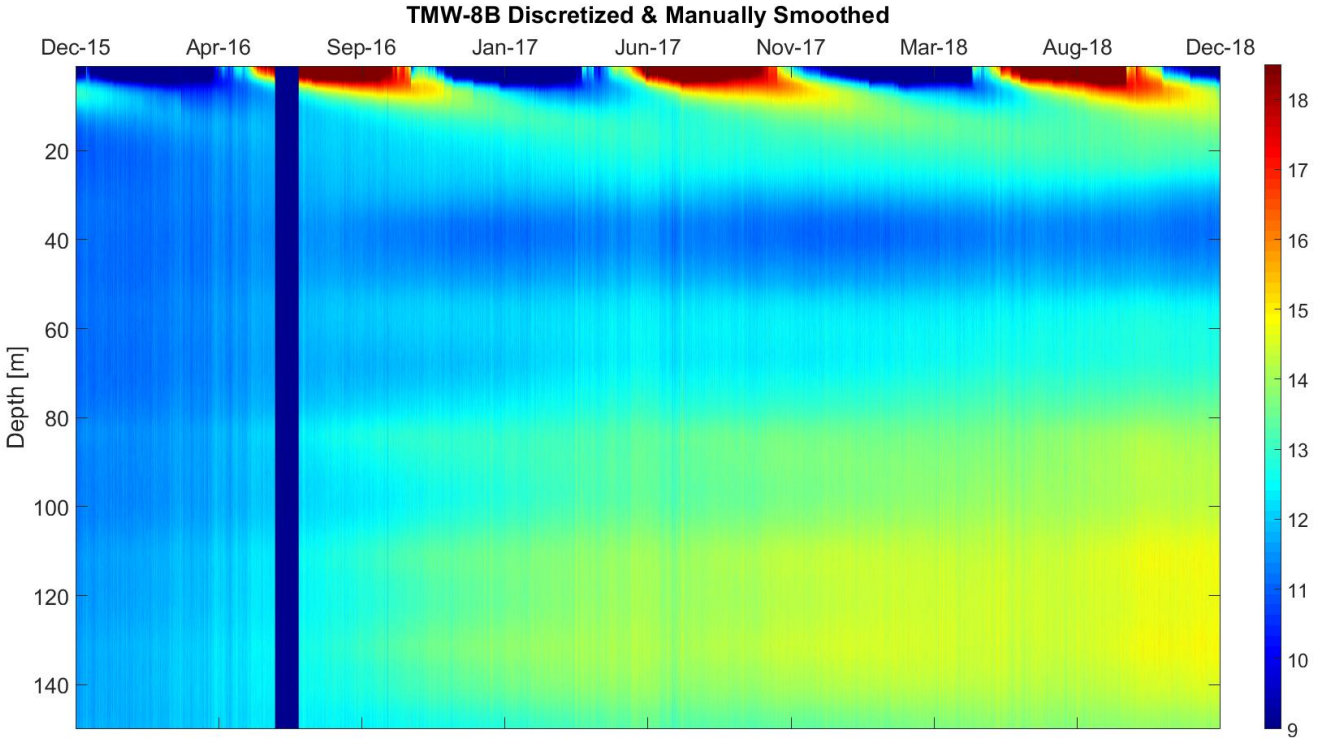

Figure 62. Discretized average gamma calibration and manual smoothing using interpolation of calibrated temperatures for TMW-8B.

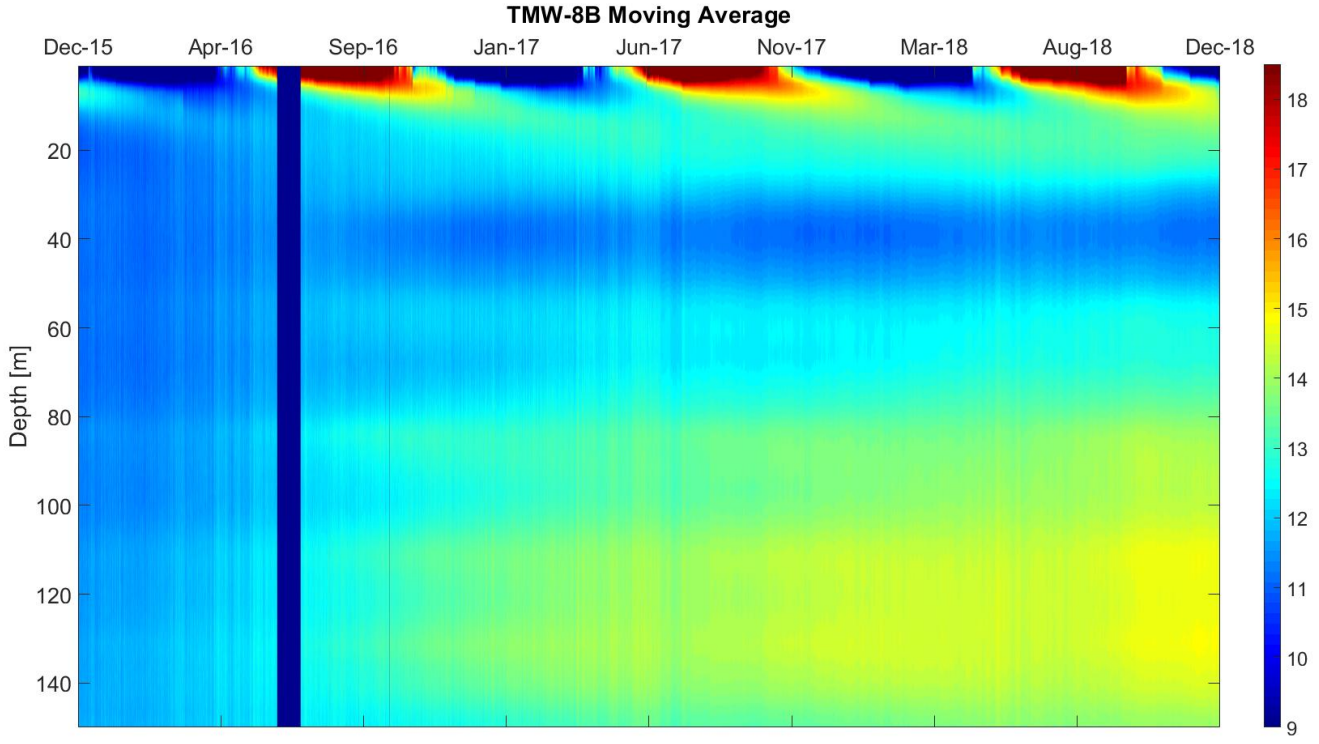

Figure 63. Discretized average gamma calibration figure with moving average applied for TMW-8B.

The color floods of the calibrated temperatures above show that the fluctuations in calibration bath temperature significantly affect the resulting calibration parameters. While using an average gamma and variable C value provides the most reliable calibrated temperature data, averaging a gamma value for the entirety of the data set will lead to miscalculated or noisy temperatures if the calibration bath temperatures are not held constant. The implementation of a refridgerator for the cold bath, rather than the use of an ambient bath that is subject to temperature variation, will help maintain and low and constant lower-bracket reference temperature. In turn, applying an average gamma for the temperatures collected since the implentation of the refrigerated cold bath will yield more reliable results with less noise, because there is little temperature flucuation in the fridge. It is important to continue to monitor the calilbration bath temperature with the thermistors so that any disruptions to the calibration setup can be documented.

Appendix B: Relevant Scripts and Data for Epic FO DTS Analysis and Heat Budget Calculation

Sample of Fixed Gamma calibration MATLAB script:

```
%%Calibration and Outputting of TMW-3B & TMW-4B Temperature Data for Epic
%%Real Time Onservation
clear
close
clc
%%Input data files
Process_Sensornet('E:\Research\Raw Data
Files\TMW3&4\2018\dec\',0,2127,'TMW34.mat');
load('TMW34.mat');
%%Averaged Fixed Gamma
GammaF_Average = 479.1551976;
GammaR_Average = 477.5144409;
%%Loop to run over multiple files
numfiles = size(Stokes,2);
%Prefine Multiple File Variables
GammaF = zeros(1,numfiles);
cF = zeros(1,numfiles);
GammaR = zeros(1,numfiles);
cR = zeros(1,numfiles);
DAsections = zeros(5,numfiles);
TMW3Keep = zeros(151,numfiles); %Length of TMW calibrated vector... can't use
variable since it is defined first.
TMW4Keep = zeros(149,numfiles);
RMSEKeep = zeros(5,numfiles);
TMW3CimKeep = zeros(5,numfiles);
TMW4CimKeep = zeros(5,numfiles);
for x = 1:numfiles
%%Flip reverse light data
AntiStokesR(:,x) = flipud(AntiStokesR(:,x)); %#ok<SAGROW>
StokesR(:,x) = flipud(StokesR(:,x)); %#ok<SAGROW>
%%Create raw local differential attenuation vector
indexend = length(distance);
EQ1 = zeros(indexend,1);
for i = 1:(indexend-1)
    EQ1(i) = (log(Stokes(i+1,x)/AntiStokes(i+1,x)) -
log(Stokes(i,x)/AntiStokes(i,x)) + log(StokesR(i,x)/AntiStokesR(i,x)) -
log(StokesR(i+1,x)/AntiStokesR(i+1,x)))/2;
end
%%Create raw cumulative differential attenuation vector
CumEQ1 = zeros(indexend,1);
for i = 2:(indexend-1)
   CumEQ1(i) = EQ1(i)+ CumEQ1(i-1);
end
CumEQ1(indexend) = CumEQ1(indexend-1);
%%Create vectors for natural log ratios forward and reverse
LnFor = log(Stokes(:,x)./AntiStokes(:,x));
LnRev = log(StokesR(:,x)./AntiStokesR(:,x));
%%Splice indexing
SP1B = 301;
SP1A = 308;
```

```
SP2B = 638;
SP2A = 647;
SP3B = 1049;
SP3A = 1058;
SP4B = 1365;
SP4A = 1374;
%%Bath indexing
B1B = 14;       %Hot
B1A = 25;       %Hot
B2B = 32;       %Cold
B2A = 45;       %Cold
B3B = 2038;     %Cold
B3A = 2052;     %Cold
B4B = 2059;     %Hot
B4A = 2071;     %Hot
%%Forward Splice Corrections
%Splice 1
FC1 = LnFor(SP1A) - LnFor(SP1B);
LnFor(SP1B:SP1A,1) = LnFor(SP1B);
LnFor(SP1A+1:indexend) = LnFor(SP1A+1:indexend)- FC1;
%Splice 2
FC2 = LnFor(SP2A) - LnFor(SP2B);
LnFor(SP2B:SP2A,1) = LnFor(SP2B);
LnFor(SP2A+1:indexend) = LnFor(SP2A+1:indexend)- FC2;
%Splice 3
FC3 = LnFor(SP3A) - LnFor(SP3B);
LnFor(SP3B:SP3A,1) = LnFor(SP3B);
LnFor(SP3A+1:indexend) = LnFor(SP3A+1:indexend)- FC3;
%Splice 4
FC4 = LnFor(SP4A) - LnFor(SP4B);
LnFor(SP4B:SP4A,1) = LnFor(SP4B);
LnFor(SP4A+1:indexend) = LnFor(SP4A+1:indexend)- FC4;
%%Reverse Splice Corrections
%Splice 4
RC4 = LnRev(SP4B) - LnRev(SP4A);
LnRev(SP4B:SP4A,1) = LnRev(SP4A);
LnRev(1:SP4B-1,1) = LnRev(1:SP4B-1) - RC4;
%Splice 3
RC3 = LnRev(SP3B) - LnRev(SP3A);
LnRev(SP3B:SP3A,1) = LnRev(SP3A);
LnRev(1:SP3B-1,1) = LnRev(1:SP3B-1) - RC3;
%Splice 2
RC2 = LnRev(SP2B) - LnRev(SP2A);
LnRev(SP2B:SP2A,1) = LnRev(SP2A);
LnRev(1:SP2B-1,1) = LnRev(1:SP2B-1) - RC2;
%Splice 1
RC1 = LnRev(SP1B) - LnRev(SP1A);
LnRev(SP1B:SP1A,1) = LnRev(SP1A);
%%Create corrected local differential attenuation vector
CorrectedEQ1 = zeros(indexend,1);
for i = 1:(indexend-1)
CorrectedEQ1(i) = (LnFor(i+1) - LnFor(i) + LnRev(i) - LnRev(i+1))/2;
end
%%Create corrected cumulative differential attenuation vector
CorrectedCumEQ1 = zeros(indexend,1);
for i = 2:(indexend-1)
   CorrectedCumEQ1(i) = CorrectedEQ1(i)+ CorrectedCumEQ1(i-1);
```

```
end
CorrectedCumEQ1(indexend) = CorrectedCumEQ1(indexend-1);
%%Find Sectional Differential Attenuations
A = CorrectedCumEQ1;
B = ones(indexend,2);
B(:,2) = distance;
DA = zeros(5,1);
%Section 1
A1 = A(50:SP1B-1);
B1 = B(50:SP1B-1,:);
X1 = B1\A1;
DA(1) = X1(2);
%Section 2
A1 = A(SP1A:SP2B-1);
B1 = B(SP1A:SP2B-1,:);
X1 = B1\A1;
DA(2) = X1(2);
%Section 3
A2 = A(SP2A:SP3B-1);
B2 = B(SP2A:SP3B-1,:);
X2 = B2\A2;
DA(3) = X2(2);
%Section 4
A3 = A(SP3A:SP4B-1);
B3 = B(SP3A:SP4B-1,:);
X3 = B3\A3;
DA(4) = X3(2);
%Section 5
A4 = A(SP4A:2034);
B4 = B(SP4A:2034,:);
X4 = B4\A4;
DA(5) = X4(2);
%%Creation of Piecewise Linear Function
PWF = zeros(indexend,1);
n = 1;
%Section 1
while n<=SP1B+2
PWF(n) = distance(n)*DA(1);
n = n+1;
end
%Section 2
while n<=SP2B+2
PWF(n) = PWF(SP1B+2)+ (distance(n)-distance(SP1B+2))*DA(2);
n = n+1;
end
%Section 3
while n<=SP3B+2
PWF(n) = PWF(SP2B+2)+ (distance(n)-distance(SP2B+2))*DA(3);
n = n+1;
end
%Section 4
while n<=SP4B+2
PWF(n) = PWF(SP3B+2)+ (distance(n)-distance(SP3B+2))*DA(4);
n = n+1;
end
%Section 5
while n<=indexend
```

```
PWF(n) = PWF(SP4B+2)+ (distance(n)-distance(SP4B+2))*DA(5);
n = n+1;
end
%%Determine Calibration Parameters
%Bath 1                              %Hot
T_1 = tref_1(1,x) + 273.15;
Ratio_1F = mean(LnFor(B1B:B1A));
Ratio_1R = mean(LnRev(B1B:B1A));
PWF_1 = mean(PWF(B1B:B1A));
%Bath 2                              %Cold
T_2 = tref_2(1,x) + 273.15;
Ratio_2F = mean(LnFor(B2B:B2A));
Ratio_2R = mean(LnRev(B2B:B2A));
PWF_2 = mean(PWF(B2B:B2A));
%Bath 3                              %Cold
T_3 = tref_2(1,x) + 273.15;
Ratio_3F = mean(LnFor(B3B:B3A));
Ratio_3R = mean(LnRev(B3B:B3A));
PWF_3 = mean(PWF(B3B:B3A));
%Bath 4
T_4 = tref_1(1,x) + 273.15;         %Hot
Ratio_4F = mean(LnFor(B4B:B4A));
Ratio_4R = mean(LnRev(B4B:B4A));
PWF_4 = mean(PWF(B4B:B4A));
% % Forward
% AF = [1,-T_1;1,-T_2;1,-T_3;1,-T_4];
% BF = [T_1*(Ratio_1F-PWF_1);T_2*(Ratio_2F-PWF_2);T_3*(Ratio_3F-
PWF_3);T_4*(Ratio_4F-PWF_4)];
% XF = AF\BF;
% Gamma_Forward = XF(1);
% C_Forward = XF(2);
C_Forward1 = GammaF_Average/T_1 + PWF_1 - Ratio_1F;
C_Forward2 = GammaF_Average/T_2 + PWF_2 - Ratio_2F;
C_Forward3 = GammaF_Average/T_3 + PWF_3 - Ratio_3F;
C_Forward4 = GammaF_Average/T_4 + PWF_4 - Ratio_4F;
C_Forward = (C_Forward1 + C_Forward2 + C_Forward3 + C_Forward4)/4;
% %Reverse
% AR = [1,-T_1;1,-T_2;1,-T_3;1,-T_4];
% BR = [T_1*(Ratio_1R-PWF_1);T_2*(Ratio_2R-PWF_2);T_3*(Ratio_3R-
PWF_3);T_4*(Ratio_4R-PWF_4)];
% XR = AR\BR;
% Gamma_Reverse = XR(1);
% C_Reverse = XR(2);
C_Reverse1 = GammaR_Average/T_1 + PWF_1 - Ratio_1R;
C_Reverse2 = GammaR_Average/T_2 + PWF_2 - Ratio_2R;
C_Reverse3 = GammaR_Average/T_3 + PWF_3 - Ratio_3R;
C_Reverse4 = GammaR_Average/T_4 + PWF_4 - Ratio_4R;
C_Reverse = (C_Reverse1 + C_Reverse2 + C_Reverse3 + C_Reverse4)/4;
%%Calibrated Temperatures
%Forward
ForwardTemp = zeros(indexend,1);
for i = 1:indexend
ForwardTemp(i) = GammaF_Average/(LnFor(i)+C_Forward-PWF(i)) - 273.15;
end
%Reverse
ReverseTemp = zeros(indexend,1);
LnRev2 = flipud(LnRev);
```

```
for i = 1:indexend
ReverseTemp(i) = GammaR_Average/(LnRev2(i)+C_Reverse-PWF(i)) - 273.15;
end
ReverseTemp = flipud(ReverseTemp);
%Average of Forward and Reverse Calibrations
CalTemp = (ReverseTemp+ForwardTemp)/2;
%%Create TMW-3B Temperature with Depth Orientation
%Pull Temperatures
TMW3Entry = 315;
TMW3Bottom = 465;
TMW3Exit = 615;
TMW3Down = CalTemp(TMW3Entry:TMW3Bottom,1);
TMW3Up = CalTemp(TMW3Bottom:TMW3Exit,1); %May need to change TMW1Bottom+1 /
TMW1Bottom if the vectors are not the same size (perfectly symmetrical).
TMW3Up = flipud(TMW3Up);
TMW3 = (TMW3Down+TMW3Up)/2;
TMW3F = TMW3*(9/5)+32; %Convert Celcius temperatures into Fahrenheight
%Apply appropriate depths to Temperatures
TMW3Depthm = distance(TMW3Entry:TMW3Bottom) - distance(TMW3Entry);
TMW3Depthft = TMW3Depthm .* 3.28084; %Convert meters to feet
%%Find TMW-3B Temperatures at 100 ft intervals for Cimplicity
TMW3Cim = zeros(5,2);      %%Temperature Monitoring Well 3B Temperature with
Depth
i=1;
for n = 1:4
while TMW3Depthft(i)<=100*n
    i = i+1;
    TMW3Cim(n,2) = (TMW3F(i)+TMW3F(i-1)+TMW3F(i+1))/3;
    TMW3Cim(n,1) = TMW3Depthft(i);
end
end
%Bottom of the well values inputed into 500 ft vector
TMW3Cim(5,2) = TMW3F(length(TMW3));
TMW3Cim(5,1) = TMW3Depthft(length(TMW3));
%%Create TMW-4B Temperature with Depth Orientation
%Pull Temperatures
TMW4Entry = 1064;
TMW4Bottom = 1212;
TMW4Exit = 1360;
TMW4Down = CalTemp(TMW4Entry:TMW4Bottom,1);
TMW4Up = CalTemp(TMW4Bottom:TMW4Exit,1);
TMW4Up = flipud(TMW4Up);
TMW4 = (TMW4Down+TMW4Up)/2;
TMW4F = TMW4*(9/5)+32; %Convert Temperatures from Celcius to Fahrenheight
%Apply appropriate depths to Temperatures
TMW4Depthm = distance(TMW4Entry:TMW4Bottom) - distance(TMW4Entry);
TMW4Depthft = TMW4Depthm .* 3.28084;    %Convert meters to feet
%%Find TMW-4B Temperatures at 100 ft intervals for Cimplicity
TMW4Cim = zeros(5,2);      %%Temperature Monitoring Well 4B Temperature with
Depth
i=1;
for n = 1:4
while TMW4Depthft(i)<=100*n
    i = i+1;
    TMW4Cim(n,2) = (TMW4F(i)+TMW4F(i-1)+TMW4F(i+1))/3;
    TMW4Cim(n,1) = TMW4Depthft(i);
end
```

```
end
%Bottom of the well values inputed into 500 ft vector
TMW4Cim(5,2) = TMW4F(length(TMW4));
TMW4Cim(5,1) = TMW4Depthft(length(TMW4));
CimMatrix = zeros(12,2);
CimMatrix(2:6,:) = TMW3Cim;
CimMatrix(8:12,:) = TMW4Cim;
% %Create File for Cimplicity Location
% csvwrite('cimplicityfiberfile.csv',CimMatrix);
%Calculate RMSE of Baths %
Bath1Error = (CalTemp(B1B:B1A) - tref_1(1,x)).^2;
B1_RMSE = sqrt(sum(Bath1Error)/length(Bath1Error));

Bath2Error = (CalTemp(B2B:B2A) - tref_2(1,x)).^2;
B2_RMSE = sqrt(sum(Bath2Error)/length(Bath2Error));

Bath3Error = (CalTemp(B3B:B3A) - tref_2(1,x)).^2;
B3_RMSE = sqrt(sum(Bath3Error)/length(Bath3Error));

Bath4Error = (CalTemp(B4B:B4A) - tref_1(1,x)).^2;
B4_RMSE = sqrt(sum(Bath4Error)/length(Bath4Error));

AvgRMSE = (B1_RMSE+B2_RMSE+B3_RMSE+B4_RMSE)/4;
RMSE = [B1_RMSE;B2_RMSE;B3_RMSE;B4_RMSE;AvgRMSE];
%Keep track of variables of Interest
%%Keep Track of Variables of Interest
% GammaF(1,x) = Gamma_Forward;
cF(1,x) = C_Forward;
% GammaR(1,x) = Gamma_Reverse;
cR(1,x) = C_Reverse;
DAsections(:,x) = DA;
TMW3Keep(:,x) = TMW3;
TMW4Keep(:,x) = TMW4;
RMSEKeep(:,x) = RMSE;
TMW3CimKeep(:,x) = TMW3Cim(:,2);
TMW4CimKeep(:,x) = TMW4Cim(:,2);
end
```

Matlab Script for Data Visualization:

```
%%Data Visualization for TMW-3B and TMW-4B
clear
close
clc
cd('E:\Research\Matlab Files for Vis');
load('TMW-34_MonthlyFixed_Gamma.mat') %New monthly fixed gamma
%TMW-3B Plot
startDate = datenum('12-03-2015');
endDate = datenum('12-31-2018');
xData = linspace(startDate,endDate,8);
figure
contour(Time,Depth3,TMW3);
pcolor(TMW3);
shading interp;
shading interp;
set(gca,'XAxisLocation','top','YAxisLocation','left','ydir','reverse','FontSi
ze',20,'layer','top');
ylabel('Depth [m]');
title('TMW-3B All Data');
% xticklabels({'Dec-15','Apr-16','Sep-16','Jan-17','Jun-17','Nov-17','Mar-
18','Aug-18','Dec-18'})
%% x-axis labeling %%COMMENT ME OUT TO SHOW COLOR
ax = gca;
ax.XTick = xData;
datetick('x','mmm-yy','keepticks');
hold on
%colorbar coloring
colormap jet
colorbar
caxis([9 18.5]) %%49 - 65 F
%%%%%%%%%%%%%%%%%%%%%%%%%%%%%%
%TMW-4B Plot
startDate = datenum('12-03-2015');
endDate = datenum('12-31-2018');
xData = linspace(startDate,endDate,9);
figure
contour(Time,Depth4,TMW4);
pcolor(TMW4);
shading interp;
shading interp;
set(gca,'XAxisLocation','top','YAxisLocation','left','ydir','reverse','FontSi
ze',20,'layer','top');
ylabel('Depth [m]');
title('TMW-4B All Data');
% xticklabels({'Dec-15','Apr-16','Sep-16','Jan-17','Jun-17','Nov-17','Mar-
18','Aug-18','Dec-18'})
%%x-axis labeling %% COMMENT ME OUT TO SHOW COLOR
ax = gca;
ax.XTick = xData;
datetick('x','mmm-yy','keepticks'); %trial date line
hold on
%colorbar coloring
colormap jet
colorbar
caxis([9 18.5])
```

Matlab Script for collecting Epic Operations Data:

```
%%Borefield Heat Flow, Internal Building Heat Flow, and Mechanical Energy
%%Tracking Script
clear
close all
clc
%%Define the number of excel files and number of datapoints pulled from
%%each one.
path = cd('E:\LT RA\Heat Budget\Epic Power Data\Geo data\2019\jan');  %%ENTER
HERE THE FOLDER NAME WHERE FILES ARE STORED
listgeofiles = dir('*.csv');
numgeofiles = numel(listgeofiles); %%number of days/excel files to read.
datapoints = 96; %number of datapoints in the given file - datapoint every 15
minutes for 1 day (24*4)
%%Define Relevant Constants - Metric Units
Rho = 999.6018;    %%kg/m^3, taken at 11 [C] - average temperature of water
Cp = 4.186; %%kJ/kg*C

%%Borefield Heat Flow Section
%%Predefine Loop Vector Sizes
%%Borefield 1
BF1ST = zeros(datapoints,numgeofiles);
BF1RT = zeros(datapoints,numgeofiles);
BF1F = zeros(datapoints,numgeofiles);
BF1Q = zeros(datapoints,numgeofiles);
BF1 = zeros(numgeofiles,1);
%%Borefield 2
BF2ST = zeros(datapoints,numgeofiles);
BF2RT = zeros(datapoints,numgeofiles);
BF2F = zeros(datapoints,numgeofiles);
BF2Q = zeros(datapoints,numgeofiles);
BF2 = zeros(numgeofiles,1);
%%Borefield 3
BF3ST = zeros(datapoints,numgeofiles);
BF3RT = zeros(datapoints,numgeofiles);
BF3F = zeros(datapoints,numgeofiles);
BF3Q = zeros(datapoints,numgeofiles);
BF3 = zeros(numgeofiles,1);
%%Borefield 4
BF4ST = zeros(datapoints,numgeofiles);
BF4RT = zeros(datapoints,numgeofiles);
BF4F = zeros(datapoints,numgeofiles);
BF4Q = zeros(datapoints,numgeofiles);
BF4 = zeros(numgeofiles,1);
%%Pond
P10ST = zeros(datapoints,numgeofiles);
P10RT = zeros(datapoints,numgeofiles);
P11ST = zeros(datapoints,numgeofiles);
P11RT = zeros(datapoints,numgeofiles);
PF = zeros(datapoints,numgeofiles);
PQ = zeros(datapoints,numgeofiles);
Pond = zeros(numgeofiles,1);
%%Total Heat from geothermal system by Day
GeoHeat = zeros(numgeofiles,1);
```

```
%%Geowater to Outside of Buildings Section
%%Building 1
C1_B1_ST = zeros(datapoints,numgeofiles);
C1_B1_RT = zeros(datapoints,numgeofiles);
C1_B1_F = zeros(datapoints,numgeofiles);
C1_B1_Q = zeros(datapoints,numgeofiles);
C1_B1_Q_Daily = zeros(numgeofiles,1);
%%Building 2
C1_B2_ST = zeros(datapoints,numgeofiles);
C1_B2_RT = zeros(datapoints,numgeofiles);
C1_B2_F = zeros(datapoints,numgeofiles);
C1_B2_Q = zeros(datapoints,numgeofiles);
C1_B2_Q_Daily = zeros(numgeofiles,1);
%%Building 3
C1_B3_ST = zeros(datapoints,numgeofiles);
C1_B3_RT = zeros(datapoints,numgeofiles);
C1_B3_F = zeros(datapoints,numgeofiles);
C1_B3_Q = zeros(datapoints,numgeofiles);
C1_B3_Q_Daily = zeros(numgeofiles,1);
%%Building 4
C1_B4_ST = zeros(datapoints,numgeofiles);
C1_B4_RT = zeros(datapoints,numgeofiles);
C1_B4_F = zeros(datapoints,numgeofiles);
C1_B4_Q = zeros(datapoints,numgeofiles);
C1_B4_Q_Daily = zeros(numgeofiles,1);
%%Building 5
C1_B5_ST = zeros(datapoints,numgeofiles);
C1_B5_RT = zeros(datapoints,numgeofiles);
C1_B5_F = zeros(datapoints,numgeofiles);
C1_B5_Q = zeros(datapoints,numgeofiles);
C1_B5_Q_Daily = zeros(numgeofiles,1);
%%Building 6
C1_B6_ST = zeros(datapoints,numgeofiles);
C1_B6_RT = zeros(datapoints,numgeofiles);
C1_B6_F = zeros(datapoints,numgeofiles);
C1_B6_Q = zeros(datapoints,numgeofiles);
C1_B6_Q_Daily = zeros(numgeofiles,1);
%%Campus 1 Total
C1_Q = zeros(datapoints,numgeofiles);
C1_Q_Daily = zeros(numgeofiles,1);
%%Campus 2
C2_ST = zeros(datapoints,numgeofiles);
C2_RT = zeros(datapoints,numgeofiles);
C2_F = zeros(datapoints,numgeofiles);
C2_Q = zeros(datapoints,numgeofiles);
C2_Q_Daily = zeros(numgeofiles,1);
%%Learning Campus
LC_ST = zeros(datapoints,numgeofiles);
LC_RT = zeros(datapoints,numgeofiles);
LC_F = zeros(datapoints,numgeofiles);
LC_Q = zeros(datapoints,numgeofiles);
LC_Q_Daily = zeros(numgeofiles,1);
%%Learning Campus
DS_ST = zeros(datapoints,numgeofiles);
DS_RT = zeros(datapoints,numgeofiles);
DS_F = zeros(datapoints,numgeofiles);
DS_Q = zeros(datapoints,numgeofiles);
```

```
DS_Q_Daily = zeros(numgeofiles,1);
%%FARM "internal"
FARM_ST = zeros(datapoints,numgeofiles);
FARM_RT = zeros(datapoints,numgeofiles);
FARM_F = zeros(datapoints,numgeofiles);
FARM_Q = zeros(datapoints,numgeofiles);
FARM_Q_Daily = zeros(numgeofiles,1);
%%Total Buildings
Buildings_Q_Daily = zeros(numgeofiles,1);
%%UBENDvsRYGAN
UBEND_ST = zeros(datapoints,numgeofiles);
UBEND_RT = zeros(datapoints,numgeofiles);
UBEND_F = zeros(datapoints,numgeofiles);
UBEND_Q = zeros(datapoints,numgeofiles);
UBEND_Q_Daily = zeros(numgeofiles,1);
UBEND_avgF_Daily = zeros(numgeofiles,1);
UBEND_running_ST = zeros(numgeofiles*datapoints,1);
UBEND_running_RT = zeros(numgeofiles*datapoints,1);
UBEND_F_running = zeros(numgeofiles*datapoints,1);
RYGAN_ST = zeros(datapoints,numgeofiles);
RYGAN_RT = zeros(datapoints,numgeofiles);
RYGAN_F = zeros(datapoints,numgeofiles);
RYGAN_Q = zeros(datapoints,numgeofiles);
RYGAN_Q_Daily = zeros(numgeofiles,1);
RYGAN_avgF_Daily = zeros(numgeofiles,1);
RYGAN_running_ST = zeros(numgeofiles*datapoints,1);
RYGAN_running_RT = zeros(numgeofiles*datapoints,1);
RYGAN_F_running = zeros(numgeofiles*datapoints,1);
%%Internal Building Heat Flow Section
%Internal Campus 1 Building 1
INT_C1B1_HWS = zeros(datapoints,numgeofiles);
INT_C1B1_HWR = zeros(datapoints,numgeofiles);
INT_C1B1_F = zeros(datapoints,numgeofiles);
INT_C1B1_Q = zeros(datapoints,numgeofiles);
INT_C1B1_Q_Daily = zeros(numgeofiles,1);
%Internal Campus 1 Building 2
INT_C1B2_HWS = zeros(datapoints,numgeofiles);
INT_C1B2_HWR = zeros(datapoints,numgeofiles);
INT_C1B2_F = zeros(datapoints,numgeofiles);
INT_C1B2_Q = zeros(datapoints,numgeofiles);
INT_C1B2_Q_Daily = zeros(numgeofiles,1);
%Internal Campus 1 Building 4
INT_C1B4_HWS = zeros(datapoints,numgeofiles);
INT_C1B4_HWR = zeros(datapoints,numgeofiles);
INT_C1B4_F = zeros(datapoints,numgeofiles);
INT_C1B4_Q = zeros(datapoints,numgeofiles);
INT_C1B4_Q_Daily = zeros(numgeofiles,1);
%Internal Campus 1 Building 5
INT_C1B5_HWS = zeros(datapoints,numgeofiles);
INT_C1B5_HWR = zeros(datapoints,numgeofiles);
INT_C1B5_F = zeros(datapoints,numgeofiles);
INT_C1B5_Q = zeros(datapoints,numgeofiles);
INT_C1B5_Q_Daily = zeros(numgeofiles,1);
%Internal Campus 1 Building 6
INT_C1B6_HWS = zeros(datapoints,numgeofiles);
INT_C1B6_HWR = zeros(datapoints,numgeofiles);
INT_C1B6_F = zeros(datapoints,numgeofiles);
```

```
INT_C1B6_Q = zeros(datapoints,numgeofiles);
INT_C1B6_Q_Daily = zeros(numgeofiles,1);
%%Internal Campus 2 Total Hot Water
INT_C2TOT_HWS = zeros(datapoints,numgeofiles);
INT_C2TOT_HWR = zeros(datapoints,numgeofiles);
INT_C2TOT_F = zeros(datapoints,numgeofiles);
INT_C2TOT_Q = zeros(datapoints,numgeofiles);
INT_C2TOT_Q_Daily = zeros(numgeofiles,1);
%%Internal Campus 2 Total Chilled Water
INT_C2TOT_CHWS = zeros(datapoints,numgeofiles);
INT_C2TOT_CHWR = zeros(datapoints,numgeofiles);
INT_C2TOT_CWF = zeros(datapoints,numgeofiles);
INT_C2TOT_CWQ = zeros(datapoints,numgeofiles);
INT_C2TOT_CWQ_Daily = zeros(numgeofiles,1);
%%Internal Campus 2 Building K (Kouhotek) Hot Water
INT_C2K_HWS = zeros(datapoints,numgeofiles);
INT_C2K_HWR = zeros(datapoints,numgeofiles);
INT_C2K_F = zeros(datapoints,numgeofiles);
INT_C2K_Q = zeros(datapoints,numgeofiles);
INT_C2K_Q_Daily = zeros(numgeofiles,1);
%%Internal Campus 2 Building K (Kouhotek) Chilled Water
INT_C2K_CHWS = zeros(datapoints,numgeofiles);
INT_C2K_CHWR = zeros(datapoints,numgeofiles);
INT_C2K_CWF = zeros(datapoints,numgeofiles);
INT_C2K_CWQ = zeros(datapoints,numgeofiles);
INT_C2K_CWQ_Daily = zeros(numgeofiles,1);
%%Internal Learning Center
INT_LC_HWS = zeros(datapoints,numgeofiles);
INT_LC_HWR = zeros(datapoints,numgeofiles);
INT_LC_F = zeros(datapoints,numgeofiles);
INT_LC_Q = zeros(datapoints,numgeofiles);
INT_LC_Q_Daily = zeros(numgeofiles,1);
%%Internal Campus 4/5 Hot Water
INT_C45_HWS = zeros(datapoints,numgeofiles);
INT_C45_HWR = zeros(datapoints,numgeofiles);
INT_C45_F = zeros(datapoints,numgeofiles);
INT_C45_Q = zeros(datapoints,numgeofiles);
INT_C45_Q_Daily = zeros(numgeofiles,1);
%%Internal Campus 4/5  Chilled Water
INT_C45_CHWS = zeros(datapoints,numgeofiles);
INT_C45_CHWR = zeros(datapoints,numgeofiles);
INT_C45_CWF = zeros(datapoints,numgeofiles);
INT_C45_CWQ = zeros(datapoints,numgeofiles);
INT_C45_CWQ_Daily = zeros(numgeofiles,1);
%%Internal Farm Campus Hot Water
INT_DS_HWS = zeros(datapoints,numgeofiles);
INT_DS_HWR = zeros(datapoints,numgeofiles);
INT_DS_F = zeros(datapoints,numgeofiles);
INT_DS_Q = zeros(datapoints,numgeofiles);
INT_DS_Q_Daily = zeros(numgeofiles,1);
%%Internal Farm Campus  Chilled Water
INT_DS_CHWS = zeros(datapoints,numgeofiles);
INT_DS_CHWR = zeros(datapoints,numgeofiles);
INT_DS_CWF = zeros(datapoints,numgeofiles);
INT_DS_CWQ = zeros(datapoints,numgeofiles);
INT_DS_CWQ_Daily = zeros(numgeofiles,1);
```

```
%%Internal FARM Hot Water
INT_FARM_HWS = zeros(datapoints,numgeofiles);
INT_FARM_HWR = zeros(datapoints,numgeofiles);
INT_FARM_F = zeros(datapoints,numgeofiles);
INT_FARM_Q = zeros(datapoints,numgeofiles);
INT_FARM_Q_Daily = zeros(numgeofiles,1);
%%Internal FARM 4/5  Chilled Water
INT_FARM_CHWS = zeros(datapoints,numgeofiles);
INT_FARM_CHWR = zeros(datapoints,numgeofiles);
INT_FARM_CWF = zeros(datapoints,numgeofiles);
INT_FARM_CWQ = zeros(datapoints,numgeofiles);
INT_FARM_CWQ_Daily = zeros(numgeofiles,1);
%%Internal Campus UB3 Hot Water
INT_UB3_HWS = zeros(datapoints,numgeofiles);
INT_UB3_HWR = zeros(datapoints,numgeofiles);
INT_UB3_F = zeros(datapoints,numgeofiles);
INT_UB3_Q = zeros(datapoints,numgeofiles);
INT_UB3_Q_Daily = zeros(numgeofiles,1);
%%Internal Campus UB3  Chilled Water
INT_UB3_CHWS = zeros(datapoints,numgeofiles);
INT_UB3_CHWR = zeros(datapoints,numgeofiles);
INT_UB3_CWF = zeros(datapoints,numgeofiles);
INT_UB3_CWQ = zeros(datapoints,numgeofiles);
INT_UB3_CWQ_Daily = zeros(numgeofiles,1);
%%Campus UB3  Heat Exchangers
INT_UB3_HXS = zeros(datapoints,numgeofiles);
INT_UB3_HXR = zeros(datapoints,numgeofiles);
INT_UB3_HXF = zeros(datapoints,numgeofiles);
INT_UB3_HXQ = zeros(datapoints,numgeofiles);
INT_UB3_HXQ_Daily = zeros(numgeofiles,1);
%%Internal Pluto Hot Water
INT_PL_HWS = zeros(datapoints,numgeofiles);
INT_PL_HWR = zeros(datapoints,numgeofiles);
INT_PL_F = zeros(datapoints,numgeofiles);
INT_PL_Q = zeros(datapoints,numgeofiles);
INT_PL_Q_Daily = zeros(numgeofiles,1);
%%Internal Pluto Chilled Water
INT_PL_CHWS = zeros(datapoints,numgeofiles);
INT_PL_CHWR = zeros(datapoints,numgeofiles);
INT_PL_CWF = zeros(datapoints,numgeofiles);
INT_PL_CWQ = zeros(datapoints,numgeofiles);
INT_PL_CWQ_Daily = zeros(numgeofiles,1);
%%Predefine Campus Energy Variables
%%GeoBus'
GBA = zeros(datapoints,numgeofiles);
GBB = zeros(datapoints,numgeofiles);
GBC = zeros(datapoints,numgeofiles);
GBD = zeros(datapoints,numgeofiles);
GBF = zeros(datapoints,numgeofiles);
GBA_ME_Daily = zeros(numgeofiles,1);
GBB_ME_Daily = zeros(numgeofiles,1);
GBC_ME_Daily = zeros(numgeofiles,1);
GBD_ME_Daily = zeros(numgeofiles,1);
GBF_ME_Daily = zeros(numgeofiles,1);
GB_Total_Daily = zeros(numgeofiles,1);
%%Campus 1
C1CEP = zeros(datapoints,numgeofiles);
```

```
C1B1 = zeros(datapoints,numgeofiles);
C1B2 = zeros(datapoints,numgeofiles);
C1B3 = zeros(datapoints,numgeofiles);
C1B4 = zeros(datapoints,numgeofiles);
C1B5 = zeros(datapoints,numgeofiles);
C1B6 = zeros(datapoints,numgeofiles);
C1CEP_ME_Daily = zeros(numgeofiles,1);
C1B1_ME_Daily = zeros(numgeofiles,1);
C1B2_ME_Daily = zeros(numgeofiles,1);
C1B3_ME_Daily = zeros(numgeofiles,1);
C1B4_ME_Daily = zeros(numgeofiles,1);
C1B5_ME_Daily = zeros(numgeofiles,1);
C1B6_ME_Daily = zeros(numgeofiles,1);
C1_ME_Daily = zeros(numgeofiles,1);
%%Campus 2
C2_ME = zeros(datapoints,numgeofiles);
C2_ME_Daily = zeros(numgeofiles,1);
C2CEP = zeros(datapoints,numgeofiles);
C2H = zeros(datapoints,numgeofiles);
C2I = zeros(datapoints,numgeofiles);
C2J = zeros(datapoints,numgeofiles);
C2K = zeros(datapoints,numgeofiles);
%%Learning Campus/Voyager Hall
LC = zeros(datapoints,numgeofiles);
LC_ME_Daily = zeros(numgeofiles,1);
%%DeepSpace
DS = zeros(datapoints,numgeofiles);
DS_ME_Daily = zeros(numgeofiles,1);
%%Farm Campus
FARMCEP = zeros(datapoints,numgeofiles);
FARM_ME_Daily = zeros(numgeofiles,1);
%%C4
C4 = zeros(datapoints,numgeofiles);
C4_ME_Daily = zeros(numgeofiles,1);
%%UB3
UB3 = zeros(datapoints,numgeofiles);
UB3_ME_Daily = zeros(numgeofiles,1);
%%Total Mechanical Energy
Campus_Total_ME = zeros(numgeofiles,1);
%%Day Index
Day = zeros(numgeofiles,1);
%%Process Data Loop
for k=1:numgeofiles

%%Read Files
filename = ['E:\LT RA\Heat Budget\Epic Power Data\Geo
data\2019\jan\Geo_Data_2019-1-',num2str(k),'.csv'];
X = xlsread(filename);
X(isnan(X)) = 0;
%%Borefield 1
BF1ST(:,k) = (X(:,1)-32).*(5/9);        %Supply Temp [C]
BF1RT(:,k) = (X(:,2)-32).*(5/9);        %Return Temp [C]
BF1F(:,k) = X(:,3).*6.30901964*10^-5;   %Flow [m3/s]
BF1Q(:,k) = BF1F(:,k).*Rho.*Cp.*(BF1RT(:,k)-BF1ST(:,k));   %Hourly Heat Flow
BF1(k) = mean(BF1Q(:,k))*24;            %%Vector that contains kWh for each
day.
BF2ST(:,k) = (X(:,4)-32).*(5/9);        %Supply Temp [C]
```

```
BF2RT(:,k) = (X(:,5)-32).*(5/9);        %Return Temp [C]
BF2F(:,k) = X(:,6).*6.30901964*10^-5;   %Flow [m3/s]
BF2Q(:,k) = BF2F(:,k).*Rho.*Cp.*(BF2RT(:,k)-BF2ST(:,k));   %Hourly Heat Flow
BF2(k) = mean(BF2Q(:,k))*24; %%Vector that contains kWh for each day.
BF3ST(:,k) = (X(:,12)-32).*(5/9);       %Supply Temp [C]
BF3RT(:,k) = (X(:,13)-32).*(5/9);       %Return Temp [C]
BF3F(:,k) = X(:,14).*6.30901964*10^-5;  %Flow [m3/s]
BF3Q(:,k) = BF3F(:,k).*Rho.*Cp.*(BF3RT(:,k)-BF3ST(:,k));   %Hourly Heat Flow
BF3(k) = mean(BF3Q(:,k))*24;        %%Vector that contains kWh for each day.
BF4ST(:,k) = (X(:,15)-32).*(5/9);   %Supply Temp [C]
BF4RT(:,k) = (X(:,16)-32).*(5/9);   %Return Temp [C]
BF4F(:,k) = X(:,17).*6.30901964*10^-5;  %Flow [m3/s]
BF4Q(:,k) = BF4F(:,k).*Rho.*Cp.*(BF4RT(:,k)-BF4ST(:,k));   %Hourly Heat Flow
BF4(k) = mean(BF4Q(:,k))*24;   %%Vector that contains kWh for each day.
P10ST(:,k) = (X(:,7)-32).*(5/9);    %Supply Temp [C]
P10RT(:,k) = (X(:,8)-32).*(5/9);    %Return Temp [C]
P11ST(:,k) = (X(:,9)-32).*(5/9);    %Supply Temp [C]
P11RT(:,k) = (X(:,10)-32).*(5/9);   %Return Temp [C]
PF(:,k) = X(:,11).*6.30901964*10^-5;    %Flow [m3/s]
PQ(:,k) = (PF(:,k)/2).*Rho.*Cp.*(P10RT(:,k)-P10ST(:,k)) +
(PF(:,k)/2).*Rho.*Cp.*(P11RT(:,k)-P11ST(:,k)); %Hourly Heat Flow
Pond(k) = mean(PQ(:,k))*24; %%Vector that contains kWh for each day.
GeoHeat(k) = BF1(k)+ BF2(k) + BF3(k) + BF4(k) + Pond(k); %%Total Heat of
Borefield System for each day
%%Geowater to Outside of Buildings Section
%%Building 1
C1_B1_ST(:,k) = (X(:,19)-32).*(5/9);    %Supply Temp [C]
C1_B1_RT(:,k) = (X(:,20)-32).*(5/9);        %Return Temp [C]
C1_B1_F(:,k) = X(:,18).*6.30901964*10^-5;   %Flow [m3/s]
C1_B1_Q(:,k) = abs(C1_B1_F(:,k).*Rho.*Cp.*(C1_B1_RT(:,k)-C1_B1_ST(:,k)));
%Hourly Heat Flow
C1_B1_Q_Daily(k) = mean(C1_B1_Q(:,k))*24;%%Daily kWh provided due to heatflow
%%Building 2
C1_B2_ST(:,k) = (X(:,22)-32).*(5/9);    %Supply Temp [C]
C1_B2_RT(:,k) = (X(:,23)-32).*(5/9);        %Return Temp [C]
C1_B2_F(:,k) = X(:,21).*6.30901964*10^-5;   %Flow [m3/s]
C1_B2_Q(:,k) = abs(C1_B2_F(:,k).*Rho.*Cp.*(C1_B2_RT(:,k)-C1_B2_ST(:,k)));
%Hourly Heat Flow
C1_B2_Q_Daily(k) = mean(C1_B2_Q(:,k))*24;%Daily kWh provided due to heat flow
%%UB3
C1_B3_ST(:,k) = (X(:,43)-32).*(5/9);    %Supply Temp [C]
C1_B3_RT(:,k) = (X(:,44)-32).*(5/9);        %Return Temp [C]
C1_B3_F(:,k) = X(:,42).*6.30901964*10^-5;   %Flow [m3/s]
C1_B3_Q(:,k) = abs(C1_B3_F(:,k).*Rho.*Cp.*(C1_B3_RT(:,k)-C1_B3_ST(:,k)));
%Hourly Heat Flow
C1_B3_Q_Daily(k) = mean(C1_B3_Q(:,k))*24;%Daily kWh provided due to heat flow
%%Building 4
C1_B4_ST(:,k) = (X(:,25)-32).*(5/9);    %Supply Temp [C]
C1_B4_RT(:,k) = (X(:,26)-32).*(5/9);        %Return Temp [C]
C1_B4_F(:,k) = X(:,24).*6.30901964*10^-5;   %Flow [m3/s]
C1_B4_Q(:,k) = abs(C1_B4_F(:,k).*Rho.*Cp.*(C1_B4_RT(:,k)-C1_B4_ST(:,k)));
%Hourly Heat Flow
C1_B4_Q_Daily(k) = mean(C1_B4_Q(:,k))*24;  %%Daily kWh provided due to heat
flow
%%Building 5
C1_B5_ST(:,k) = (X(:,28)-32).*(5/9);    %Supply Temp [C]
C1_B5_RT(:,k) = (X(:,29)-32).*(5/9);        %Return Temp [C]
```

```
C1_B5_F(:,k) = X(:,27).*6.30901964*10^-5;   %Flow [m3/s]
C1_B5_Q(:,k) = abs(C1_B5_F(:,k).*Rho.*Cp.*(C1_B5_RT(:,k)-C1_B5_ST(:,k)));
%Hourly Heat Flow
C1_B5_Q_Daily(k) = mean(C1_B5_Q(:,k))*24;%Daily kWh provided due to heat flow
%%Building 6
C1_B6_ST(:,k) = (X(:,31)-32).*(5/9);    %Supply Temp [C]
C1_B6_RT(:,k) = (X(:,32)-32).*(5/9);        %Return Temp [C]
C1_B6_F(:,k) = X(:,30).*6.30901964*10^-5;   %Flow [m3/s]
C1_B6_Q(:,k) = abs(C1_B6_F(:,k).*Rho.*Cp.*(C1_B6_RT(:,k)-C1_B6_ST(:,k)));
%Hourly Heat Flow
C1_B6_Q_Daily(k) = mean(C1_B6_Q(:,k))*24;%Daily kWh provided due to heat flow
%%Campus Heat Flow
C1_Q(:,k) = C1_B1_Q(:,k) + C1_B2_Q(:,k) + C1_B3_Q(:,k) + C1_B4_Q(:,k) +
C1_B5_Q(:,k) + C1_B6_Q(:,k);
C1_Q_Daily(k) = mean(C1_Q(:,k))*24;  %%Daily kWh provided due to heat flow
%%Campus 2
C2_ST(:,k) = (X(:,34)-32).*(5/9);       %Supply Temp [C]
C2_RT(:,k) = (X(:,35)-32).*(5/9);        %Return Temp [C]
C2_F(:,k) = X(:,33).*6.30901964*10^-5;   %Flow [m3/s]
C2_Q(:,k) = abs(C2_F(:,k).*Rho.*Cp.*(C2_RT(:,k)-C2_ST(:,k)));%Hourly Heat
Flow
C2_Q_Daily(k) = mean(C2_Q(:,k))*24;  %%Daily kWh provided due to heat flow
%%Learning Campus
LC_ST(:,k) = (X(:,51)-32).*(5/9);       %Supply Temp [C]
LC_RT(:,k) = (X(:,52)-32).*(5/9);        %Return Temp [C]
LC_F(:,k) = X(:,50).*6.30901964*10^-5;   %Flow [m3/s]
LC_Q(:,k) = abs(LC_F(:,k).*Rho.*Cp.*(LC_RT(:,k)-LC_ST(:,k)));%Hourly Heat
Flow
LC_Q_Daily(k) = mean(LC_Q(:,k))*24; %%Daily kWh provided due to heat flow
%% Deep Space
DS_ST(:,k) = (X(:,40)-32).*(5/9);       %Supply Temp [C]
DS_RT(:,k) = (X(:,41)-32).*(5/9);        %Return Temp [C]
DS_F(:,k) = X(:,39).*6.30901964*10^-5;   %Flow [m3/s]
DS_Q(:,k) = abs(DS_F(:,k).*Rho.*Cp.*(DS_RT(:,k)-DS_ST(:,k)));%Hourly Heat
Flow
DS_Q_Daily(k) = mean(DS_Q(:,k))*24;%%Daily kWh provided due to heat flow
%% FARM Campus
FARM_ST(:,k) = (X(:,48)-32).*(5/9);       %Supply Temp [C]
FARM_RT(:,k) = (X(:,49)-32).*(5/9);        %Return Temp [C]
FARM_F(:,k) = X(:,47).*6.30901964*10^-5;   %Flow [m3/s]
FARM_Q(:,k) = abs(FARM_F(:,k).*Rho.*Cp.*(FARM_RT(:,k)-FARM_ST(:,k)));
%Hourly Heat Flow
FARM_Q_Daily(k) = mean(FARM_Q(:,k))*24;%Daily kWh provided due to heat flow
%%Total Heat Flow Daily to all Buildings
Buildings_Q_Daily(k) = FARM_Q_Daily(k) + DS_Q_Daily(k) + LC_Q_Daily(k) +
C2_Q_Daily(k) + C1_Q_Daily(k);
% Absolute Value Performance of UBend vs Rygan Comparison section
UBEND_ST(:,k) = (X(:,73)-32).*(5/9);       %Supply Temp [C]
UBEND_RT(:,k) = (X(:,74)-32).*(5/9);        %Return Temp [C]
UBEND_F(:,k) = X(:,72).*6.30901964*10^-5;   %Flow [m3/s]
UBEND_Q(:,k) = abs(UBEND_F(:,k).*Rho.*Cp.*(UBEND_RT(:,k)-UBEND_ST(:,k)));
%Hourly Heat Flow
UBEND_Q_Daily(k) = mean(UBEND_Q(:,k))*24;%Daily kWh provided due to heat flow
UBEND_avgF_Daily(k) = mean(UBEND_F(:,k));      %%Average UBEND FLow
UBEND_running_ST((datapoints*(k-1))+1:datapoints*k) = UBEND_ST(:,k);
%%Running Compilation of UBEND return temperatures.
```

```
UBEND_running_RT((datapoints*(k-1))+1:datapoints*k) = UBEND_RT(:,k);
%%Running Compilation of UBEND return temperatures.
UBEND_F_running((datapoints*(k-1))+1:datapoints*k) = UBEND_F(:,k);
%%Running Compilation of UBEND Flow.
RYGAN_ST(:,k) = (X(:,76)-32).*(5/9);       %Supply Temp [C]
RYGAN_RT(:,k) = (X(:,77)-32).*(5/9);        %Return Temp [C]
RYGAN_F(:,k) = X(:,75).*6.30901964*10^-5;   %Flow [m3/s]
RYGAN_Q(:,k) = abs(RYGAN_F(:,k).*Rho.*Cp.*(RYGAN_RT(:,k)-RYGAN_ST(:,k)));
%Hourly Heat Flow
RYGAN_Q_Daily(k) = mean(RYGAN_Q(:,k))*24;%Daily kWh provided due to heat flow
RYGAN_avgF_Daily(k) = mean(RYGAN_F(:,k));      %%Average Rygan FLow
RYGAN_running_ST((datapoints*(k-1))+1:datapoints*k) = RYGAN_ST(:,k);
%%Running Compilation of RYGAN supply temperatures.
RYGAN_running_RT((datapoints*(k-1))+1:datapoints*k) = RYGAN_RT(:,k);
%%Running Compilation of RYGAN  return temperatures.
RYGAN_F_running((datapoints*(k-1))+1:datapoints*k) = RYGAN_F(:,k);
%%Running Compilation of RYGAN  flow.
%Internal Building Heat Flow Section
%%Internal Campus 1 Building 1
INT_C1B1_HWS(:,k) = (X(:,78)-32).*(5/9);       %Hot Water Supply Temp [C]
INT_C1B1_HWR(:,k) = (X(:,79)-32).*(5/9);       %Hot Water Return Temp [C]
INT_C1B1_F(:,k) = X(:,80).*6.30901964*10^-5;      %Hot Water Flow [m3/s]
INT_C1B1_Q(:,k) = abs(INT_C1B1_F(:,k).*Rho.*Cp.*(INT_C1B1_HWR(:,k)-
INT_C1B1_HWS(:,k)));   %Hourly Heat Flow
INT_C1B1_Q_Daily(k) = mean(INT_C1B1_Q(:,k))*24;%Daily kWh provided due to
heat flow
%%Internal Campus 1 Building 2
INT_C1B2_HWS(:,k) = (X(:,81)-32).*(5/9);       %Hot Water Supply Temp [C]
INT_C1B2_HWR(:,k) = (X(:,82)-32).*(5/9);       %Hot Water Return Temp [C]
INT_C1B2_F(:,k) = X(:,83).*6.30901964*10^-5;      %Hot Water Flow [m3/s]
INT_C1B2_Q(:,k) = abs(INT_C1B2_F(:,k).*Rho.*Cp.*(INT_C1B2_HWR(:,k)-
INT_C1B2_HWS(:,k)));   %Hourly Heat Flow
INT_C1B2_Q_Daily(k) = mean(INT_C1B2_Q(:,k))*24;  %%Daily kWh provided due to
heat flow
%%Internal Campus 1 Building 4
INT_C1B4_HWS(:,k) = (X(:,84)-32).*(5/9);       %Hot Water Supply Temp [C]
INT_C1B4_HWR(:,k) = (X(:,85)-32).*(5/9);       %Hot Water Return Temp [C]
INT_C1B4_F(:,k) = X(:,86).*6.30901964*10^-5;      %Hot Water Flow [m3/s]
INT_C1B4_Q(:,k) = abs(INT_C1B4_F(:,k).*Rho.*Cp.*(INT_C1B4_HWR(:,k)-
INT_C1B4_HWS(:,k)));   %Hourly Heat Flow
INT_C1B4_Q_Daily(k) = mean(INT_C1B4_Q(:,k))*24;  %%Daily kWh provided due to
heat flow
%%Internal Campus 1 Building 5
INT_C1B5_HWS(:,k) = (X(:,87)-32).*(5/9);       %Hot Water Supply Temp [C]
INT_C1B5_HWR(:,k) = (X(:,88)-32).*(5/9);       %Hot Water Return Temp [C]
INT_C1B5_F(:,k) = X(:,89).*6.30901964*10^-5;      %Hot Water Flow [m3/s]
INT_C1B5_Q(:,k) = abs(INT_C1B5_F(:,k).*Rho.*Cp.*(INT_C1B5_HWR(:,k)-
INT_C1B5_HWS(:,k)));   %Hourly Heat Flow
INT_C1B5_Q_Daily(k) = mean(INT_C1B5_Q(:,k))*24;  %%Daily kWh provided due to
heat flow
%%Internal Campus 1 Building 6
INT_C1B6_HWS(:,k) = (X(:,90)-32).*(5/9);       %Hot Water Supply Temp [C]
INT_C1B6_HWR(:,k) = (X(:,91)-32).*(5/9);       %Hot Water Return Temp [C]
INT_C1B6_F(:,k) = X(:,92).*6.30901964*10^-5;      %Hot Water Flow [m3/s]
INT_C1B6_Q(:,k) = abs(INT_C1B6_F(:,k).*Rho.*Cp.*(INT_C1B6_HWR(:,k)-
INT_C1B6_HWS(:,k)));   %Hourly Heat Flow
```

```
INT_C1B6_Q_Daily(k) = mean(INT_C1B6_Q(:,k))*24;  %%Daily kWh provided due to
heat flow
%%Internal Campus 2 Total Hot Water
INT_C2TOT_HWS(:,k) = (X(:,93)-32).*(5/9);       %Hot Water Supply Temp [C]
INT_C2TOT_HWR(:,k) = (X(:,94)-32).*(5/9);       %Hot Water Return Temp [C]
INT_C2TOT_F(:,k) = X(:,95).*6.30901964*10^-5;      %Hot Water Flow [m3/s]
INT_C2TOT_Q(:,k) = abs(INT_C2TOT_F(:,k).*Rho.*Cp.*(INT_C2TOT_HWR(:,k)-
INT_C2TOT_HWS(:,k)));   %Hourly Heat Flow
INT_C2TOT_Q_Daily(k) = mean(INT_C2TOT_Q(:,k))*24;  %%Daily kWh provided due
to heat flow
%%Internal Campus 2 Total Chilled Water
INT_C2TOT_CHWS(:,k) = (X(:,99)-32).*(5/9);       %Hot Water Supply Temp [C]
INT_C2TOT_CHWR(:,k) = (X(:,100)-32).*(5/9);       %Hot Water Return Temp [C]
INT_C2TOT_CWF(:,k) = X(:,101).*6.30901964*10^-5;      %Hot Water Flow [m3/s]
INT_C2TOT_CWQ(:,k) = abs(INT_C2TOT_CWF(:,k).*Rho.*Cp.*(INT_C2TOT_CHWR(:,k)-
INT_C2TOT_CHWS(:,k)));   %Hourly Heat Flow
INT_C2TOT_CWQ_Daily(k) = mean(INT_C2TOT_CWQ(:,k))*24;  %%Daily kWh provided
due to heat flow
%%Internal Campus 2 Building K (Kouhotek) Hot Water
INT_C2K_HWS(:,k) = (X(:,96)-32).*(5/9);       %Hot Water Supply Temp [C]
INT_C2K_HWR(:,k) = (X(:,97)-32).*(5/9);       %Hot Water Return Temp [C]
INT_C2K_F(:,k) = X(:,98).*6.30901964*10^-5;      %Hot Water Flow [m3/s]
INT_C2K_Q(:,k) = abs(INT_C2K_F(:,k).*Rho.*Cp.*(INT_C2K_HWR(:,k)-
INT_C2K_HWS(:,k)));   %Hourly Heat Flow
INT_C2K_Q_Daily(k) = mean(INT_C2K_Q(:,k))*24;  %%Daily kWh provided due to
heat flow
%%Internal Campus 2 Building K (Kouhotek) Chilled Water
INT_C2K_CHWS(:,k) = (X(:,102)-32).*(5/9);       %Hot Water Supply Temp [C]
INT_C2K_CHWR(:,k) = (X(:,103)-32).*(5/9);       %Hot Water Return Temp [C]
INT_C2K_CWF(:,k) = X(:,104).*6.30901964*10^-5;      %Hot Water Flow [m3/s]
INT_C2K_CWQ(:,k) = abs(INT_C2K_CWF(:,k).*Rho.*Cp.*(INT_C2K_CHWR(:,k)-
INT_C2K_CHWS(:,k)));   %Hourly Heat Flow
INT_C2K_CWQ_Daily(k) = mean(INT_C2K_CWQ(:,k))*24;  %%Daily kWh provided due
to heat flow
%%Internal Learning Center
INT_LC_HWS(:,k) = (X(:,105)-32).*(5/9);       %Hot Water Supply Temp [C]
INT_LC_HWR(:,k) = (X(:,106)-32).*(5/9);       %Hot Water Return Temp [C]
INT_LC_F(:,k) = X(:,107).*6.30901964*10^-5;      %Hot Water Flow [m3/s]
INT_LC_Q(:,k) = abs(INT_LC_F(:,k).*Rho.*Cp.*(INT_LC_HWR(:,k)-
INT_LC_HWS(:,k)));   %Hourly Heat Flow
INT_LC_Q_Daily(k) = mean(INT_LC_Q(:,k))*24;  %%Daily kWh provided due to heat
flow
%%Internal Campus 4/5 Hot Water
INT_C45_HWS(:,k) = (X(:,108)-32).*(5/9);       %Hot Water Supply Temp [C]
INT_C45_HWR(:,k) = (X(:,109)-32).*(5/9);       %Hot Water Return Temp [C]
INT_C45_F(:,k) = X(:,110).*6.30901964*10^-5;      %Hot Water Flow [m3/s]
INT_C45_Q(:,k) = abs(INT_C45_F(:,k).*Rho.*Cp.*(INT_C45_HWR(:,k)-
INT_C45_HWS(:,k)));   %Hourly Heat Flow
INT_C45_Q_Daily(k) = mean(INT_C45_Q(:,k))*24;  %%Daily kWh provided due to
heat flow
%%Internal Campus 4/5 Chilled Water
INT_C45_CHWS(:,k) = (X(:,111)-32).*(5/9);       %Hot Water Supply Temp [C]
INT_C45_CHWR(:,k) = (X(:,112)-32).*(5/9);       %Hot Water Return Temp [C]
INT_C45_CWF(:,k) = X(:,113).*6.30901964*10^-5;      %Hot Water Flow [m3/s]
INT_C45_CWQ(:,k) = abs(INT_C45_CWF(:,k).*Rho.*Cp.*(INT_C45_CHWR(:,k)-
INT_C45_CHWS(:,k)));   %Hourly Heat Flow
```

```
INT_C45_CWQ_Daily(k) = mean(INT_C45_CWQ(:,k))*24;  %%Daily kWh provided due
to heat flow
%%Internal Deep Space Hot Water
INT_DS_HWS(:,k) = (X(:,114)-32).*(5/9);       %Hot Water Supply Temp [C]
INT_DS_HWR(:,k) = (X(:,115)-32).*(5/9);       %Hot Water Return Temp [C]
INT_DS_F(:,k) = X(:,116).*6.30901964*10^-5;      %Hot Water Flow [m3/s]
INT_DS_Q(:,k) = abs(INT_DS_F(:,k).*Rho.*Cp.*(INT_DS_HWR(:,k)-
INT_DS_HWS(:,k)));   %Hourly Heat Flow
INT_DS_Q_Daily(k) = mean(INT_DS_Q(:,k))*24;  %%Daily kWh provided due to heat
flow
%%Internal Deep Space Chilled Water
INT_DS_CHWS(:,k) = (X(:,117)-32).*(5/9);       %Hot Water Supply Temp [C]
INT_DS_CHWR(:,k) = (X(:,118)-32).*(5/9);       %Hot Water Return Temp [C]
INT_DS_CWF(:,k) = X(:,119).*6.30901964*10^-5;      %Hot Water Flow [m3/s]
INT_DS_CWQ(:,k) = abs(INT_DS_CWF(:,k).*Rho.*Cp.*(INT_DS_CHWR(:,k)-
INT_DS_CHWS(:,k)));   %Hourly Heat Flow
INT_DS_CWQ_Daily(k) = mean(INT_DS_CWQ(:,k))*24;  %%Daily kWh provided due to
heat flow
%%Internal Farm Campus Hot Water
INT_FARM_HWS(:,k) = (X(:,120)-32).*(5/9);       %Hot Water Supply Temp [C]
INT_FARM_HWR(:,k) = (X(:,121)-32).*(5/9);       %Hot Water Return Temp [C]
INT_FARM_F(:,k) = X(:,122).*6.30901964*10^-5;      %Hot Water Flow [m3/s]
INT_FARM_Q(:,k) = abs(INT_FARM_F(:,k).*Rho.*Cp.*(INT_FARM_HWR(:,k)-
INT_FARM_HWS(:,k)));   %Hourly Heat Flow
INT_FARM_Q_Daily(k) = mean(INT_FARM_Q(:,k))*24;  %%Daily kWh provided due to
heat flow
%%Internal Farm Campus Chilled Water
INT_FARM_CHWS(:,k) = (X(:,123)-32).*(5/9);       %Hot Water Supply Temp [C]
INT_FARM_CHWR(:,k) = (X(:,124)-32).*(5/9);       %Hot Water Return Temp [C]
INT_FARM_CWF(:,k) = X(:,125).*6.30901964*10^-5;      %Hot Water Flow [m3/s]
INT_FARM_CWQ(:,k) = abs(INT_FARM_CWF(:,k).*Rho.*Cp.*(INT_FARM_CHWR(:,k)-
INT_FARM_CHWS(:,k)));   %Hourly Heat Flow
INT_FARM_CWQ_Daily(k) = mean(INT_FARM_CWQ(:,k))*24;  %%Daily kWh provided due
to heat flow
%%Internal UB3 Hot Water
INT_UB3_HWS(:,k) = (X(:,126)-32).*(5/9);       %Hot Water Supply Temp [C]
INT_UB3_HWR(:,k) = (X(:,127)-32).*(5/9);       %Hot Water Return Temp [C]
INT_UB3_F(:,k) = X(:,128).*6.30901964*10^-5;      %Hot Water Flow [m3/s]
INT_UB3_Q(:,k) = abs(INT_UB3_F(:,k).*Rho.*Cp.*(INT_UB3_HWR(:,k)-
INT_UB3_HWS(:,k)));   %Hourly Heat Flow
INT_UB3_Q_Daily(k) = mean(INT_UB3_Q(:,k))*24;  %%Daily kWh provided due to
heat flow
%%Internal UB3 Chilled Water
INT_UB3_CHWS(:,k) = (X(:,129)-32).*(5/9);       %Hot Water Supply Temp [C]
INT_UB3_CHWR(:,k) = (X(:,130)-32).*(5/9);       %Hot Water Return Temp [C]
INT_UB3_CWF(:,k) = X(:,131).*6.30901964*10^-5;      %Hot Water Flow [m3/s]
INT_UB3_CWQ(:,k) = abs(INT_UB3_CWF(:,k).*Rho.*Cp.*(INT_UB3_CHWR(:,k)-
INT_UB3_CHWS(:,k)));   %Hourly Heat Flow
INT_UB3_CWQ_Daily(k) = mean(INT_UB3_CWQ(:,k))*24;  %%Daily kWh provided due
to heat flow
%%Internal UB3 Heat Exchangers
INT_UB3_HXS(:,k) = (X(:,136)-32).*(5/9);       %Hot Water Supply Temp [C]
INT_UB3_HXR(:,k) = (X(:,137)-32).*(5/9);       %Hot Water Return Temp [C]
INT_UB3_HXF(:,k) = X(:,138).*6.30901964*10^-5;      %Hot Water Flow [m3/s]
INT_UB3_HXQ(:,k) = abs(INT_UB3_HXF(:,k).*Rho.*Cp.*(INT_UB3_HXR(:,k)-
INT_UB3_HXS(:,k)));   %Hourly Heat Flow
```

```
INT_UB3_HXQ_Daily(k) = mean(INT_UB3_HXQ(:,k))*24;  %%Daily kWh provided due
to heat flow
%%Internal Pluto Hot Water
INT_PL_HWS(:,k) = (X(:,139)-32).*(5/9);       %Hot Water Supply Temp [C]
INT_PL_HWR(:,k) = (X(:,140)-32).*(5/9);       %Hot Water Return Temp [C]
INT_PL_F(:,k) = X(:,141).*6.30901964*10^-5;      %Hot Water Flow [m3/s]
INT_PL_Q(:,k) = abs(INT_PL_F(:,k).*Rho.*Cp.*(INT_PL_HWR(:,k)-
INT_PL_HWS(:,k)));   %Hourly Heat Flow
INT_PL_Q_Daily(k) = mean(INT_PL_Q(:,k))*24;  %%Daily kWh provided due to heat
flow
%%Internal Pluto Chilled Water
INT_PL_CHWS(:,k) = (X(:,142)-32).*(5/9);       %Hot Water Supply Temp [C]
INT_PL_CHWR(:,k) = (X(:,143)-32).*(5/9);       %Hot Water Return Temp [C]
INT_PL_CWF(:,k) = X(:,144).*6.30901964*10^-5;      %Hot Water Flow [m3/s]
INT_PL_CWQ(:,k) = abs(INT_PL_CWF(:,k).*Rho.*Cp.*(INT_PL_CHWR(:,k)-
INT_PL_CHWS(:,k)));   %Hourly Heat Flow
INT_PL_CWQ_Daily(k) = mean(INT_PL_CWQ(:,k))*24;  %%Daily kWh provided due to
heat flow
%%Building Mechanical Energy Section
GBA(:,k) = X(:,145);
GBA_ME_Daily(k) = sum(GBA(:,k));
GBB(:,k) = X(:,146);
GBB_ME_Daily(k) = sum(GBB(:,k));
GBC(:,k) = X(:,147);
GBC_ME_Daily(k) = sum(GBC(:,k));
GBD(:,k) = X(:,148);
GBD_ME_Daily(k) = sum(GBD(:,k));
GBF(:,k) = X(:,149);
GBF_ME_Daily(k) = sum(GBF(:,k));
GB_Total_Daily(k) = GBA_ME_Daily(k) + GBB_ME_Daily(k) + GBC_ME_Daily(k) +
GBD_ME_Daily(k) + GBF_ME_Daily(k);
%%Campus 1
C1CEP(:,k) = X(:,150);
C1CEP_ME_Daily(k) = sum(C1CEP(:,k));
C1B1(:,k) = X(:,151);
C1B1_ME_Daily(k) = sum(C1B1(:,k));
C1B2(:,k) = X(:,152);
C1B2_ME_Daily(k) = sum(C1B2(:,k));
C1B3(:,k) = X(:,153);
C1B3_ME_Daily(k) = sum(C1B3(:,k));
C1B4(:,k) = X(:,154);
C1B4_ME_Daily(k) = sum(C1B4(:,k));
C1B5(:,k) = X(:,155);
C1B5_ME_Daily(k) = sum(C1B5(:,k));
C1B6(:,k) = X(:,156);
C1B6_ME_Daily(k) = sum(C1B6(:,k));
C1_ME_Daily(k) = C1CEP_ME_Daily(k) + C1B6_ME_Daily(k) + C1B5_ME_Daily(k) +
C1B4_ME_Daily(k) + C1B3_ME_Daily(k) + C1B2_ME_Daily(k) + C1B1_ME_Daily(k);
%%Campus 2
C2CEP(:,k) = X(:,157);
C2H(:,k) = X(:,158);
C2I(:,k) = X(:,159);
C2J(:,k) = X(:,160);
C2K(:,k) = X(:,161);
C2_ME(:,k) = C2CEP(:,k) + C2H(:,k) + C2I(:,k) + C2J(:,k) + C2K(:,k);
C2_ME_Daily(k) = sum(C2_ME(:,k));
%%Learning Campus
```

```
LC(:,k) = X(:,162);
LC_ME_Daily(k) = sum(LC(:,k));
%%Deep Space
DS(:,k) = X(:,163);
DS_ME_Daily(k) = sum(DS(:,k));
%%Farm Campus
FARMCEP(:,k) = X(:,164);
FARM_ME_Daily(k) = sum(FARMCEP(:,k));
%%Campus 4
C4(:,k) = X(:,165);
C4_ME_Daily(k) = sum(C4(:,k));
%%UB3
UB3(:,k) = X(:,166);
UB3_ME_Daily(k) = sum(UB3(:,k));
%%Total
Campus_Total_ME(k) =
UB3_ME_Daily(k)+C4_ME_Daily(k)+FARM_ME_Daily(k)+DS_ME_Daily(k)+LC_ME_Daily(k)
+C2_ME_Daily(k)+C1_ME_Daily(k);
%%Day Index
Day(k) = k;
End

%Write Excel Document Summarizing Data
path = cd('E:\LT RA\Heat Budget\Epic Power Data\Matlab
Processed\2019\January'); %%Change path to desired folder of exported excel
file - Change to Appropriate Month
warning('off','MATLAB:xlswrite:AddSheet') %%Turn off warning that alerts when
writing over a pre-existing excel file.
%%Borefield Heat Flow Tab
Borefield_Headers = {'Day','Borefield 1 Total Heat Transported
[kWh]','Borefield 2 Total Heat Transported [kWh]','Borefield 3 Total Heat
Transported [kWh]','Borefield 4 Total Heat Transported [kWh]','Pond Total
Heat Transported [kWh]','Overall Total Heat Transported [kWh]'};
xlswrite('Monthly Summary.xls',Borefield_Headers,'Borefield Heat Flow','A1');
Borefield_Summary = [Day,BF1,BF2,BF3,BF4,Pond,GeoHeat];
xlswrite('Monthly Summary.xls',Borefield_Summary,'Borefield Heat Flow','A2');
%%Geowater to External Building Sensors Tab
External_Building_GeoHeat_Headers = {'Day','Campus 1 Building 1 Heat Moved
[kWh]','Campus 1 Building 2 Heat Moved [kWh]','Campus 1 Building 3 Heat Moved
[kWh]','Campus 1 Building 4 Heat Moved [kWh]','Campus 1 Building 5 Heat Moved
[kWh]','Campus 1 Building 6 Heat Moved [kWh]','Campus 1 Total Heat Moved
[kWh]','Campus 2 Total Heat Moved [kWh]','Learning Center Total Heat Moved
[kWh]','Deep Space Total Heat Moved [kWh]','Farm Campus Total Heat Moved
[kWh]','Buildings Total Heat Moved [kWh]'};
xlswrite('Monthly Summary.xls',External_Building_GeoHeat_Headers,'External
Building GeoHeat Flow','A1');
External_GeoHeat_Summary =
[Day,C1_B1_Q_Daily,C1_B2_Q_Daily,C1_B3_Q_Daily,C1_B4_Q_Daily,C1_B5_Q_Daily,C1
_B6_Q_Daily,C1_Q_Daily,C2_Q_Daily,LC_Q_Daily,DS_Q_Daily,FARM_Q_Daily,Building
s_Q_Daily];
xlswrite('Monthly Summary.xls',External_GeoHeat_Summary,'External Building
GeoHeat Flow','A2');
%%UBEND vs Rygan Tab
GHX_comparison_Headers = {'Day','UBend Absolute Heat Moved [kWh]','Rygan
Absolute Heat Moved [kWh]','UBend Average Flow [m^3/s]','Rygan Average Flow
[m^3/s]',};
```

```
xlswrite('Monthly Summary.xls',GHX_comparison_Headers,'UBEND vs Rygan
Comparison','A1');
GHX_comparison_Summary =
[Day,UBEND_Q_Daily,RYGAN_Q_Daily,UBEND_avgF_Daily,RYGAN_avgF_Daily];
xlswrite('Monthly Summary.xls',GHX_comparison_Summary,'UBEND vs Rygan
Comparison','A2');
%%Internal Building Heat Flow Tab
Internal_Q_Headers = {'Day','C1B1 Heat Moved [kWh]','C1B2 Heat Moved
[kWh]','C1B4 Heat Moved [kWh]','C1B5 Heat Moved [kWh]','C1B6 Heat Moved
[kWh]','Campus 2 Total Hot Water Heat Moved [kWh]','Campus 2 Total Chilled
Water Heat Moved [kWh]','C2 Kohoutek Total Hot Water Heat Moved [kWh]','C2
Kohoutek Total Chilled Water Heat Moved [kWh]','Learning Center Heat Moved
[kWh]','Campus 4/5 Hot Water Heat Moved [kWh]','Campus 4/5 Hot Water Chilled
Moved [kWh]','Deep Space Hot Water Heat Moved [kWh]','Deep Space Chilled
Water Heat Moved [kWh]','FARM Hot Water Heat Moved [kWh]','FARM Chilled Water
Heat Moved [kWh]','UB3 Hot Water Heat Moved [kWh]','UB3 Chilled Water Heat
Moved [kWh]','UB3 Heat Exchanger Heat Moved [kWh]','Pluto Hot Water Heat
Moved [kWh]','Pluto Chilled Water Heat Moved [kWh]'};
xlswrite('Monthly Summary.xls',Internal_Q_Headers,'Internal Building Heat
Flows','A1');
Internal_Building_Heat_Summary =
[Day,INT_C1B1_Q_Daily,INT_C1B2_Q_Daily,INT_C1B4_Q_Daily,INT_C1B5_Q_Daily,INT_
C1B6_Q_Daily,INT_C2TOT_Q_Daily,INT_C2TOT_CWQ_Daily,INT_C2K_Q_Daily,INT_C2K_CW
Q_Daily,INT_LC_Q_Daily,INT_C45_Q_Daily,INT_C45_CWQ_Daily,INT_DS_Q_Daily,INT_D
S_CWQ_Daily,INT_FARM_Q_Daily,INT_FARM_CWQ_Daily,INT_UB3_Q_Daily,INT_UB3_CWQ_D
aily,INT_UB3_HXQ_Daily,INT_PL_Q_Daily,INT_PL_CWQ_Daily];
xlswrite('Monthly Summary.xls',Internal_Building_Heat_Summary,'Internal
Building Heat Flows','A2');
%%Mechanical Energy to Run Geothermal System Tab
Mechanical_Energy_Headers = {'Day','PumpHouse Mechanical Energy
[kWh]','Campus 1 CEP Mechanical Energy [kWh]','C1B1 Mechanical Energy
[kWh]','C1B2 Mechanical Energy [kWh]','C1B3 Mechanical Energy [kWh]','C1B4
Mechanical Energy [kWh]','C1B5 Mechanical Energy [kWh]','C1B5 Mechanical
Energy [kWh]','Campus 1 Total Mechanical Energy [kWh]','Campus 2 Total
Mechanical Energy [kWh]','Learning Center Mechanical Energy [kWh]','Deep
Space Mechanical Energy [kWh]','Farm Campus Mechanical Energy [kWh]','Campus
4 Mechanical Energy [kWh]','UB3 Mechanical Energy [kWh]','Overal Total Campus
Mechanical Energy [kWh]'};
xlswrite('Monthly Summary.xls',Mechanical_Energy_Headers,'Campus Mechanical
Energy','A1');
Mechanical_Energy_Summary =
[Day,GB_Total_Daily,C1CEP_ME_Daily,C1B1_ME_Daily,C1B2_ME_Daily,C1B3_ME_Daily,
C1B4_ME_Daily,C1B5_ME_Daily,C1B6_ME_Daily,C1_ME_Daily,C2_ME_Daily,LC_ME_Daily
,DS_ME_Daily,FARM_ME_Daily,C4_ME_Daily,UB3_ME_Daily,Campus_Total_ME];
xlswrite('Monthly Summary.xls',Mechanical_Energy_Summary,'Campus Mechanical
Energy','A2');
```

Appendix C: Life Cycle Assessment Spreadsheet Tool Guide

The goal of the LCA spreadsheet tool is to allow a user to analyze the environmental impacts of deep-direct use geothermal systems throughout the life span of the system. The spreadsheet was developed with a specific DDU system in mind, but the inputs can be manipulated to calculate an estimate of the life cycle impacts. The spreadsheet is divided into eight main tabs: Design Inputs, Inventory, Impacts, Summary, Offsets, Spider, Reference, and Strategies.

The Design Inputs tab is where the user can enter in the known design parameters for the DDU system. There is a section for the well design, drill rig inputs, operation equipment inputs, chiller inputs (if applicable), submersible pump inputs, and central heating/surface equipment inputs. The primary function of this tab is to assist in performing the necessary material quantity calculations in order to determine the impact of those materials, but it also serves as a way to catalog the various design components of the DDU system. The lower half of this tab will calculate the amount of material used for the general components of a DDU system, with a focus on the well material calculations. If a chiller is used in the design, a drop-down menu with three different chiller schemes can be used to determine the generalized material calculations of chiller components. This tab will also provide calculations for the surface components of the system (e.g. fuel use, surface connection materials, etc.), however these parameters can also be estimated using other methods. The material calculations within this tab are simply estimates to provide the user with an idea of the quantity of materials needed for their respective design, and should be verified based on specific project design.

The Inventory tab is a catalog of the collected SimaPro impacts for the components in each lifecycle stage. The impacts are for 1 unit of each material, so that the impacts can be manipulated for various designs. The SimaPro processes were selected with a focus on material sourcing and

use within the United States, however some processes are labeled for global use. The inventory collected here is by no means a thorough collection of all of the materials necessary for a DDU system, however it offers general insight into the impacts associated with each phase of the system.

The Impacts tab will calculate the total environmental impacts of each component of the DDU system using the Impact Inventory developed in the previous tab. There are two columns that require the user's attention on this tab: the design input column and the functional input column. This where the design parameters are converted from the design units to the SimaPro unit, if necessary. Many of the cells in the design inputs column in this tab pull from the previous Design Inputs tab, however some of the values are manually entered using assumptions made by the user. There is a Notes column to the far right that allows the user to keep track of any assumptions made to calculate the impact. It is very important to keep track of the units being used for these impact calculations, as there are many transitions from English to metric units throughout the spreadsheet. The following Summary tab automatically calculates sums of impacts in a variety of groupings. This allows the user to quickly review the relative impacts of various parts of the system so that the user can understand what components of the DDU design contribute the most to its overall environmental impact.

The Spider tab, along with the corresponding Reference and Strategies tabs, allow the user to create a Spider Diagram that compares the DDU system to an alternative source of thermal energy. The Reference tab is a table in which the User can enter in the total impacts in five different categories, and the Strategies tab is a table in which impacts for the DDU system are calculated based on different areas of the spreadsheet. Within the Spider tab, the user can then select which Reference and Strategy to compare, and the relative performance will be determined. The user can also assign point values to correspond to certain benchmarks of performance, the resulting Spider

diagram will then produce a graph showing how well the DDU system performs based on which impact categories are most important to them.

The impacts calculated and results presented in this spreadsheet tool provide a general estimate of the life cycle environmental impact associated with DDU systems. There are areas of this spreadsheet that could be refined to more specifically and accurately break down the environmental impacts of the system, however this spreadsheet still has the potential to serve as a useful tool to investigate the environmental impacts and overall benefits of a DDU system. To see the results and analysis from using this spreadsheet tool for a proposed DDU system, see Chapter 4 of this thesis.

Appendix D: LCA and LCOH Supplemental Information

Table 13. Stratigraphy of geologic units in the ILB (Stumpf, et al., 2018).

Formation	Thickness (m)	Top (m)	Description of Formation
Quaternary	58	0	Silt, clay, sand, till; sand and gravel, water bearing
Pennsylvanian	46–61	58	Shale, siltstone, sandstone, coal beds
Mississippian	37–73	111	Largely siltstone; Chouteau Limestone at base
New Albany	21–27	162–177	Dark colored, hard shale
Grand Tower (Devonian)	21–27	186–201	Limestone, commonly sandstone at base
Silurian	189–207	210–229	Vuggy dolomite, lower part limestone; shows of oil likely
Maquoketa (Ordovician)	61	418	Shale; limestone in middle
Kimmswick	140	479	Limestone
Decorah and Platteville	300	521	Limestone, thin shale layers
Joachim	21	613	Dolomite and sandstone, shale layers
St. Peter	61–76	634	Pure quartz sandstone, water bearing
Knox Group	396	701	Dominantly dolomite, partly sandy and cherty
Ironton	46	1,097	Pure quartz sandstone, water bearing
Eau Claire	137	1,143	Shale, sandstone, and limestone; shale increasing downward
Mt. Simon	762+	1,280	Sandstone, commonly coarse grained; water bearing

Table 14. Assumptions for used in Material Production Phase of LCA impact assessment.

Material Production					
Injection Well (IW)	**Design Input**	**Unit**	**Functional Input**	**Unit**	**NOTES/ASSUMPTIONS:**
Casing 1 (surface)	1.12	m3	8988.34	kg	assumes density of 8000 kg/m3
Casing 2 (int.)	15.61	m3	124844.95	kg	assumes density of 8000 kg/m3
Casing 3 (prod.)	11.30	m3	90396.98	kg	assumes density of 8000 kg/m3
Concrete 1 (surface)	16.55	m3	16.55	m3	
Concrete 2 (int.)	104.29	m3	104.29	m3	
Concrete 3 (prod.)	61.37	m3	61.37	m3	
Tubing	1645.92	m		kg	unsure of units/materials
Tube lining	1645.92	m		kg	unsure of units
Injection Packer	0.25	kg	0.25	kg	assumes small amount of insulation
Drilling (prod. of fuel)	12000.00	gal	38640.00	kg	assumes 25 gal/hr use, 1 gal diesel weighs 3.22 kg
Drilling (water)	221456.69	kg	221456.69	kg	assumes 15 kg/m use
Production Well (PW)	**Design Input**	**Unit**	**Functional Input**	**Unit**	
Casing 1 (surface)	1.91	m3	15250.89	kg	assumes density of 8000 kg/m3
Casing 2 (int.)	20.27	m3	162129.33	kg	assumes density of 8000 kg/m3
Casing 3 (long string)	18.49	m3	147897.68	kg	assumes density of 8000 kg/m3
Concrete 1 (surface)	21.61	m3	21.61	m3	
Concrete 2 (int.)	151.20	m3	151.20	m3	
Concrete 3 (long string)	93.23	m3	93.23	m3	
Tubing	1828.80	m		kg	unsure of units/materials
Tube lining	1828.80	m		kg	unsure of units
Production Packer	0.25	kg	0.25	kg	assumes small amount of insulation
Drilling (prod. of fuel)	12000.00	gal	38640.00	kg	assumes 25 gal/hr use, 1 gal diesel weighs 3.22 kg
Drilling (water)	29030.78	kg	29030.78	kg	assumes 15 kg/m use
Submersible Pump	**Design Input**	**Unit**	**Functional Input**	**Unit**	
Copper Wire	16.00	kg	16	kg	from (Sullivan, Clark, Han, & & Wang, 2010)
Steel	19.35	kg	19.35	kg	from Sullivan et al. 2010
Lead	0.70	kg	0.7	kg	from Sullivan et al. 2010
Lubricant oil	1.00	kg	1	kg	from Sullivan et al. 2010
Chiller	**Design Input**	**Unit**	**Functional Input**	**Unit**	
Refrigerant	1191	kg	1191	kg	from (Lijung Gu, 2019)
Steel	24397	kg	24397	kg	from (Lijung Gu, 2019)
Aluminum	435	kg	435	kg	from (Lijung Gu, 2019)
Copper	6506	kg	6506	kg	from (Lijung Gu, 2019)
Surface Components	**Design Input**	**Unit**	**Functional Input**	**Unit**	
Heat Exchanger	8810	kg	8810	kg	from (Adolfsson & Rashid, 2016)
HDPE	40	m	20.2	kg	typical 20 m trench --> 10.1 kg piping

Table 15. Assumptions for used in Material Transport, Use, and End of Life Phases of LCA impact assessment.

Material Transport & Construction					
Transportation of Materials	**Design Input**	**Unit**	**Functional Input**	**Unit**	**NOTES/ASSUMPTIONS:**
Transport of Concrete	45	mi	34761.74	tkm	assumes 30 truck loads, 15 tons on each truck, 3 miles
Transport of Steel	200	mi	45061.52	tkm	assumes 5 truckloads, 40 miles, can hold 35 tons
Transport of construction equip.	45	mi	13035.65	tkm	assumes equip is 40 tons
Construction of Wells	**Design Input**	**Unit**	**Functional Input**	**Unit**	
Drilling IW (comb. of fuel)	20	d	480	hr	assumes operations run 24/7
Pumping cement IW (comb. of fuel)	20	d	480	hr	assumes operations run 24/7
Pumping water IW (comb. of fuel)	20	d	480	hr	assumes operations run 24/7
Drilling PW (comb. of fuel)	20	d	480	hr	assumes operations run 24/7
Pumping cement PW (comb. of fuel)	20	d	480	hr	assumes operations run 24/7
Pumping water PW (comb. of fuel)	20	d	480	hr	assumes operations run 24/7
Trenching	**Design Input**	**Unit**	**Functional Input**	**Unit**	
Excavating (comb. of fuel)	20	d	480	hr	assumes operations run 24/7
Use of System					
Operation of Wells	**Design Input**	**Unit**	**Functional Input**	**Unit**	
Electricity for pumps	2053125	kWh	2053125	kWh	450 B/D, 2.5 kWh per barrel
Operation of chiller	2285	kW	11046.37	kWh	
Operation of heat exchanger	504	kWh/h	6622560	kWh	504 kWh/h, operate 30% of year. From Adolfsson et al.
Maintenance	1	p	1	p	
End of Life					
Deconstruction	**Design Input**	**Unit**	**Functional Input**	**Unit**	
Pump removal	24	hr	24	hr	
Surface equip. removal	24	hr	24	hr	
Sealing IW	15	m	79.08	m3	assumes seal to 20 m depth
Sealing PW	15	m	104.04	m3	assumes seal to 20 m depth
Waste	900	kg	900	kg	assume ~1 ton of waste
Waste Transport	60	mi	96.56	tkm	landfill ~60 mi away

References

Adolfsson, M., & Rashid, S. (2016). *Life Cycle Assessment and Life Cycle Cost of Heat Exchangers.* Thesis, Chalmers University of Technology. Retrieved from http://publications.lib.chalmers.se/records/fulltext/237796/237796.pdf

Beckers, K., & McCabe, K. (2018). Introducing GEOPHIRES v2.0: Updated Geothermal Techno-Economic Simulation Tool. *43rd Workshop on Geothermal Reservoir Engineering.* Standford University.

Boiarski, A. (1993). Distributed Fiber Optic Temperature Sensing. *Applications of Fiber Optic Sensors in Engineering Mechanics*, 210-24.

Bosman, R. (2016). *Water footprint of widely used construction materials - steel, cement, and glass.* Civil Engineering and Management. Enschede, The Netherlands: University of Twente. Retrieved May 2019, from https://essay.utwente.nl/69751/1/MA%20thesis%20Bosman,%20R..pdf

Clauser, C., & Huenges, E. (2013). Thermal Conductivity of Rocks and Minerals. In *Rock Physics & Phase Relations: A Handbook of Physcal Constants, Volume 3.*

Eckaus, R. S. (1992). Comparing the Effects of Greenhouse Gas Emissions on Global Warming. *The Energy Journal, 13*(1), 25-35. Retrieved from http://www.jstor.org/stable/41322452

EIA. (2016, February 2). *Carbon Dioxide Emissions Coefficients by Fuel*. Retrieved May 2019, from https://www.eia.gov/environment/emissions/co2_vol_mass.php

Energy, O. o. (n.d.). *Geothermal FAQs*. Retrieved 2019, from Energy.gov: https://www.energy.gov/eere/geothermal/geothermal-faqs

EPA, U. (n.d.). *Geothermal Heating and Cooling Technologies*. Retrieved April 2019, from United States Environmental Protection Agency: https://www.epa.gov/rhc/geothermal-heating-and-cooling-technologies

F&S, U. (2017). *Energy Billing System (EBS) Data.*

Fridleifsson, I. R. (2008). The possible role and contribution of geothermal energy to the mitigation of climate change. *IPCC Scoping Meeting on Renewable Energy Sources.* Luebeck, Germany.

Giesen, N. V.-D. (2012). Double-Ended Calibration of Fiber-Optic Raman Spectra Distributed Temperature Sensing Data. *Sensors*, 5471-485.

Green Building Alliance. (2019, May). *Geothermal Energy*. Retrieved from Green Building Alliance: https://www.go-gba.org/resources/green-building-methods/geothermal-energy/

GTO. (2018). *Geothermal Technologies Office.* Retrieved from Energy.gov: https://www.energy.gov/eere/geothermal/low-temperature-deep-direct-use-program-draft-white-paper

Harris, T. D., Smith, V. H., Graham, J. L., Van de Waal, D. B., Tedesco, L. P., & Clercin, N. (2017). Combined effects of nitrogen to phosphorus and nitrate to ammonia ratios on cyanobacterial metabolite concentrations in eutrophic Midwestern USA reservoirs. *Inland Waters, 6*(2), 199-210. Retrieved from https://www.tandfonline.com/doi/ref/10.5268/IW-6.2.938?scroll=top

Hausner, M. B. (2011). Calibrating Single-Ended Fiber-Optic Raman Spectra Distributed Temperature Sensing Data. *Sensors*.

Hsu, S. (2010). *Life Cycle Assessment of Materials and Construction in Commercial Structures: Variablity and Limitiations.* Massachusetts Institute of Technology. Retrieved from http://web.mit.edu/cron/project/concrete-sustainability-hub/Literature%20Review/Building%20Energy/Thesis/Libby%20Hsu%20Thesis.pdf

ICC. (2017, September). *Ameren Environmental Disclosure Filing.* Retrieved from Illinois Commerce Commission: https://www.icc.illinois.gov/downloads/public/filing/2/12/13/178049.pdf

Illinois, U. o. (n.d.). *Abbott Power Plant*. Retrieved from Illinois Facilities & Services: http://www.fs.illinois.edu/services/utilities-energy/production/abbott-power-plant

ISO. (2006). *Life Cycle Assessment - Principles and Framework.* Retrieved from International Organization for Standardization: https://www.iso.org/obp/ui/#iso:std:iso:14040:en

Lee, J. C. (2010). *Evaluating the Sustainability of Constrution with Recycled Materials.* Dissertation, University of Wisconsin-Madison.

Lijung Gu, D. G. (2019). Life Cycle Assessment for Cooling and Heating Sources of Buildings. Retrieved from https://www.researchgate.net/publication/242418447_LIFE_CYCLE_ASSESSMENT_FOR_COOLING_AND_HEATING_SOURCES_OF_BUILDING

Lowe, R. (2011, September). Combined heat and power considered as a virtual steam cycle heat pump. *Energy Policy, 39*(9), 5528-5534. Retrieved from https://doi.org/10.1016/j.enpol.2011.05.007

McDaniel, A. (2018). Dynamic Calibration for Permanent Distributed Temperature Sensing Networks. *IEEE Sensors Journal*, 2342-2352. doi:10.1109/JSEN.2018.2795240

McDaniel, A. (2018). Long-term district-scale geothermal exchange borefield monitoring with fiber optic distributed temperature sensing. *Geothermics*, 193-204.

McDaniel, A., Tinjum, J., Hart, D., Lin, Y. F., Stumpf, A., & Thomas, L. (2018). Distributed Thermal Response Test to Analyze Thermal Properties in Heterogeneous Lithology. *Geothermics, 76*, 116-124. Retrieved from https://doi.org/10.1016/j.geothermics.2018.07.003

Mekonnen, M. M. (2015, March). The consumptive water footprint of electricity and heat: a global assessment. *Environmental Science: Water Research & Technology*. doi:10.1039/c5ew00026b

Netz, J., & Sundin, J. (2015). *Water Footprint of Concrete.* Vetenskap Och Konst, Department of Sustainable Development, Environmental Science and Engineering. Retrieved May 2019, from https://www.diva-portal.org/smash/get/diva2:855765/FULLTEXT01.pdf

NOAA. (2019, February). *NCEI ocean heat content, temperature anomalies, salinity anomalies, thermosteric sea level anomalies, halosteric sea level anomalies, and total steric sea level anomalies from 1955 to present calculated from in situ oceanographic subsurface profile data.* Retrieved from data.gov: https://catalog.data.gov/dataset/ncei-ocean-heat-content-temperature-anomalies-salinity-anomalies-thermosteric-sea-level-anomali

Ponsioen, T. (2013, March 15). *The Surplus Cost Method*. Retrieved from PRéSustainability: https://www.pre-sustainability.com/news/the-surplus-cost-method-introduction

Puttagunta, S. e. (2010). Residential ground-source heat pumps: In-field system performance and energy modeling. *GRC Trans*, 941-948. Retrieved from http://www.carb-swa.com/Collateral/Documents/CARB-SWA/Research/Ground_Source_Heat_Pumps.pdf

Rajaei, M., & Tinjum, J. M. (2013). Life Cycle Assessment of Energy Balance and Emissions of a Wind Energy Plant. *Geotechnical and Geological Engineering*. doi:10.1007/s10706-013-9637-3

Selker, J. S. (2006). Distributed Fiber-Optic Temperature Sensing for Hydrologic Systems. *Water Resources Research* .

SimaPro. (n.d.). *About SimaPro*. Retrieved from https://simapro.com/about/

Solomon, S. (1999, August). Stratospheric ozone depletion: A review of concepts and history. *Reviews of Geophysics, 37*(3), 275-316. doi:https://doi.org/10.1029/1999RG900008

Stumpf, A., Damico, J., Okwen, R., Stark, T., Elrick, S., Nelson, W. J., . . . Lin, Y.-F. (2018). Feasibility of a Deep Direct-Use Geothermal System at the University of Illinois Urbana-Champaign. *Geothermal Resources Council Transactions*.

Suarez, F. M. (2011). Heat Transfer in the Environment: Development and Use of Fiber-Optic Distributed Temperature Sensing. *Developments in Heat Transfer*.

Sullivan, J., Clark, C., Han, J., & & Wang, M. (2010). *Life-Cycle Analysis Results of Geothermal Systems in Comparison to Other Power Systems.* Argonne National Laboratory. Retrieved from https://energy.gov/sites/prod/files/2014/02/f7/lifecycle_analysis_of_geothermal_systems.pdf

Thorsteinsson, H. H., & Tester, J. W. (2009). Barriers and enablers to geothermal district heating system development in the United States. *Energy Policy*.

Tomasini-Montenegro, C. e. (2017, March 5). Life cycle assessment of geothermal power generation technologies. *Applied Thermal Engineering, 114*, 1119-1136. Retrieved from https://doi.org/10.1016/j.applthermaleng.2016.10.074

UIUC. (2015). *Illinois Climate Action Plan.* Universtiy of Illinois. Institute for Sustainability, Energy, and Environment. Retrieved from https://sustainability.illinois.edu/campus-sustainability/icap/

UIUC. (2016). *UIUC Energy Report.* University of Illinois. Retrieved from https://www.fs.illinois.edu/docs/default-source/utilities-energy/2016-combined-college-energy-report-fy16.pdf?sfvrsn=d639faea_2

UIUC. (2017). *Statement of Project Objectives, SOPO.* U.S. Department of Energy.

UN. (2018). *What is the Paris Agreement?* Retrieved from United Nations Climate Change: https://unfccc.int/process-and-meetings/the-paris-agreement/what-is-the-paris-agreement

USGCRP. (2017). *Climate Science Special Report: Fourth National Climate Assessment, Volume I.* U.S. Global Change Research Program. doi:10.7930/J0J964J6

Walker, M. D., & Meyer, L. L. (2015). Thermal Property Measurements of Stratigraphic Units with Modeled Implications for Expected Performance of Vertical Ground Source Heat Pumps. *Geotechnical and Geological Engineering*, 223-238.

Woods-Robinson, R. (2013). *Life Cycle Assessment of a Non-Conventional Deep Insulated Single Hole (DISH) Ground Source Heat Pump and Comparison with Conventional Heating, Ventilation and Cooling Methods.* University of Wisconsin-Madison, Dept. of Geological Engineering.